Mechanistic insights into the adverse effects of cisplatin employing the zebrafish model

Zur Erlangung des akademischen Grades eines
DOKTORS DER NATURWISSENSCHAFTEN
(Dr. rer. nat.)

von der KIT-Fakultät für Chemie und Biowissenschaften
des Karlsruher Instituts für Technologie (KIT)
genehmigte
DISSERTATION
von

Ding Zhang
aus Anhui, China

1. Referent: PD Dr. Carsten Weiss
2. Referent: Prof. Dr. Andrea Hartwig
3. KIT-Dekan: Prof. Dr. Martin Bastmeyer

Tag der mündlichen Prüfung: 08.02.2024

Erklärung

Bei der vorgelegten Arbeit ‘Mechanistic insights into the adverse effects of cisplatin employing the zebrafish model’ handelt es sich um meine eigenständig erbrachte Leistung. Ich habe nur die angegebenen Quellen und Hilfsmittel benutzt und mich keiner unzulässigen Hilfe Dritter bedient. Insbesondere habe ich wörtlich oder sinngemäß aus anderen Werken übernommene Inhalte als solche kenntlich gemacht. Die Richtigkeit der vorstehenden Erklärungen bestätige ich. Die Bedeutung der eidesstattlichen Versicherung und die strafrechtlichen Folgen einer unrichtigen oder unvollständigen eidesstattlichen Versicherung sind mir bekannt. Ich versichere an Eides statt, dass ich nach bestem Wissen die reine Wahrheit erklärt und nichts verschwiegen habe.

Datum: 07/12/2023 Unterschrift: Ding Zhang

Summary

Cisplatin, a widely used chemotherapeutic drug, is associated with various side effects and toxic reactions, including nephrotoxicity, neurotoxicity, and ototoxicity, which have limited its clinical use. Among these toxicities, nephrotoxicity can lead to acute kidney injury, posing a significant threat to patient safety. Understanding the mechanisms underlying cisplatin-induced nephrotoxicity is crucial for the development of preventive and therapeutic strategies to reduce the risk of renal damage during clinical use.

To analyze the potential regulatory mechanisms, this study first established a zebrafish larval model of cisplatin-induced nephrotoxicity, which involved selecting appropriate schedules for larval injection, improving injection techniques, and implementing phenotypic scoring methods. Within this model, functional inhibition of the G protein-coupled estrogen receptor (GPER) effectively reduces abnormal phenotypes and decreased the upregulation of some kidney injury markers provoked by cisplatin, suggesting a potential regulating role of GPER in cisplatin-induced nephrotoxicity. Additional biochemical analyses and inhibitor experiments revealed that inhibiting GPER function decreases the activation of Mitogen-Activated Protein Kinases (MAPK), indicating that the GPER-MAPK signaling is important for cisplatin-induced nephrotoxicity.

Zusammenfassung

Der Einsatz von Cisplatin, einem weit verbreiteten Chemotherapeutikum, ist mit verschiedenen Nebenwirkungen und toxischen Reaktionen verbunden, darunter Nierentoxizität, Neurotoxizität und Ototoxizität, die seine klinische Anwendung einschränken. Eine dieser Nebenwirkungen, die Nierentoxizität, kann zu akutem Nierenversagen führen und stellt eine erhebliche Bedrohung für die Patientensicherheit dar. Das Verständnis der Mechanismen, die der cisplatininduzierten Nierentoxizität zugrunde liegen, ist entscheidend für die Entwicklung präventiver und therapeutischer Strategien zur Verringerung des Risikos einer Nierenschädigung während der klinischen Anwendung.

Um die potenziellen Regulationsmechanismen zu analysieren, wurde in dieser Studie zunächst ein Zebrafischlarvenmodell der durch Cisplatin induzierten Nephrotoxizität etabliert. Dies umfasste die Auswahl geeigneter Zeitpläne für die Injektion der Larven, die Verbesserung der Injektionstechniken und die Umsetzung von phänotypischen Scoring-Methoden. Innerhalb dieses Modells führte die funktionelle Hemmung des G-Protein-gekoppelten Östrogenrezeptors (GPER) effektiv zu einer Verringerung abnormer Phänotypen und einer Abnahme der Hochregulationeiniger Marker für Nierenschädigung, die durch Cisplatin verursacht wurden. Dies legt eine potenzielle regulierende Rolle von GPER in der durch Cisplatin induzierten Nephrotoxizität nahe. Weitere biochemische Analysen und Inhibitorexperimente zeigten, dass die Hemmung der GPER-Funktion zu einer Verringerung der Aktivierung von Mitogen-aktivierten Proteinkinasen (MAPK) führte, was darauf hindeutet, dass die GPER-MAPK-Kaskade für die durch Cisplatin induzierte Nephrotoxizität wichtig ist.

Table of Content

List of figures

List of tables

Abbreviations

DMSO	dimethylsulfoxide
PFA	paraformaldehyde
cDNA	complementary DNA
dpf	days post fertilization
dpi	days post injection
hpi	hours post injection
hpf	hours post fertilization
ROS	reactive oxygen species
MAPK	mitogen-activated protein kinase
H2AX	H2A histone family member X
ERK	extracellular signal regulated kinase
qRT-PCR	quantitative Real-Time PCR
SDS	sodium dodecyl sulfate
ER	endoplasmic reticulum
DDR	DNA damage response
NER	nucleotide excision repair
MMR	mismatch repair
gDNA	genomic DNA
AKI	acute kidney injury
GPER	G protein-coupled estrogen receptor
GPCR	G protein-coupled receptor
WB	western blotting
ISH	*in situ* hybridization
IHC	immunohistochemistry
PBS	phosphate buffered saline
TEMED	tetramethyl ethylene diamine
HEPES	N-2-hydroxyethylpiperazine-N-2-ethane sulfonic acid
cdh17	cadherin 17
kim1	kidney injury molecule 1
clu	clusterin
ctgf	connective tissue growth factor
homx1	heme oxygenase 1
TNF	tumor necrosis factor
IL	interleukin
Tris	tris(hydroxymethyl)aminomethane
DEPC	diethyl pyrocarbonate
EDTA	ethylenediaminetetraacetic acid
Tween-20	polysorbate 20
DIG	digoxigenin
RT	room temperature
PMSF	phenylmethylsulfonyl fluoride
w/v	weight/volume

v/v	volume/volume
FDA	Food and Drug Administration
DMAP	Damage-associated molecular patterns
PTW	PBS with Tween-20
kDa	kilodalton
RTEC	renal tubular epithelial cells
SD	standard deviation
OCT2	organic cation transporter 2
CTR1	copper transporter 1
JNK	Jun N-terminal kinase

1 Introduction

1.1 The anticancer drug cisplatin

1.1.1 Platinum-based drugs

Chemotherapy is an effective treatment for cancer. Before the 1960s, all drugs used for cancer treatment were pure organic compounds. Towards the late 1960s, there was an unexpected discovery of a simple, coordinating inorganic compound with anticancer properties – cisplatin. Not only did it inhibit bacterial growth, but it also inhibited the growth of cancer cells [1, 2]. This discovery opened new possibilities for cancer chemotherapy.

Cisplatin, also known as cis-diamminedichloroplatinum(II) or cisplatinum, is a coordination complex composed of a doubly charged platinum ion surrounded by four ligands, 2 amine and 2 chloride ions. It has a square planar geometry and appears as a white or yellow-orange crystalline powder at room temperature (RT) (Table 1.1). The arrangement of the ligands around the platinum ion is such that the two amine groups are located on one side of the molecule, and the two chloride ions are located on the opposite side. This arrangement is known as the cis-configuration, hence the name cisplatin. Cisplatin was the first platinum-based drug to be approved by the US Food and Drug Administration (FDA) in 1978 [3]. Since then, it has been widely used in the treatment of testicular, ovarian, and lung cancers (Table 1.1). However, its clinical use is limited by its severe side effects, including nephrotoxicity [4], neurotoxicity [5], and ototoxicity [6].

Carboplatin was developed as a second-generation platinum-based drug in the 1970s [7]. Compared with cisplatin, carboplatin contains a cyclobutane dicarboxylate group instead of the two chloride atoms. The modification reduced the toxicity and side effects of cisplatin while retaining its anticancer properties (Table 1.1). Carboplatin was first approved by the FDA in 1989 for

the treatment of ovarian cancer [8]. Since then, it has been approved for the treatment of various other types of cancer, including lung cancer, bladder cancer and more (Table 1.1).

Oxaliplatin, a third-generation platinum-based drug, was approved by the FDA in 2002. Oxaliplatin features a chelating oxalate leaving group ligand and a chelating diaminocyclohexane (DACH) non-leaving group ligand (Table 1.1). It shows efficacy against colorectal cancer and has a different toxicity profile than cisplatin and carboplatin [9].

Drug	Structure	Year of approval	Country approved	Type of cancer treated
Cisplatin	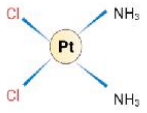	1978	Worldwide	Testicular, Ovarian, Bladder, Melanoma, NSCLC, Lymphomas, Myelomas
Carboplatin	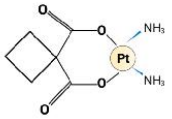	1989	Worldwide	Ovarian, Cervix, Testis, Breast, Lung, Bladder
Oxaliplatin	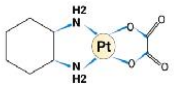	2002	Worldwide	Colon

Table 1.1 Clinically approved Pt(II)-anticancer drugs

1.1.2 Cisplatin-induced DNA damage and anticancer effect

In the clinics, after being administered to patients intravenously in the form of a sterile saline solution, cisplatin remains unchanged and neutral in the bloodstream due to the high concentration of chloride (approximately 100 mM) [10]. As a result, it continues to circulate throughout the body. However, plasma proteins such as albumin, transferrin, and the amino acid cysteine have a strong affinity for cisplatin, leading to deactivation of a significant portion of the administered drug. It has been reported that within 24 hours of administration, 65-95% of cisplatin may bind to blood plasma proteins [11].

According to current knowledge, Figure 1.1 illustrates the mechanism of action of cisplatin. The drug can reach tumor cells through passive diffusion [10] or

active transport using e.g. copper transporter protein 1 (CTR1 [12], after which it enters the low-chloride intracellular environment (Figure 1.1). In this environment, the water molecules displace the hydrolysable Cl^- ligands, creating a highly reactive species with a positive charge. These species consist of monoaqua $[Pt(NH_3)_2Cl(H_2O)]^+$ and diaqua $[Pt(NH_3)_2(H_2O)_2]^{2+}$ complexes that bind covalently to nucleophilic sites on DNA, particularly to the N-7 atom of purine bases, primarily guanine [13]. This binding leads to intrastrand and interstrand DNA crosslinks, with 90-95% of crosslinks being intrastrand, and of those, 60-65% being 1,2-d(GpG) and 20-25% being 1,2-d(ApG). Other crosslinks such as monoadduct (~2%) and 1,3-d(GpXpG) (~2%) are formed less frequently [3]. These platinum-DNA adducts interfere with DNA transcription and replication, which can lead to miscoding and single or double-strand breaks. The damage is recognized by DNA damage repair pathways including nucleotide excision repair (NER) and mismatch repair (MMR) [14]. When this damage has accumulated and DNA repair machineries are not sufficient to repair it, the DNA damage response (DDR) pathway comprised of the ATM (Ataxia telangiectasia mutated) – Chk2 (Checkpoint kinase 2) and ATR (Ataxia telangiectasia and Rad3 related) – Chk1 (Checkpoint kinase 1) [15] pathways are triggered. Downstream targets involve p53 [16], mitogen-activated protein kinases (MAPK) [17] and others, which are activated and ultimately might induce cell death either by apoptosis or necrosis. Although all cells can experience this type of DNA damage, rapidly dividing cells such as cancer cells are particularly susceptible. As a result, this is considered the primary mechanism behind cisplatin anticancer activity.

Although cisplatin's main target is genomic DNA (gDNA), only a small proportion (~1%) of intracellular cisplatin is typically bound to gDNA, suggesting additional mechanisms contributing to its anticancer activity [18]. Recent studies have revealed that cisplatin strongly impacts mitochondrial function. This dysfunction can cause changes in mitochondrial structure, disruption of mitochondrial membrane potential, and instability of electron

transport reactions, leading to the overproduction of reactive oxygen species (ROS) [19] (Figure 1.1). ROS is a normal byproduct of cellular metabolism, but excessive amounts can result in oxidative stress, which can damage proteins, lipids, and nucleic acids, leading to cellular dysfunction and cell death. *Zhang et al.* demonstrated that cisplatin-induced aberrant ROS production activates the p53 and MAPK pathways, ultimately leading to cancer cell death [20].

In addition to the reported genomic DNA damage and aberrant ROS production, cisplatin can induce abnormal calcium ion (Ca^{2+}) accumulation, leading to endoplasmic reticulum (ER) stress and ultimately resulting in apoptosis [21, 22] (Figure 1.1). The anticancer effect of cisplatin is a complex process that involves multiple cellular activities and mechanisms. It should be noted that different studies have confirmed that cisplatin-induced DNA damage and aberrant ROS production activate the MAPK and p53 signaling pathways in cancer cells, leading to cell death. However, the mechanisms by which cisplatin activates these pathways are still unknown, and potential upstream regulators remain to be investigated.

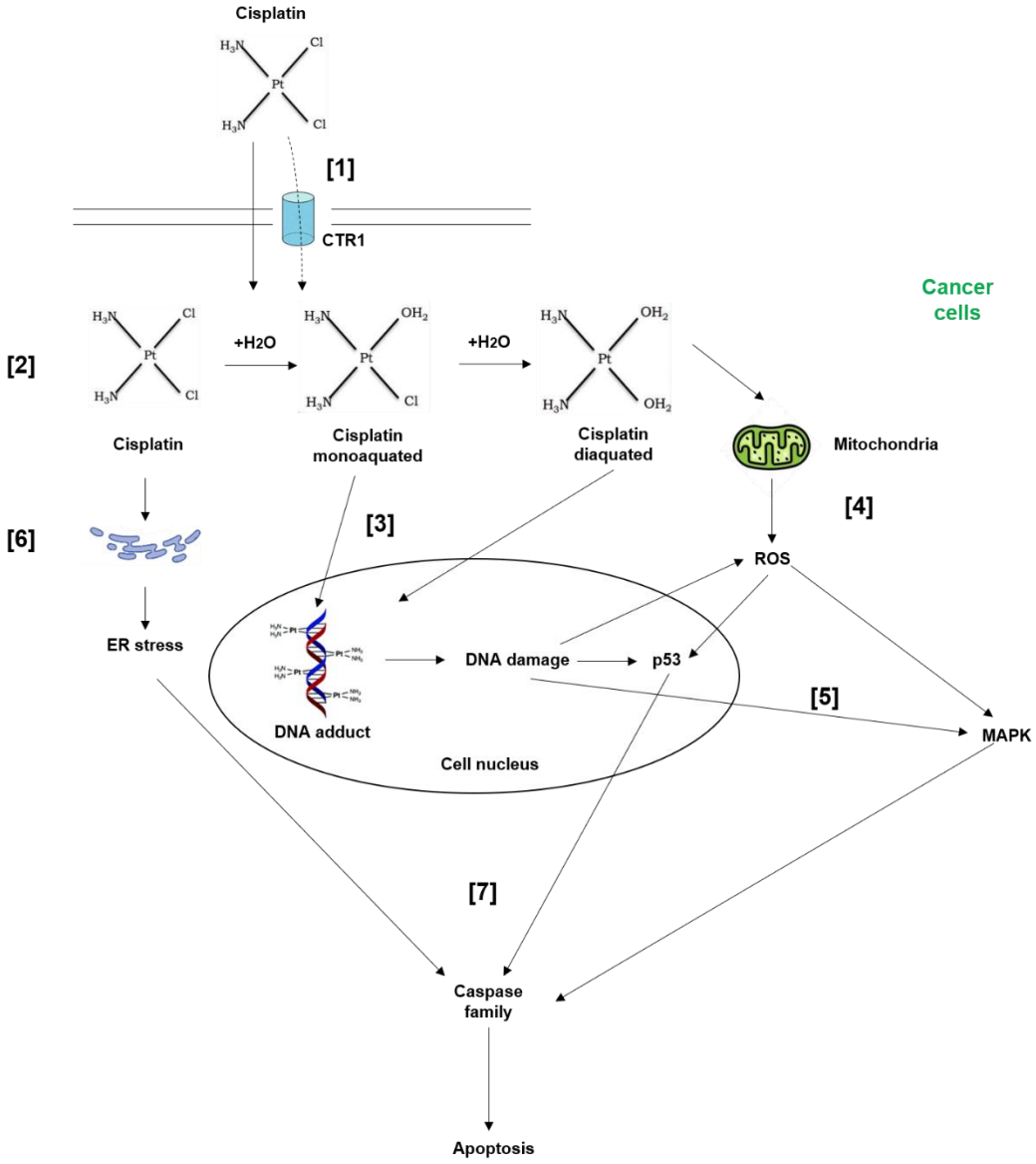

Figure 1.1 Cellular responses to cisplatin
[1] Cisplatin enters cells either through passive diffusion (as indicated by the dashed arrow) or by utilizing the carrier-mediated transport via Copper Transporter 1 (CTR1).
[2] The activation process of cisplatin involves the exchange of one or two chloride ions with water molecules, resulting in monoaqua and diaqua forms, respectively.
[3] Once activated, cisplatin interacts with DNA, inhibiting DNA synthesis to halt cell proliferation, subsequently triggering a DNA damage response.
[4] Activated cisplatin can interact with mitochondrial DNA and induce ROS.
[5] DNA damage response and ROS activate the p53 and MAPK pathways.
[6] Apart from ROS and DNA damage, cisplatin can induce endoplasmic reticulum stress.
[7] Finally, caspases are activated, inducing cell death.

1.1.3 Cisplatin-induced adverse effects

The cytotoxicity of cisplatin is not limited to cancer cells and its action on

normal non-cancerous cells generates severe side effects. Patients receiving cisplatin treatment often exhibit significant nephrotoxicity, ototoxicity, neurotoxicity, and gastrointestinal toxicity.

1. Gastrointestinal toxicity

Cisplatin chemotherapy is associated with significant gastrointestinal toxicity, leading to substantial impacts on treatment adherence (Figure 1.2). Common clinical manifestations of cisplatin-induced gastrointestinal toxicity encompass a wide range of gastrointestinal alterations. The most frequent symptoms related to cisplatin treatment include nausea, vomiting, loss of appetite, weight loss, gastrointestinal dysfunction, diarrhea, delayed gastric emptying, mucositis, malabsorption, and barrier disruption. These symptoms may persist for an extended period even after the completion of the treatment regimen [23, 24] .

2. Neurotoxicity

Cisplatin treatment can cause neurotoxicity, which is a well-known side effect that limits the dose (Figure 1.2). Distal sensory neuropathy is a common manifestation that can be distressing. There is a rough correlation between the severity of neurotoxicity and the administered dose of cisplatin, and currently there are no known treatment options. Unfortunately, neurotoxicity is often irreversible [25, 26].

3. Ototoxicity

Ototoxicity is another dose limiting side effect of cisplatin treatment (Figure 1.2). It typically results in sensorineural hearing loss starting in the high frequencies and progressing to the speech range, often accompanied by tinnitus [27]. Ototoxicity is dose-dependent [28], and radiation to the ear may increase its severity [29]. There is considerable variability in the extent of ototoxicity among individuals, possibly due to differences in pharmacokinetics, genetics, and metabolic status [27]. Unfortunately, susceptible individuals cannot be identified prior to treatment. However, early diagnosis may be possible through monitoring of high-frequency audiometry [30] or otoacoustic

emissions [31].

4. Nephrotoxicity

Cisplatin chemotherapy is associated with nephrotoxicity, which was first reported in the early clinical trials (Figure 1.2). Despite careful hydration, approximately one-third of patients develop nephrotoxicity after a single dose of cisplatin (50-100 mg/m^2) [32, 33]. The onset of clinical symptoms typically occurs around 10 days after cisplatin administration and is characterized by a lower glomerular filtration rate, elevated serum creatinine, and reduced serum magnesium and potassium levels [4]. Long-term cisplatin treatment will ultimately result in various symptoms including acute kidney injury (AKI), hypomagnesemia, Fanconi-like syndrome, distal renal tubular acidosis, hypocalcemia, renal salt wasting, and hyperuricemia [34].

Among these different organ toxicities, nephrotoxicity is considered the most important adverse effect induced by cisplatin because it can be severe and potentially life-threatening, which inevitably limits the wide clinical application of cisplatin [35]. Administering intravenous fluids such as saline or mannitol, and diuretics, e.g. furosemide, can be employed to decrease cisplatin-induced nephrotoxicity [36]. However, these strategies can only ameliorate cisplatin-induced nephrotoxicity, and permanent kidney injury still exists in patients receiving long-term treatment. In order to improve the clinical efficiency of cisplatin, different studies in the past 40 years attempted to uncover cisplatin-induced nephrotoxicity, but many of the regulatory mechanisms still remain unknown.

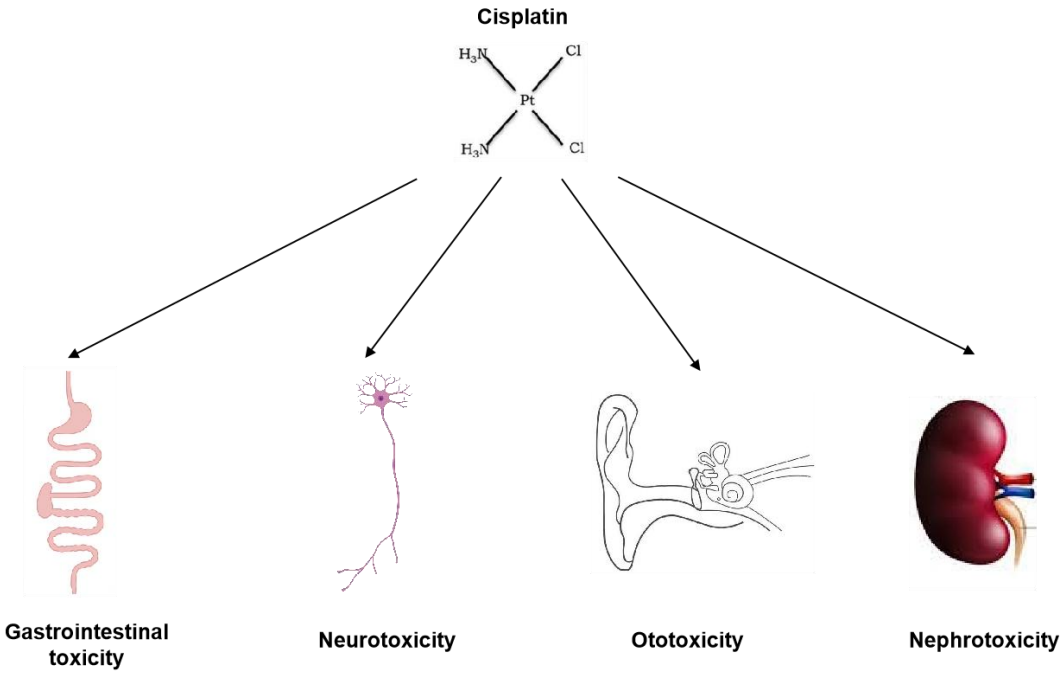

Figure 1.2 The main target organs of cisplatin-induced toxicity

1.2 Cisplatin-induced nephrotoxicity

1.2.1 The mechanisms of cisplatin-induced nephrotoxicity

Cisplatin can accumulate in the kidney during glomerular filtration and tubular secretion, with concentrations in the proximal tubules approximately five times higher than in the blood. As a result, even non-toxic serum levels of cisplatin can reach toxic levels in the kidney, leading to impaired renal function. Renal biopsies of cisplatin treated patients show severe injury to the S3 segment of the proximal tubules [37]. Cisplatin can enter renal tubular cells through passive diffusion or active transport, and it has been observed to move from the basolateral to the apical side. Basolaterally expressed transporters such as organic cation transporter 2 (OCT2) [38, 39] are responsible for removing cisplatin from the bloodstream and transferring it into renal tubular cells. Cisplatin nephrotoxicity has been found to be positively correlated with OCT2 expression.

As cisplatin accumulates in renal epithelial cells, it can trigger a series of biochemical processes and cellular signaling that ultimately lead to

nephrotoxicity.

1. Nuclear DNA damage

Cisplatin-induced damage to nuclear DNA is typically pronounced in rapidly proliferating cells. Although the proliferation rate of normal quiescent renal tubular epithelial cells is low, surviving epithelial cells enter the cell cycle and rapidly proliferate in response to tubular injury and cell death [40]. Yamashita et al. demonstrated that even with low-dose cisplatin injections, accumulation of nuclear DNA damage in renal tubular cells occurs, potentially promoting the transition from acute kidney injury (AKI) to chronic kidney damage in mice [41].

2. Mitochondrial dysregulation and oxidative stress

Several lines of evidence suggest that the nephrotoxicity of cisplatin is closely related to reactive oxygen species (ROS) produced by mitochondria. The abundant mitochondrial content in proximal tubule epithelial cells makes them susceptible targets of cisplatin. After entering the proximal tubule epithelial cells, cisplatin can form more potent toxins in addition to generating positively charged metabolites by hydrolysis. This process begins with the formation of glutathione adducts from circulation, followed by catalysis by various metabolic enzymes to form highly reactive thiols [42].

Highly reactive thiols can directly impact the activity of the electron transport chain, which is a source of free radical generation within cells. When mitochondria are impaired, electron leakage becomes particularly problematic, leading to reduced or blocked electron transfer. Under these conditions, mitochondria produce an abundance of ROS in various forms. Furthermore, thiols can also modulate the mitochondrial permeability transition pore, controlling the flow of molecules in and out of the mitochondria, such as cytochrome c and apoptosis-inducing factor (AIF) [19].

3. Inflammation

cisplatin-induced nephrotoxicity is closely associated with inflammation. After influx into the renal cell, cisplatin induces the expression of pro-inflammatory cytokines, such as Tumor necrosis factor-α (TNF-α), Interleukin-1β (IL-1β),

and Interleukin-6 (IL-6), and Damage-associated molecular patterns (DAMPs), such as ATP, which trigger a cascade of inflammatory responses [43]. The activation of inflammatory cells, such as macrophages and T cells, further amplifies the inflammatory response, leading to renal tissue damage and dysfunction. In addition, cisplatin can activate the nuclear factor kappa-light-chain-enhancer of activated B cells (NF-κB) pathway, a key signaling pathway that regulates inflammation, leading to the expression of various inflammatory genes [44]. The activation of NF-κB also contributes to the recruitment of inflammatory cells and the release of pro-inflammatory cytokines. The induction of inflammation by cisplatin is considered one of the major mechanisms underlying cisplatin-induced nephrotoxicity.

4. Apoptosis and necrosis

As previously mentioned, cisplatin-induced apoptosis in renal tubular epithelial cells (RTECs) is primarily dependent on the activation of downstream signaling pathways in response to DNA damage, oxidative stress, and inflammation. These pathways include the extrinsic pathway activated through death receptors, such as TNF- or Fas-receptors, the intrinsic mitochondrial pathway, and the endoplasmic reticulum stress pathway.

Intriguingly, evidence suggests that cisplatin activates these apoptotic pathways by increasing the activity of p53, MAPK, and caspases [45]. Caspases are a family of cell death proteases that play a crucial role in the execution phase of cisplatin-induced RTECs apoptosis. However, the induction of cell death by p53 or MAPK, as upstream regulators of caspases, is a complex and multifactorial process.

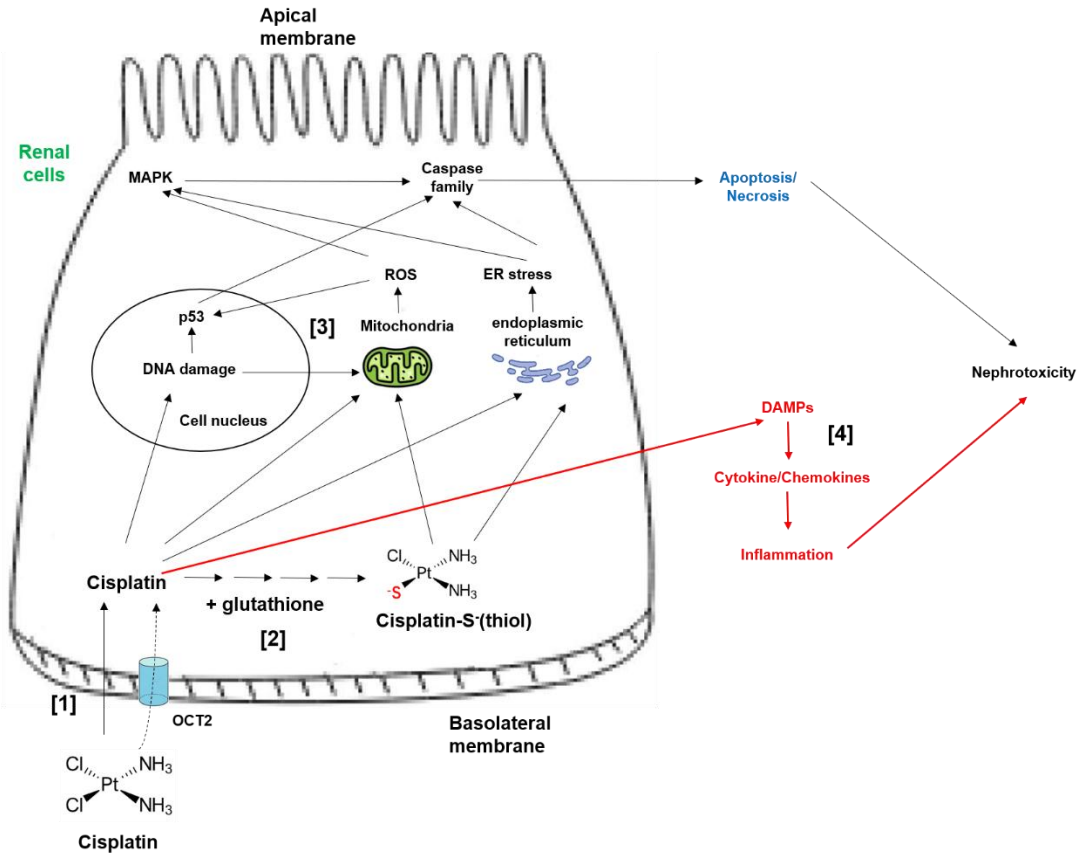

Figure 1.3 Mechanisms of cisplatin-induced nephrotoxicity
[1] Cisplatin enters kidney cells either via passive diffusion (as indicated by the dashed arrow) or through organic cation transporter 2 (OCT2) carriers.
[2] Bioactivation of cisplatin to the nephrotoxin, cisplatin-S^- (thiol).
[3] Summary of cisplatin-induced renal cell death. Cisplatin and its thiol derivatives promote oxidative stress, endoplasmic reticulum stress, and DNA damage, reported to be associated with the activation of p53 and MAPK. Finally, caspases are activated, inducing cell death.
[4] Summary of cisplatin-induced inflammation. Cisplatin-induced injury to renal epithelial cells leads to the release of DAMPs and cytokines/chemokines, ultimately resulting in local inflammation.

1.2.2 p53 pathway

Cisplatin treatment activates p53 both *in vivo* in kidneys [46] and *in vitro* in renal epithelial cells [47]. Inhibition of p53 transcriptional activity through either pharmacologic or genetic means reduces cisplatin-induced caspase activation and apoptosis *in vitro* [47], as well as cisplatin-induced apoptosis and renal injury *in vivo* [48].

cisplatin-induced DNA damage activates ATM and ATR, which in turn

phosphorylate and activate p53. Activated p53 then induces the transcription of several apoptotic genes, including p53 up-regulated modulator of apoptosis-alpha (PUMA-α) and p53-induced protein with a death domain (PIDD), both of which are downstream mediators of p53-induced apoptosis [49]. PIDD activates caspase 2 by forming PIDDosomes, resulting in the release of apoptosis-inducing factor (AIF) from mitochondria, leading to caspase-independent apoptosis [50]. On the other hand, PUMA-α translocates to mitochondria and interacts with and neutralizes the antiapoptotic protein Bcl-XL, freeing pro-apoptotic protein Bax and Bak to form pores on the outer membrane of mitochondria. This results in the release of cytochrome c into the cytosol, activating caspases and leading to caspase-dependent apoptosis [51]. These findings indicate that p53 plays a central role in cisplatin-induced nephrotoxicity.

In recent research conducted by Yuan et al., it was demonstrated that p53 contributes to the mitochondrial production of ROS [52]. Moreover, inhibition of p53 transcriptional activity reduced cisplatin-induced oxidative stress and apoptosis [53].

In conclusion, there is ample evidence suggesting that the activation of p53 plays a central role in cisplatin-induced nephrotoxicity, and inhibition of p53 decreases cisplatin-induced nephrotoxicity. However, it is noteworthy that inhibition of p53 might increase the survival of cancer cells and thus reduce the therapeutic efficiency of cisplatin. This depends on the p53 status, as in many types of cancer p53 is mutated [54, 55]. In this situation, inhibition of p53 might reduce kidney injury without impairing the anticancer activity of cisplatin.

1.2.3 MAPK pathway

The mitogen-activated protein kinase (MAPK) signaling pathways encompass multiple tiers of highly conserved serine/threonine protein kinases, culminating in the activation of extracellular signal-regulated kinase (ERK), p38, and Jun N-terminal kinase (JNK) [56]. These pathways play a crucial role in regulating

cellular homeostasis and processes such as proliferation, differentiation, and apoptosis. In the context of cisplatin-induced nephrotoxicity, activation of MAPKs has been observed in various experimental models. However, the specific roles of individual MAPKs in mediating renal cell injury induced by cisplatin are complex and can vary between different studies [57-61]. Moreover, these roles may be influenced by the specific cell types and experimental models under investigation.

A study conducted by Nowak et al. demonstrated that during cisplatin treatment of primary cultures of renal tubular cells, ERK1/2 were activated and accumulated in mitochondria. Inhibiting ERK1/2 using PD98059 and U0126, two pharmacological MEK inhibitors, showed potential in mitigating cisplatin-induced mitochondrial dysfunction and apoptosis [62].

The roles of p38 and JNK in cisplatin nephrotoxicity are less well-defined compared to ERK. In immortalized mouse proximal tubule cells, although cisplatin activated all three MAPKs, only ERK was found to contribute to apoptosis [63]. Conversely, Ramesh et al. demonstrated the involvement of p38 in cisplatin nephrotoxicity through both *in vitro* and *in vivo* models [59]. Renoprotective effects were observed with pharmacological inhibitors of p38 (SB203580 and SKF-86002) [64]. Interestingly, rather than directly regulating tubular cell injury and death, p38 may play a role in regulating TNF-α expression in renal tubular cells, thereby influencing the associated inflammatory response accompanying cisplatin nephrotoxicity.

Activation of JNK protein by cisplatin has been observed in cultured renal tubular cells and kidney tissues [58, 63]. Francescato et al. conducted an *in vivo* rat study and demonstrated that treatment with the JNK inhibitor SP600125 reduced renal apoptosis and inflammation in response to cisplatin [58]. However, the evidence regarding the role of JNK in cisplatin-induced nephrotoxicity remains inconclusive.

In order to address the varying outcomes observed in different studies, it is essential to investigate the concurrent activation of ERK, p38, and JNK in the

same samples during cisplatin treatment [63]. A systematic assessment of their temporal and spatial activation is warranted to gain a comprehensive understanding. Furthermore, the usage of pharmacological inhibitors should be supported by rigorous examination to ensure their specificity and validity.

1.3 GPER and cisplatin-induced nephrotoxicity

1.3.1 Preliminary work and potential mechanisms

Previous studies confirmed the existence of similarities in the mechanisms underlying cisplatin-induced nephrotoxicity and its anticancer effects. cisplatin-induced DNA damage and generation of ROS are found in both cancer cells and renal cells. These cellular stressors activate the p53 and MAPK signaling pathways, subsequently leading to caspase activation and initiation of apoptotic pathways. This finding suggests that conclusions drawn from studies on the anticancer mechanisms of cisplatin might also help to understand the mechanisms underlying cisplatin-induced nephrotoxicity.

With the aim to identify regulators of cisplatin-induced cell death, a doctoral student in our laboratory, Iris Hansjosten, previously co-exposed two human cancer cell lines to 1120 bioactive chemicals, including FDA-approved drugs, and cisplatin [65]. Among several hits, G protein-coupled estrogen receptor (GPER) inhibitors were found to significantly suppress cisplatin-induced cancer cell death. This discovery implies the involvement of GPER in cisplatin-induced cancer cell death. Considering the similarities in the mechanisms of cisplatin-induced nephrotoxicity and its anticancer effects, this result prompted our speculation on whether GPER could regulate cisplatin-induced nephrotoxicity.

1.3.2 GPER

GPER (G protein-coupled estrogen receptor), also known as GPR30, is a

transmembrane receptor that belongs to the G protein-coupled receptor (GPCR) family [66]. It was first identified in 1996 as a novel estrogen receptor that mediates estrogen signaling pathways independently of the classical estrogen receptors, ERα and ERβ. Unlike ERα and ERβ, which are predominantly localized in the nucleus [67]. GPER is primarily located on the cell membrane and endoplasmic reticulum (ER), allowing for rapid signaling responses [68] (Figure 1.4).

GPER is widely expressed in various tissues and cell types, including reproductive organs, cardiovascular system, nervous system, and cancer cells. Its expression pattern suggests that it plays a critical role in mediating estrogen's diverse physiological functions beyond the classical estrogen-responsive tissues [69]. Activation of GPER by estrogen or selective agonists leads to the activation of intracellular signaling cascades, including cyclic adenosine monophosphate (cAMP) pathway [70], calcium (Ca^{2+}) signaling pathway [71], phosphoinositide 3-kinase (PI3K) pathway [72], and mitogen-activated protein kinase (MAPK) pathway [73] (Figure 1.4).

The involvement of GPER in various cellular processes has attracted significant attention in recent years. Studies have demonstrated its role in regulating cell proliferation, migration, and apoptosis, which are critical for normal tissue development and homeostasis [74] (Figure 1.4).

One of the key physiological functions of GPER is its involvement in cell proliferation. Activation of GPER has been shown to stimulate cell growth and promote cell cycle progression in different cell types. This suggests that GPER signaling is crucial for regulating the balance between cell proliferation and differentiation. Furthermore, GPER has been implicated in the growth and development of reproductive organs, including the uterus, ovaries, and mammary glands, where estrogen signaling is known to play a significant role.

GPER also influences cell migration, which is a fundamental process in tissue development, wound healing, and metastasis. Activation of GPER has been shown to enhance cell motility and promote invasive behavior in various

cancer cell lines. Additionally, GPER-mediated signaling has been implicated in the regulation of epithelial to mesenchymal transition (EMT) [75], a critical process involved in tissue remodeling and metastatic dissemination of cancer cells.

Although the majority of studies have highlighted the role of GPER in promoting cell proliferation, emerging evidence suggests that it can also modulate apoptotic pathways under specific conditions. Liliana et al. elucidated that G-1, a GPER agonist, causes an early rise of intracellular Ca^{2+}, arrests the cell cycle in G2/M, reduces viability, and provokes apoptosis in T cell lines derived from patients with acute lymphoblastic leukemia [76]. Interestingly, the apoptotic effects of GPER signaling can vary depending on the cellular context and the specific stimuli involved. Han et al. found that GPER activation protects the brain after ischemia/reperfusion injury and reduces apoptosis via the endoplasmic reticulum stress-mediated apoptotic pathway. [77] The precise mechanisms underlying GPER-mediated apoptosis are still being elucidated, and further research is needed to fully understand the conditions and cellular contexts in which GPER elicits pro-apoptotic effects.

Overall, GPER exerts diverse physiological functions beyond its role in disease contexts. Its involvement in cell proliferation, migration, and apoptosis highlights its significance in tissue development, homeostasis, and regeneration. Understanding the intricate mechanisms underlying GPER signaling in these physiological processes may provide insights into potential therapeutic interventions for various diseases and contribute to the development of personalized medicine approaches. Further research is needed to unravel the complexities of GPER-mediated signaling and its precise role in different physiological contexts.

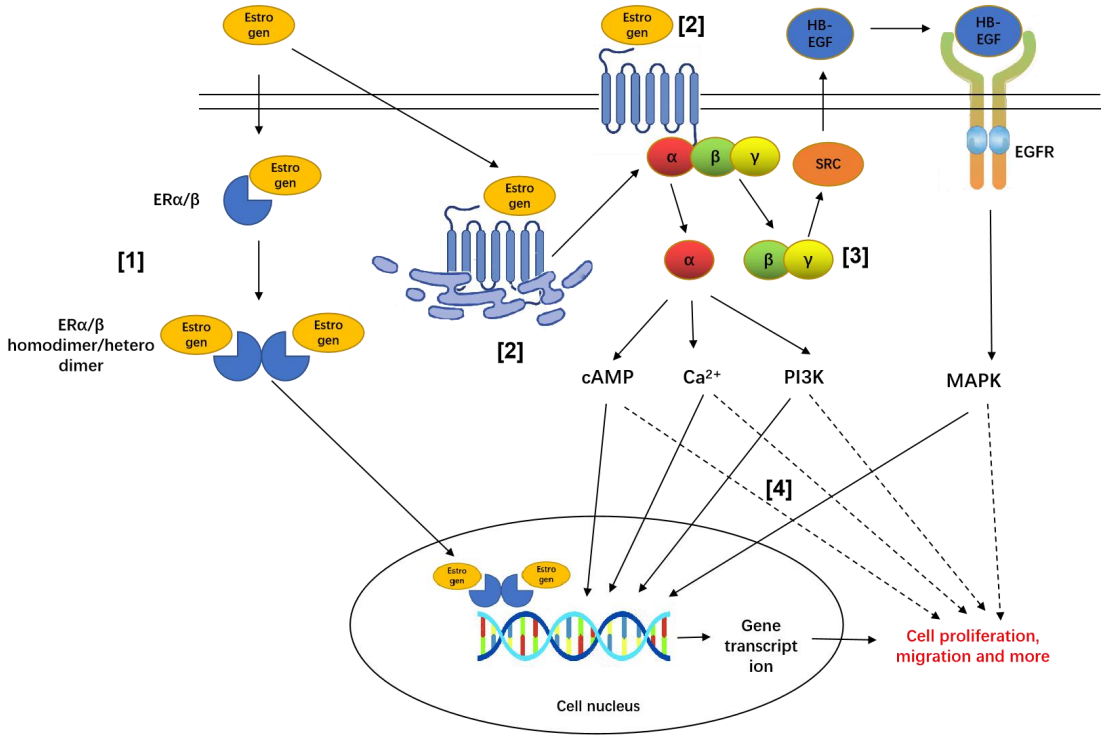

Figure 1.4 Cellular signaling mechanisms of GPER

[1] The classic estrogen receptors ERα and ERβ primarily exist in the cytoplasm and nucleus of cells, and upon dimerization, interact with estrogen response elements (ERE), driving genomic responses.

[2] GPER was found in the endoplasmic reticulum and cell membrane. Unlike the nuclear estrogen receptors, GPER signaling occurs through signaling cascades. GPER activation induces heterotrimer G protein Gαβγ dissociation. The Gα-subunit then leads to the activation of cAMP, PI3K and calcium signaling pathway.

[3] Gβγ-subunit and Src family kinase-dependent intracellular signals transactivate the epidermal growth factor receptor (EGFR), leading to the release of heparin-binding epidermal growth factor-like growth factor (HB-EGF) from the cell surface. The released, active HB-EGF then binds to the EGFR, initiating downstream activation of the MAPK pathways.

[4] MAPK, cAMP, PI3K and calcium signaling pathway can induce nongenomic effects (indicated by dotted arrows), or genomic effects regulating gene transcription (indicated by solid arrows), finally leading to cell proliferation, migration and more.

1.3.3 GPER and kidney

GPER expression has been detected in various renal cell types, including renal tubular and epithelial cells. Specifically, GPER has been found in the cortical epithelia [78], brush border of proximal tubules [79], and distal convoluted tubule [78].

Different studies confirmed that GPER exerts renoprotective effects through

various mechanisms, including reducing oxidative stress, renal hypertrophy, and glomerular permeability [74]. GPER activation inhibits podocyte apoptosis by decreasing ROS production, highlighting its anti-apoptotic effects [80]. Similarly, G1 treatment has been shown to enhance the activity of superoxide dismutase and reduce the levels of malondialdehyde in renal epithelial cells that are subjected to methotrexate treatment [81]. These findings further emphasize the antioxidant properties associated with the activation of GPER.

Interestingly, nearly all studies consistently attribute nephroprotective abilities to GPER in various contexts or under different stimuli, whether it's AKI [82] or chronic kidney disease (CKD) [83]. Only Hutchens et al. reported that the genetic deletion of GPR30 (GPER) could reduce serum creatinine levels in male mice, indicating that GPER deficiency also possesses kidney-protective functions under certain specific conditions or stimuli [84]. Further research is warranted to unravel the intricate mechanisms underlying GPER mediated effects in the kidney and explore its potential as a therapeutic target for renal diseases.

1.3.4 GPER and cisplatin

Except for one article, previous studies have not reported on the involvement of GPER in cisplatin-induced nephrotoxicity. Gohar et al. investigated whether the deletion of the GPER1 gene would exacerbate cisplatin-induced AKI in male mice. The results indicated that the absence of GPER1 promoted renal cell apoptosis and attenuated the upregulation of heme oxygenase-1 induced by cisplatin, suggesting that GPER1 may play a role in cellular protection and anti-apoptosis in AKI [80]. However, this study also mentioned that the data obtained from their research did not support a role for GPER1 in cisplatin-induced renal injury because the deletion of the GPER1 gene did not alter relevant parameters of cisplatin-induced kidney damage, including serum urea, kidney injury molecular 1 (KIM1) and others.

It's worth noting that many aspects were not clearly explained by Gohar and

colleagues, including 1) conducting experiments only on male mice rather than female mice, and 2) not extensively examining whether GPER gene knockout would affect changes in the proximal tubules, which are the most severely affected areas in cisplatin-induced kidney injury.

Interestingly, not only are there limited studies addressing the involvement of GPER in cisplatin-induced nephrotoxicity or anticancer effects, but also the research on other GPCRs and their role in cisplatin-induced effects is scarce.

In the following some hypothesis on the potential interaction of cisplatin with GPER are summarized:

1) Direct Binding:

Babolmorad et al. demonstrated that cisplatin can directly bind to Toll-like receptor 4 (TLR4) to regulate cisplatin-induced ototoxicity [85]. While the specific molecular details and structural requirements for the binding between cisplatin and TLR4 require further investigation, Babolmorad et al. proposed that cisplatin may directly bind to TLR4, similar to the TLR4 agonist lipopolysaccharide [85]. Moreover, Pan et al. found that cisplatin binds to the C622 (Cysteine 622) residue in the glucocorticoid receptor (GR) that induces platinum resistance [86]. These discovery supports the possibility of cisplatin directly modulating other receptors.

2) Indirect Regulation:

Instead of directly binding to the GPER, cisplatin might indirectly impact GPER function through the activation of other processes, for example, cisplatin-induced DNA damage, ROS generation, or calcium signaling. These initial events in turn ultimately result in the onset of apoptosis or release of pro-inflammatory factors, including tumor necrosis factor α (TNF-α), interleukin 6 (IL-6), and others. Although the extent to which these pathways affect GPER remains unknown, various past studies still provide us with valuable reference points. For example, calmodulin [87] and CCL-18 (chemokine) [88] have been shown to regulate GPER-dependent signaling.

1.3.5 GPER and MAPK

Similar to most GPCRs, GPER activation leads to significant activation of MAPK in different cell types [89-91]. Compared to other members of the GPCR family, there is not a great deal of research on the specific mechanisms by which GPER activates MAPK. There are no studies reporting that the traditional G protein Gα can directly activate the MAPK signaling pathway. Instead, more reports show that the Gβγ complex can activate the Src-related tyrosine kinase family, leading to the transactivation of EGFR. Activated EGFR ultimately signals to MAPK (Figure 1.4) [92, 93].

In most cases, GPER activation-induced MAPK activation promotes proliferation and migration (Figure 1.4). Scaling et al. demonstrated that in *in vitro* experiments, estrogen (E2) can promote proliferation of the MCF10A cell line (non-tumorigenic human breast cells) by activating ERK through GPER [94].

However, the cellular outcomes following MAPK activation are context-dependent, varying across cell types, stimuli, and physiological conditions. Thus, the GPER-MAPK signaling cascade can also induces cell apoptosis. For example, Qiu et al. confirmed that the GPER agonist G1 promotes apoptosis and inhibits cell growth in hepatocellular carcinoma cells via the GPER/ERK signaling pathway [90], and Ding et al. demonstrated that estrogen-induced vascular smooth muscle cell apoptosis requires the GPER/ERK signaling cascade [95].

1.4 Nephrotoxicity research in the zebrafish embryo model

1.4.1 General strengths of the zebrafish model system

The zebrafish (*Danio rerio*) has emerged as a powerful model organism for scientific research across various disciplines [96]. Its unique characteristics

and advantages have contributed to its widespread use and popularity in biomedical, developmental, and genetic studies. Here, it's necessary to explain that Balon et al. first proposed a nomenclature for the different developmental stages of zebrafish [97]. Considering that our experiment only used zebrafish from 0-5 dpf, this stage is still referred to as the embryonic period. The embryonic period is defined as extending from fertilization until the developing fish is no longer dependent on the yolk for nutrition. The term 'embryo' generally refers to prehatching stages (0-2 dpf). The term 'eleutheroembryo' refers to posthatching embryonic stages, which some other researchers call 'sac fry' or 'yolk sac larvae' (2-5 dpf). However, the nomenclature has not been overly emphasized in past studies, and the term 'eleutheroembryo' is rarely used in current literature, with 'larva' being more common [98, 99]. In our study, to avoid unnecessary ambiguity, the term 'embryo' is used to encompass zebrafish from 0-5 dpf, and the term 'larvae' specifically refers to zebrafish from 2-5 dpf.

One of the major strengths of the zebrafish model is its high degree of genetic similarity to humans [100] (Figure 1.5). The zebrafish genome shares a significant level of conservation with the human genome, making it an invaluable tool for investigating human genetic disorders and disease mechanisms. Researchers can easily manipulate zebrafish genes using techniques such as gene knockout, knockdown, and transgenesis, allowing for the study of gene function and the modeling of human diseases [101].

Another advantage of zebrafish is their external and rapid development (Figure 1.5). Zebrafish embryos are transparent, enabling researchers to directly observe and study embryonic development in real-time [102]. This transparency, combined with the external development, facilitates the visualization and tracking of organogenesis, tissue interactions, and cellular behavior during different stages of embryogenesis. This feature has been particularly useful in studying early embryonic development and organ formation.

Zebrafish also possess a remarkable regenerative capacity, making them an excellent model for studying tissue repair and regeneration [103] (Figure 1.5). They can regenerate various organs, including the heart [104], spinal cord [105], and fins [106]. By studying the regenerative processes in zebrafish, researchers can gain insights into the cellular and molecular mechanisms underlying tissue regeneration, which could have implications for regenerative medicine and therapies in humans.

The large clutch size of zebrafish is another advantageous characteristic (Figure 1.5). Zebrafish produce a large number of offspring in each mating, resulting in hundreds of embryos. This abundance of embryos allows for high-throughput experimental approaches, such as genetic [107] and chemical screens [108], which can identify novel genes, pathways, and drug candidates involved in various biological processes and diseases.

Zebrafish are also amenable to pharmacological studies (Figure 1.5). Their small size and external development make them suitable for drug administration and screening [109]. Researchers can test the efficacy and toxicity of potential drug candidates in zebrafish models, providing valuable insights into drug mechanisms and safety profiles.

In addition to these advantages, zebrafish are relatively easy and cost-effective to maintain in the laboratory [110] (Figure 1.5). They have a short generation time and require minimal space and resources compared to other vertebrate model organisms. This accessibility and affordability make zebrafish an attractive model for both academic and industrial research.

In conclusion, the zebrafish model system offers a wide range of strengths and advantages for scientific research. Its genetic similarity to humans, external and rapid development, regenerative capacity, large clutch size, and suitability for pharmacological studies make it a versatile and valuable tool for investigating various biological processes, genetic diseases, and potential therapeutics. The zebrafish model continues to make significant contributions to our understanding of human biology and disease, and it holds great promise

for future discoveries and advancements in biomedical research.

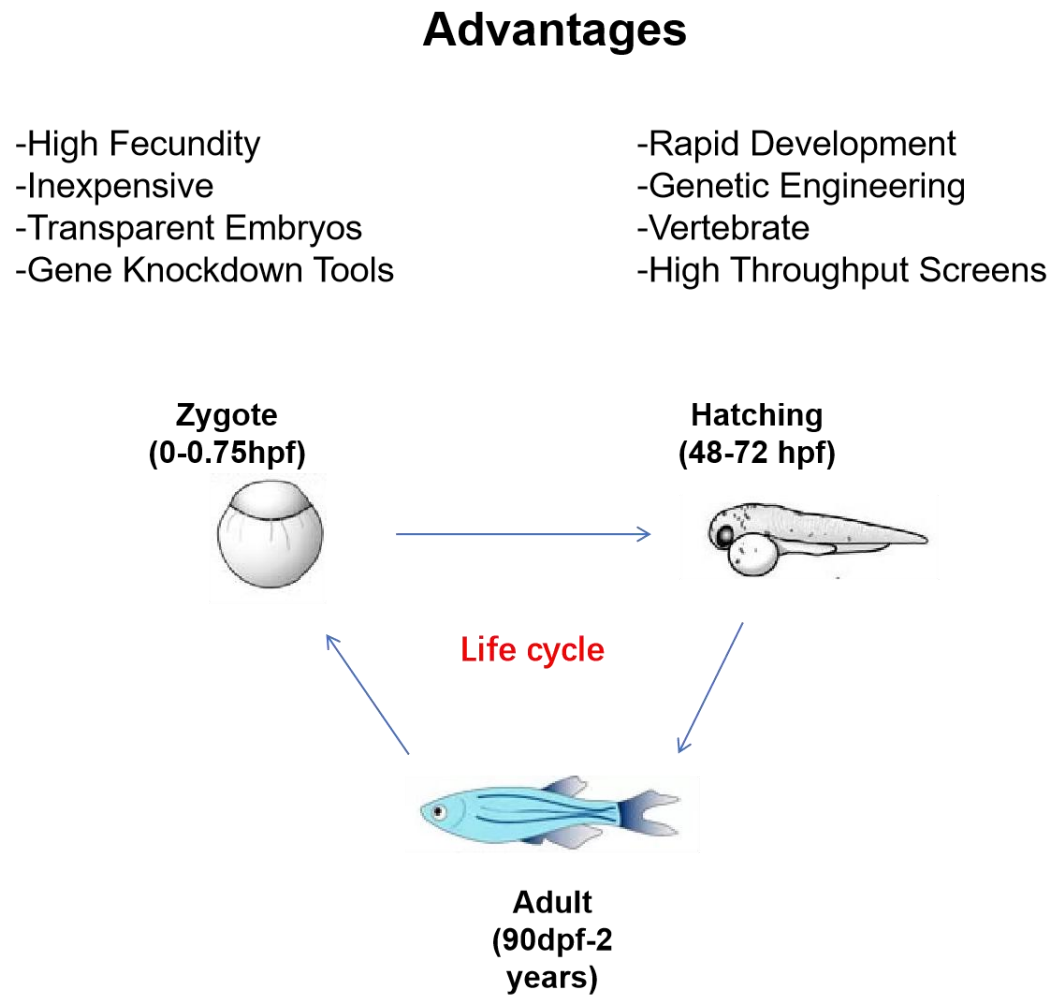

Figure 1.5 Zebrafish Model System
Schematic illustrating the advantages of zebrafish as a model system.

1.4.2 Conservation of kidney development, structure and function in zebrafish larvae and mammals

Kidney development in humans undergoes three distinct stages characterized by the appearance of the pronephros, mesonephros, and metanephros [111]. The first two structures are transient in mammals and eventually only the metanephros persists throughout life. The pronephros is the functional kidney during embryonic development of lower vertebrates such as amphibians and fish, and is later replaced by the mesonephros as the functional kidney.

While the overall complexity of the human kidney far exceeds that of zebrafish,

the nephron is the structural and functional unit of all kidney types. Nephron development involves four sequential stages: A) induction of the intermediate mesoderm to form the renal primordium, B) epithelialization and growth of the renal tubules, C) specialization of the nephron into distinct segments, and D) vascularization of the nephron for blood filtration [112].

The nephron is divided into three parts: 1) the glomerulus, which filters blood; 2) the tubules, which absorb and secrete solutes; and 3) the collecting ducts, which collect and excrete waste and metabolic materials [113]. The tubular epithelium is divided into different segments to perform specific functions. The zebrafish pronephros segmental organization resembles that of the mammalian metanephros, as shown in Figure 1.6. The zebrafish pronephric tubules are divided into proximal tubule, distal tubules which resemble the segmentation pattern of mammalian metanephric nephrons (Figure 1.6). One of the main differences between zebrafish and mammalian nephrons is the absence of the loop of Henle (intermediate tubule) in zebrafish, which acts as a countercurrent multiplier to generate a medullary osmotic gradient for water conservation [114]. This segment would serve no purpose in zebrafish as it is a freshwater fish. Each segment has distinct cell types and segment-specific gene expression, which are conserved in vertebrates [115].

Apart from the structural conservation, zebrafish larval and human nephron also exhibit functional similarities. Zebrafish possess one pair of pronephros, which starts to form after 12 hpf and becomes fully functional by 48 hpf [116]. By 48 hpf, the larval glomerulus already contains specialized cells, such as supporting mesangial cells and podocytes, that aid in blood filtration. The capillaries in the glomerulus have fenestrations and are leaky, allowing components from the plasma to be filtered into the renal corpuscular filtrate. Ions and water are reabsorbed from the renal corpuscular filtrate as it passes through the tubules composed of polarized epithelium. The remaining filtrate then enters the ducts for final processing [113].

In Europe, in line with recommendations of the European Union Legislation

(EU Directive 2010/63/EU), research on zebrafish larvae is permitted without any additional approval by regulatory agencies up to 5 dpf [117]. The pronephros development is fully established [113]. Considering the highly conserved and similar functional and structural characteristics between zebrafish larvae and human nephron, zebrafish larvae fulfill the basic requirements for an alternative model in nephrotoxicity testing.

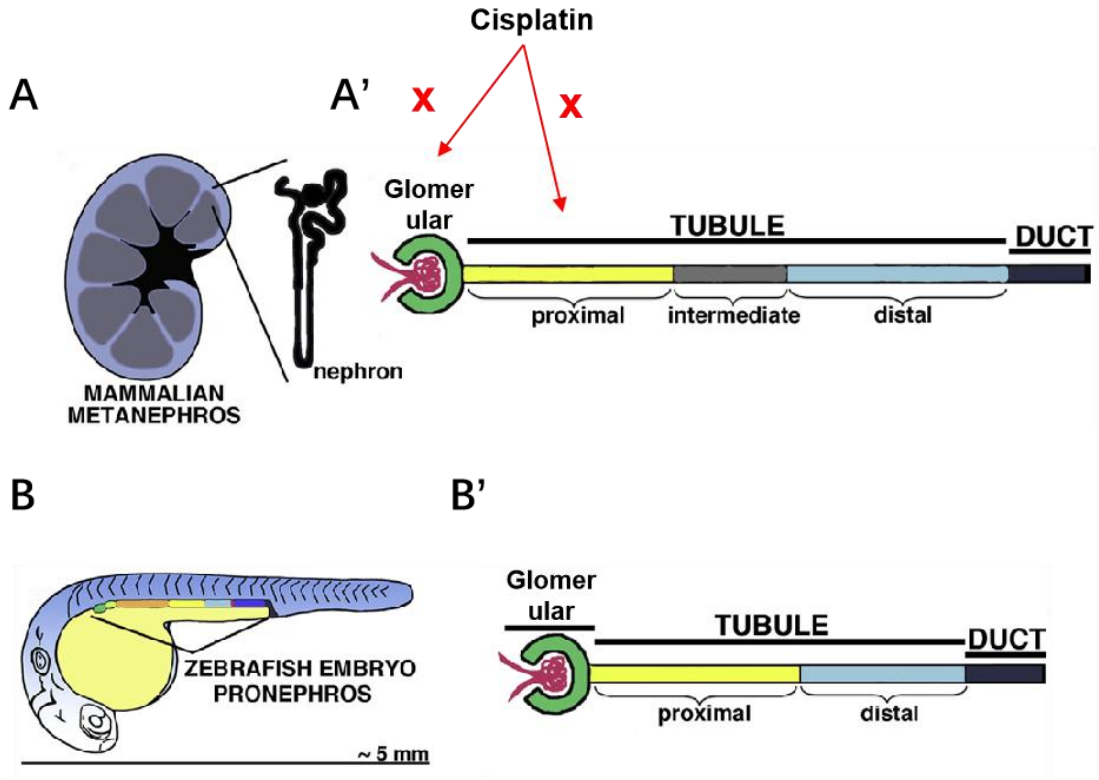

Figure 1.6 The structure of the kidneys varies among vertebrates, but the composition of nephron segments is broadly conserved

Figure is modified from McCampbell et al [118].

(A) The mammalian kidney is composed of a variable number of nephrons, ranging from thousands to millions. Each nephron is a convoluted tubule with a complex arrangement of epithelial cells.

(A') After straightening the mammalian nephron, it primarily consists of the glomerulus (green), proximal tubule (yellow), intermediate tubule (grey), distal tubule (light blue), and collecting duct (black).

(B) At 2 days post-fertilization (dpf), zebrafish embryos develop linear pronephrons, consisting of a pair of nephrons. The schematic diagram in lateral view illustrates a single nephron.

(B') The zebrafish pronephric nephron, consisting of the glomerulus (green), proximal tubule (yellow), distal tubule (light blue), and collecting duct (black).

As cisplatin primarily damages the glomerular and proximal tubule regions (marked by an ✕) of the nephron, which are conserved in zebrafish larvae and mammals (A'). zebrafish

larvae possess the full potential to serve as a model for studying cisplatin-induced nephrotoxicity.

1.4.3 Zebrafish larval model in nephrotoxicity research

Previous research confirmed that various nephrotoxins, including chemotherapy drugs (cisplatin [119] and adriamycin [120]) and aminoglycoside antibiotics (gentamicin [121] and puromycin [122]), can induce renal cell death through different mechanisms in both humans and rodent animal models, ultimately leading to varying degrees of kidney injury. Over the past two decades, the zebrafish model gradually evoked the interest of researchers, and both adult and larval zebrafish models have become essential tools for assessing different nephrotoxins.

In previous studies, zebrafish embryos and larvae have been considered as rapid screening models for assessing nephrotoxicity [123]. However, when it comes to studying drug-induced nephrotoxicity mechanisms, researchers tend to favor the use of adult zebrafish, as it allows for easier access to organ- or tissue-specific responses [124]. Nevertheless, in recent years, with the advancement of various biochemical and transgenic technologies, several pioneering research groups have successfully established zebrafish larvae as a robust model for studying nephrotoxicity. Utilizing zebrafish larvae model to assess various nephrotoxins, including chemotherapy drugs (cisplatin [125] and adriamycin [126]) and aminoglycoside antibiotics (gentamicin [118] and puromycin [127]), has highlighted the significant advantages of this approach.

1). Different nephrotoxins induce varying degrees of edema in zebrafish larvae, including cardiac edema, yolk sac edema, and eye edema, cerebral edema, kidney edema [128], among others [129].

2). Just as demonstrated in Section 1.4.2, the patterns of segments and cellular compositions in zebrafish kidney nephrons are more accessible and easier to observe compared to those in humans and mice [130, 131].

3). Some parameters related to kidney injury still apply to zebrafish larvae,

such as glomerulus filtration rate [129], proteinuria [132], and kidney injury markers [133].

In this context, I chose to use gentamicin as an example to elucidate the methods and endpoints employed in nephrotoxicity research using the zebrafish larval model. Gentamicin is an aminoglycoside antibiotic that is widely used as a model drug to investigate nephrotoxicity.

1. Edema formation

McCampbell et al. injected 2.5 mg/ml of gentamicin into zebrafish embryos at 48 hpf and observed notable morphological changes in zebrafish larvae [118]. At 24 hours post injection (hpi), the yolk sac of the embryo exhibited a darkened color, accompanied by some pericardial edema, consistent with the renal insufficiency phenotype previously observed in other studies [125, 134]. By 48 hpi, the darkening of the yolk sac intensified, and the edema increased to a moderate level. Severe pericardial edema and body curvature were observed in embryos at 72 hpi.

In summary, this progressive phenotype begins with the formation of pericardial edema and gradually progresses to yolk sac edema formation, ultimately resulting in excessive fluid accumulation and body curvature. These morphological changes in zebrafish are not exclusively triggered by gentamicin but are also observed in response to other nephrotoxic agents, such as aristolochic acid [135] or puromycin aminonucleoside [136]. Thus, formation of edema serves as a read-out of nephrotoxicity induced by nephrotoxic drugs. Particularly in the study of nephrotoxicity, zebrafish models offer a more convenient and rapid assessment of morphological changes compared to other rodent models.

2. Mortality

Although the injuries caused by gentamicin are similar in different species, several research groups have now reported that gentamicin treatment leads to the death of zebrafish embryos [98, 125]. McCampbell et al. also found, through further testing of different gentamicin doses, that all embryos that

developed edema were unable to survive [118]. It seems that gentamicin exposure causes severe damage to the nephron tubules, from which the embryos cannot recover. Considering that embryonic zebrafish have only two nephrons, exposure to gentamicin easily results in damage to both nephrons, complete loss of renal function, and eventually embryonic death.

This high mortality in zebrafish resulting from nephrotoxicity is not limited to gentamicin but is also observed with other nephrotoxic substances, such as the phytochemical aristolochic acid (AA), cadmium chloride ($CdCl_2$), the mycotoxin ochratoxin A (OTA) and potassium bromate ($KBrO_3$) [99]. Compared to rodent models, which often require long-term systemic administration to induce nephrotoxicity-related deaths, zebrafish embryos experience high mortality within a short period of days. Alongside the formation of edema, this high mortality provides an additional marker of severe nephrotoxicity.

3. Kidney reporter lines

Over the past 20 years, several transgenic zebrafish lines have been established by researchers to study kidney development and function. These transgenic lines often express fluorescent proteins to localize kidney specific markers, allowing researchers to visualize and track the development and morphology of kidney structures in real-time. According to the zebrafish kidney development atlas, the first established transgenic zebrafish lines for kidney research were Tg(*wt1b*:EGFP), Tg(*wt1a*:EGFP) [137], and Tg(*pax2a*:GFP) [138]. However, in these transgenic fish lines, at 3 dpf, the fluorescent signals are not limited to the pronephros region but are also expressed in other organs. For example, at 3 dpf, Tg(*wt1b*:EGFP) exhibits strong signals in the exocrine pancreas. In recent years, Tg(*cdh17*:GFP) [139] and Tg(*gtshβ*:GFP) [140] have become available as reporter lines with specific fluorescence expression in the pronephros region between 2 dpf and 5 dpf in early zebrafish embryos.

4. Kidney injury markers

Unlike in clinical and other animal models, certain commonly used kidney injury indices, such as serum creatinine and blood urea nitrogen, cannot be

used in zebrafish larval models. However, several kidney injury markers can be measured or observed to evaluate the extent of kidney damage or study the effects of different treatments or conditions on the zebrafish kidney, including kidney injury molecule 1 (*kim1*) [141, 142], clusterin (*clu*) [143], and connective tissue growth factor (*ctgf*) [144]. Among these markers, *kim1* is the most extensively studied kidney injury marker in different models. *kim1* is a transmembrane protein expressed in the proximal tubules of the zebrafish kidney. Its expression is upregulated in response to kidney injury, making it a valuable marker for detecting and assessing kidney damage.

5. Histopathological changes

Histological sectioning is a common technique to study internal structures and tissues at a microscopic level. Combined with the commonly used biochemical methods, such as in situ hybridization (ISH) and immunohistochemistry (IHC), histological sectioning allows for specific visualization of tissue or organ pathological changes at the cellular level and by employing different antibodies or staining techniques also at the molecular level. Cosentino et al. and Bauer et al. performed immunostaining using ATP1A1 (α6f) antibody [98] or hematoxylin and eosin (H&E) staining [99], respectively. The sections revealed gentamicin mediated injury, characterized by flattening and loss of the pronephric tubule brush border, tubular swelling, and the presence of debris in the tubular lumen.

1.5 Aims of this thesis

Nephrotoxicity is a major problem associated with the use of cisplatin, a potent chemotherapeutic drug widely used against various cancers. Unfortunately, up to one third of patients undergoing cisplatin therapy experience severe side effects, particularly in normal non-target tissues, including the kidneys. To enhance the clinical benefits of cisplatin treatment, it is crucial to prioritize the development of innovative strategies aimed at preventing nephrotoxicity.

Our group’s previous work discovered that inhibiting the function of G

protein-coupled estrogen receptor (GPER) effectively suppresses cisplatin-induced cancer cell death. As mentioned earlier, the similarities between cisplatin-induced nephrotoxicity and its anticancer effects suggest the possibility of GPER involving in regulating cisplatin-induced nephrotoxicity.

Based on the conserved nephron structure and physiological similarities to humans, zebrafish larvae have been chosen as the animal model in this study to investigate the mechanisms underlying cisplatin-induced nephrotoxicity. There have been limited studies on cisplatin-induced nephrotoxicity in zebrafish larvae, and specific methods for reference are lacking. The specific objectives of this project are as follows:

1. Establishment of a zebrafish larval model for cisplatin-induced nephrotoxicity.
2. Investigation of the potential mechanisms of cisplatin-induced nephrotoxicity, particularly examining the role of GPER.

By employing the zebrafish model, we aimed to gain a better understanding of the cellular and molecular events associated with cisplatin-induced nephrotoxicity, with a specific focus on the potential involvement of GPER. This research may provide valuable insights into the development of novel therapeutic targets to mitigate kidney damage associated with cisplatin treatment.

2 Materials and Methods

2.1 Materials

2.1.1 Solutions and buffers

Table 2.1 Composition of the different solutions and buffers

Name	Purpose	Recipe
60x E3 medium (stock solution)	Zebrafish culture	5 mM NaCl, 0.17 mM KCl, 10 mM HEPES, 0.33 mM $MgSO_4$, 0.33 mM $CaCl_2$
10x Phosphate-buffered saline (PBS)	Washing	1.37 M NaCl, 27 mM KCl, 100 mM Na_2HPO_4, 18 mM KH_2PO_4
PBS with Tween-20 (PTW)	Washing	1x PBS, 0.1% Tween-20 (v/v)
Ringer's buffer	Washing	125 mM NaCl, 5 mM KCl, 0.8 mM Na_2HPO_4, 1.5 mM $CaCl_2$ (pH ~ 7.4)
4% paraformaldehyde (PFA) solution	Fixation	1x PBS, 4% PFA (w/v) (pH ~ 7.2)
1.6% agarose gel	Microinjection	1.6% UltraPure low melting point agarose (w/v), 1x E3 medium
20x SSC buffer (stock solution)	ISH	3 M NaCl, 0.3 M sodium citrate
Blocking buffer (ISH)	ISH	100 mM Tris pH9.5, 50 mM $MgCl_2$, 100 mM NaCl, 0.1% Tween-20
Hybridization buffer	ISH	50% formamide (v/v), 5x SSC buffer, 500 µg/ml yeast RNA, 50 µg/ml heparin, 5mM ethylenediaminetetraacetic acid (EDTA), 0.1% Tween-20 (v/v)
Staining buffer	ISH	100 mM Tris-HCl pH 9.5, 50 mM MgCl2, 100 mM NaCl, 0.1% Tween-20 (v/v)
Wash buffer 1	ISH	50% formamide (v/v), 50% 2x SSC buffer, 0.1% Tween-20 (v/v)
Wash buffer 2	ISH	2x SSC buffer, 0.1% Tween-20 (v/v)
Wash buffer 3	ISH	0.2x SSC buffer, 0.1% Tween-20 (v/v)
Wash buffer 4	ISH	33.3% PTW, 66.7% 0.2x SSC buffer, 0.1% Tween-20 (v/v)
Wash buffer 5	ISH	66.7% PTW, 33.3% 0.2x SSC buffer, 0.1% Tween-20 (v/v)
Bleaching buffer	ISH and IHC	1.79 mM KOH, 3% H_2O_2 (v/v)

Proteinase K solution	ISH and IHC	1x PTW, 10 µg/ml proteinase K
PBT	IHC	1x PBS, 1% Triton (v/v)
Dent's fixative	IHC	80% methanol, 20% dimethyl sulfoxide (DMSO)
RIPA buffer	WB	50 mM Tris pH 7.5, 150 mM NaCl, 1% NP-40 lysis buffer, 0.5% sodium deoxycholate (w/v), 5 mM phenylmethylsulfonyl fluoride (PMSF)
Loading buffer	WB	4% sodium dodecyl sulfate (SDS) (v/v), 10% 2-mercaptoethanol (v/v), 20% glycerol (v/v), 0.004% bromophenol blue (w/v), 0.125 M Tris-HCl (pH ~ 6.8)
10% Separating gel (10 ml)	WB	4 ml H_2O, 3.3 ml 30% acrylamide mix, 2.5 ml 1M Tris (pH 8.8), 0.1 ml 10% SDS, 0.1 ml 10% ammonium persulphate solution (APS), 10 µl tetramethylethylenediamine (TEMED)
5% Stacking gel (10 ml)	WB	6.8 ml H2O, 1.7 ml 30% acrylamide mix, 1.25 ml 1 M Tris (pH 6.8), 0.1 ml 10% SDS, 0.1 ml 10% APS, 10 µl TEMED
Running Buffer	WB	25 mM Tris, 190 mM glycine, 0.1% SDS
Transfer buffer	WB	25 mM Tris, 190 mM glycine, 20% methanol, 0.1% SDS
10 x Tris-buffered saline (TBS) (stock solution)	WB	1 M Tris-HCl, 5 M NaCl (pH ~ 7.4)
TBS with with Tween-20 (TBST)	WB	1x TBS, 0.1% Tween-20 (v/v)
Blocking buffer (WB)	WB	1x TBST, 5% skim milk powder / bovine serum albumin (w/v)

2.1.3 Commercial reagents

Table 2.2 Commercial reagents

Name	Purpose	Company	Catalog number
qPCR kits	RT-qPCR	Promega	A6010
Maxima first strand cDNA synthesis kit for RT-qPCR	cDNA synthesis	ThermoFisher	K1641
SacI-HF restriction enzyme	ISH	NEB	R3156S
SacII restriction enzyme	ISH	NEB	R0157S
T7 RNA polymerase	ISH	Promega	P2075
RNasin ribonuclease inhibitor	ISH	Promega	N2511
SP6 RNA Polymerase	ISH	Promega	P1085
GeneJET gel extraction kit	ISH	ThermoFisher	K0691

Plasmid midi kit	ISH	QIAGEN	12145
XL1-blue competent cells	ISH	Agilent	200249
Digoxigenin RNA labeling mix	ISH	Roche	11277073910
Anti-digoxigenin-AP, fab fragments	ISH	Roche	11093274910
pGEM-T easy vector systems	ISH	Promega	A1360
ProbeQuant G-50 micro columns	ISH	Cytiva	GE28-9034-08
Anti-ATP1A1 primary antibody	IHC	DSHB	α6f
Anti-Vinculin primary antibody	WB	Sigma	V9131
Anti-p53 primary antibody	WB	Genetex	GTX12813
Phospho-P44/42 MAPK (Erk1/2) (Thr202/Tyr204) primary antibody	WB	Cell Signaling Technology	9101
Anti-phospho-p53 (p-p53) (Ser15) primary antibody	WB	Cell Signaling Technology	9284
Anti-phospho-p38 (p-p38) (Thr180/Tyr182) primary antibody	WB	Cell Signaling Technology	4511
Anti-phospho-H2A.X (p-H2AX) (Ser139) primary antibody	WB	Cell Signaling Technology	2577
UltraPure low melting point agarose	Microinjection	ThermoFisher	16520100
Cisplatin	Microinjection	Cayman Chemical	13119
Carboplatin	Microinjection	Cayman Chemical	13112
Oxaliplatin	Microinjection	Cayman Chemical	13106
G36	Incubation	Tocris Bioscience	4759
G15	Incubation	Tocris Bioscience	3678
TRIzol	RNA extraction	ThermoFisher	15596026
Diethyl pyrocarbonate (DEPC) water	RNA extraction	ThermoFisher	AM9906
GoTaq G2 DNA polymerase	PCR	Promega.	M7841
5x green GoTaq® reaction buffer	PCR	Promega.	M7911
Q-PCR clear seal adhesive film	RT-qPCR	Steinbrenner Laborsysteme	SL-AM 0558
96-well PCR platte	RT-qPCR	Biozym	710888
DNase	ISH	Roche	04716728001
GeneJET RNA purification kit	ISH	ThermoFisher	K0732
Proteinase K	ISH and IHC	NEB	P8107S
PageRuler™ plus prestained protein ladder	WB	ThermoFisher	26619
Anti-mouse-HRP second antibody	WB	DAKO	P0447

Anti-rabbit-HRP secondary antibody	WB	DAKO	P0448
Anti-goat-HRP secondary antibody	WB	DAKO	P04489
Anti-mouse-fluorescent 488 secondary antibody	IHC	Abcam	ab150113
Epon-812 (Glycid ether 100)	Histologic section	Serva	21045
Toluidine blue	Histologic section	Sigma	198151
Dodecenylsuccinic acid anhydride (DDSA)	Histologic section	Serva	20755
Methylenacid anhydride (MNA)	Histologic section	Serva	29452
2,4,6-tris(dimethyl-aminomethyl)phenol (DMP 30)	Histologic section	Serva	36975
Dextran, fluorescein, 70,000 MW, anionic	Microinjection	ThermoFisher	D1823
Dextran, rhodamine B, 10,000 MW, neutral	MIcroinjection	ThermoFisher	D1824
Q-VD-OPh	Incubation	MP Biomedicals	03OPH109-CF
PD98059	Incubation	Sigma	513000
U0126	Incubation	Cell Signaling Technology	9903
Gentamicin sulfate	Microinjection	Sigma	G1914
Polyvinylidene difluoride (PVDF) membrane	WB	Millipore	IPVH00010
SYTO-59 red fluorescent nucleic acid stain	Microinjection	ThermoFisher	S11341
NP-40 lysis buffer	WB	ThermoFisher	J60766.AP
PCR tubes	PCR	Eppendorf	EP0030124359

2.1.3 Instruments and equipment

Incubator for fish embryos (Heraeus, Germany)

Incubator for bacteria (Heraeus, Germany)

FemtoJet microinjector (Eppendorf, Germany)

Flaming-Brown Needle puller (Sutter Instruments, USA)

TCS SP8 confocal microscope (Leica, Germany)

Stereomicroscope SMZ645 (Nikon, Japan)

DM6 B Fluorescence LED Microscope (Leica, Germany)

NanoDrop ND-1000 (Peqlab, Germany)

Bio-analyzer 2100 (Agilent, USA)

PCR-Thermocycler Peqstar 96 HPL gradient (Peqlab, Germany)

ChemiDoc™ MP (Bio-Rad, USA)

RM2065 microtome (Leica, Germany)

Bioanalyzer 2100 (Agilent, USA)

2.1.4 Oligonucleotides

All oligonucleotides used in this thesis, were purchased from Metabion International AG and designed using the Blast tool (https://www.ncbi.nlm.nih.gov/tools/primer-blast/) and related literature.

Table 2.3 PCR primer sequences for ISH probes

Name	Accession number (Ensembl)	Sequence
fabp10a Forward	ENSDARG00000038439	5'-AGCTTCTCCAGAAAGCATGG-3'
fabp10a Reverse	ENSDARG00000038439	5'-AGTGATGGTGAAACGCTTCAG-'
cdh17 Forward	ENSDARG00000005112	5'-CAGGAAAAGGAGCCCGTAGG-3'
cdh17 Reverse	ENSDARG00000005112	5'-GGGATCCTTGGCTTCAGCTT-3'
podocin Forward	ENSDARG00000042850	5'-CAAGATCTGCCCGGATAAAG-3'
podocin Reverse	ENSDARG00000042850	5'-CAGCTCTGGAGGAAGATTG-3'
nephrin Forward	ENSDARG00000060758	5'-GCGATACAGCATGACAGGAG-3'
nephrin Reverse	ENSDARG00000060758	5'-TTCAAAGGAGCCCAGTAACG-3'
slc20a1a Forward	ENSDARG00000020114	5'-GCTGAGCGTTCATTGTTCAC-3'
slc20a1a Reverse	ENSDARG00000020114	5'-TCCCGAACGGATGGTTTCGC-3'
trpm7 Forward	ENSDARG00000036232	5'-AAGTACTCGGAGGTGTCGGA-3'
trpm7 Reverse	ENSDARG00000036232	5'-GACCAATGCGTGCGTGTATC-3'

Table 2.4 PCR primer sequences for qRT-PCR

Name	Accession number (Ensembl)	Sequence
β-actin Forward	ENSDARG00000037746	5'-CGAGCTGTCTTCCCATCCA -3'
β-actin Reverse	ENSDARG00000037746	5'- ACCAACGTAGCTGTCTTTC-3'
kim1 Forward	ENSDARG00000040178	5'-TCTCCTGTTACTGTTGGCTTT-3'
kim1 Reverse	ENSDARG00000040178	5'-ATGCCACTGTTCGTATTCGCT-3'

clu Forward	ENSDARG00000010434	5'-AGAGGATGCTGTCGGAGATG-3'
clu Reverse	ENSDARG00000010434	5'-CCTCGCTGAGCTTCTCCTT-3'
ctgf Forward	ENSDARG00000042934	5'-CTCCCCAAGTAACCGTCGTA-3'
ctgf Reverse	ENSDARG00000042934	5'-TCCACCAAACACACAAGTGG-3'
hmox1 Forward	ENSDARG00000027529	5'-GGACTTGGAGCACTTCTTCG-3'
hmox1 Reverse	ENSDARG00000027529	5'-GGACTGCTCTTGCCAATCTC-3'

Table 2.5 Morpholino sequences

Target gene	Sequence	Type	Reference
gper1	5'-ACATTGGTAGTCTGCTCCTCCATGC-3'	ATG	Chaturantabut et al. [145]
gper1	5'-GCTGCAACACCTGTTATAAGAGAAA-3'	Splice	Chaturantabut et al. [145]
p53	5'-GCGCCATTGCTTTGCAAGAATTG-3'	ATG	Weger et al. [146]
control	5'-CCTCTTACCTCAGTTACAATTTATA-3'	Random control	Finckbeiner et al. [147]

Table 2.6 PCR primer sequences to assess the efficacy to block splicing by the morpholino

Name	Sequence
gper1 Ex1 Forward	5'-ACTTTGTCATCGTTGAAGGT-3'
gper1 Int Forward	5'-TGTCAGATCCACAACAGAGA-3'
gper1 Ex2 Reverse	5'-CATTGACGTGTCTTTACTGCGCCCTCATC-3'

2.1.5 Zebrafish lines

Table 2.7 Zebrafish lines

Name	Allele	Type	Reference
AB ZIRC KA		Wild-Type	Hansjosten et al [148]
Tg(*mpeg1*:GFP)	gl22Tg	Transgenic insertion	Hayashi et al. [149]
p53 -/-	ka801	Small deletion	Elabd et al. [150]

2.2 Methods

2.2.1 Zebrafish husbandry and maintenance

Fish housing and husbandry followed the recommendations by the zebrafish book [151]. The fish were maintained in a recirculation system at 28ºC with a

14 hours light and 10 hours dark cycle [152]. They were fed a diet of commercial food and in-house hatched brine shrimp. To initiate breeding, male and female fish were separated using a grid and placed in a 1L laying cage containing recirculation system water. One or more pairs of fish were introduced into the cage. On the second day of cohabitation, the eggs would fall into a compartment below to prevent cannibalism by the parents. The collected eggs were then transferred to clean petri dishes and hatched in an incubator at 28°C.

Experiments were conducted using 2-5 days AB wild-type (WT), $p53^{-/-}$ and Tg*(mpeg1*:EGFP*)* zebrafish embryos (Table 2.7). It is worth mentioning here that the p53 -/- embryos used for the experiments are collected from the incross of homozygous mutant adults. They are maternal and zygotic homozygous mutants for p53, lacking all functional p53 protein. All animal experiments adhered to German animal protection standards and were approved by the Government of Baden-Württemberg, Regierungspräsidium Karlsruhe, Germany (Aktenzeichen 35-9185.64/BH KIT).

2.2.2 Microinjection

The zebrafish larvae at 2-3 dpf were anesthetized using 0.01% tricaine in E3 medium (Table 2.1). Under a stereomicroscope, the larvae were embedded in a drop of 1.2% UltraPure low melting point agarose (in E3 medium, 28°C) (Table 2.1) placed at the bottom of a Petri dish [153] (Figure 2.1). The samples were oriented with the injection side facing up and the Petri dish was placed on RT to allow the agarose to solidify for up to 5 minutes.

A microinjection needle was filled with a solution using a microloader tip and attached to a micromanipulator. The tip of the needle was carefully broken. Under the stereomicroscope, 10 nl different concentration cisplatin or 140 mM NaCl solution was pressure-injected into the pericardiac space using a FemtoJet express microinjector (Eppendorf, Germany) with low injection pressure (100-300 hPa) and a pulse duration of 0.5 - 1 second.

After the injection, E3 medium was added, and the agarose was carefully removed from the samples using a dissection needle. The larvae were then maintained in an incubator at 28°C.

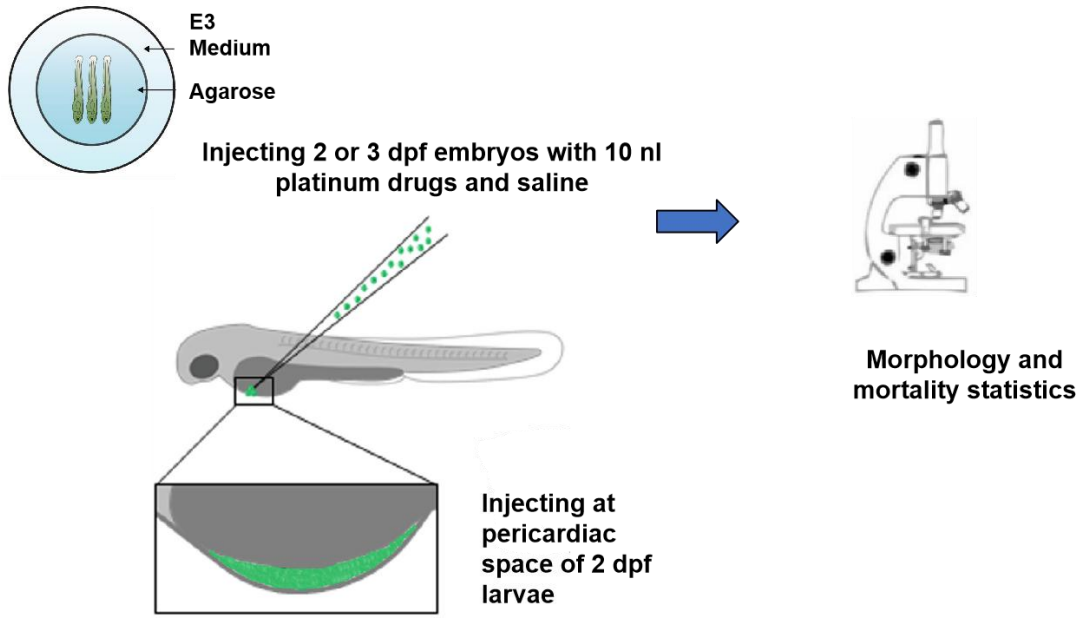

Figure 2.1 The microinjection method to research adverse effects of cisplatin in zebrafish embryos

2.2.3 Morpholino approach

Morpholino-based knockdown is a commonly used technique in various animal models, allowing researchers to investigate the functions of specific genes [154]. These knockdowns involve the use of chemically modified oligonucleotides called morpholinos. Morpholinos were designed to be 25 bases long and have a neutrally charged backbone, which differs from the phosphate backbone found in DNA. This modification makes morpholinos as uncharged molecules. When introduced into organisms or cells, morpholinos can selectively bind to the 5' untranslated region of mRNA, effectively blocking the translation of the targeted mRNA [155]. Additionally, morpholinos can also interfere with pre-mRNAs by binding to specific junctions and disrupting the splicing process [155]. In our experiment, the morpholinos stock solution was first diluted to a working concentration of 100 μM using sterile water. Then, 10 μl of the 100 μM morpholinos solution was mixed with 1 μl of 0.5% phenol red

to prepare the injection solution. Zebrafish embryos at the 0-4 cell stage (0-2 hpf) were collected, and 2 nl of the injection solution was injected into the yolk of each embryo. The injection efficiency was observed after 8 hours. If the mortality rate was around 15%, it was considered a successful injection, and the dead embryos were removed. If the mortality rate exceeded 15%, it indicated injection failure, and the injection needed to be repeated. After removing the dead embryos, the embryos were placed in fresh egg water and incubated at 28°C.

After successful injection of morpholinos, further validation of their effectiveness is necessary. In this study, four different morpholinos were mainly used: GPER ATG-blocking morpholino (GPER ATG-MO) [145], GPER splice site morpholino (GPER SP-MO) [145], p53 ATG-blocking morpholino (p53 ATG-MO) [146], and control morpholino (CON MO) [146]. The most straightforward method to evaluate the morpholinos is to examine the reduction in protein levels of the target gene's translation. This can be assessed using western blotting analysis to determine the effectiveness of the morpholinos. Given that we have suitable p53 antibody (Table 2.2), the efficacy of p53 ATG-MO can be evaluated using the western blotting method. As for the effectiveness of GPER ATG-MO and GPER SP-MO, since lacking appropriate GPER protein detecting antibodies, we can refer to the results from Chaturantabut et al. [145] and observe whether GPER MO injection leads to a reduction in liver size. The effect of GPER SP-MO could be verified by RT-PCR, and specific experimental methods can be referenced from Eisen et al. [156].

2.2.4 Quantitative real-time PCR

A. Total RNA extraction

A total of 30 zebrafish embryos were collected and placed in a 1.5 ml microcentrifuge tube, and excess water was carefully removed using a pipette. Next, 500 µl of TRIzol reagent (Table 2.2), containing phenol and to be used only under a fume hood, was immediately added to the tube containing the

embryos at RT.

The embryos were then lysed and homogenized by gently passing them through a syringe with approximately 20 strokes until the tissue was sufficiently disrupted. After homogenization, the samples were incubated for 5 minutes at RT.

To facilitate RNA extraction, 0.2 ml of chloroform was added to the sample, and the tube was gently rocked for 15 seconds to ensure proper mixing. The sample was then incubated for 2 minutes at RT before being centrifuged at 12,000 x g for 15 minutes at 4°C.

Following centrifugation, the mixture separated into a lower red phenol-chloroform phase, an interphase, and a colorless upper aqueous phase. The colorless upper aqueous phase was carefully transferred to a fresh 1.5 ml microfuge tube using a pipette with a 200 µl filter tip.

To precipitate the total RNA, 0.5 ml of isopropanol was added to the transferred aqueous phase. The sample was allowed to sit at RT for 10 minutes and was then centrifuged at 12,000 x g for 10 minutes at 4°C. The RNA formed a gel-like pellet at the bottom of the tube.

The supernatant was removed using a pipette with a 200 µl filter tip, and the RNA pellet was washed with 1 ml of 75% ethanol solution. After gentle mixing and centrifugation at 7500 x g for 5 minutes at 4°C, the ethanol was carefully removed using a pipette.

The tube was then inverted and allowed to dry for 10 minutes at RT. Subsequently, the pellet was resuspended in 30 µl of DEPC water (RNAase-free) (Table 2.2), and the sample was incubated at 55°C for 10 minutes. Finally, the concentration and total RNA integrity of the sample were assessed using a Bioanalyzer 2100 (Agilent, USA).

B. cDNA synthesis (first strand)

To perform the reaction, the steps below were followed in the indicated order, using a sterile and RNase-free tube placed on ice:

1. The components from Maxima first strand cDNA synthesis kit for RT-qPCR

(Table 2.2) were added in the following order to 0.2 ml PCR tubes (Table 2.2):

4 µl 5x Reaction Mix
4 µl Maxima Enzyme Mix
2 µg template RNA (all samples should have the same amount)
Add DEPC water (Table 2.2) to 20 µl
total volume 20 µl

2. The solutions were gently mixed and then the tubes were centrifuged at 1000 x g for 10 seconds to ensure that all droplets have settled to the bottom.

3. Mixtures were incubated for 10 minutes at 25°C, followed by 15 minutes at 50°C. If the RNA template amount exceeds 1 µg, the reaction time was extended to 30 minutes. Additionally, for RNA templates with high GC base pair content or significant secondary structure, the reaction temperature was increased to 65°C.

4. To stop the reaction, tubes were heated at 85°C for 5 minutes.

C. Quantitative real-time PCR

After obtaining the cDNA sample, the DNA was amplified according to an RT-PCR protocol based on Lubke et al [157].

1. A PCR reaction mix was prepared for each target gene, including cDNA template, PCR mix buffer from qPCR kits (Table 2.2), forward and reverse primers specific to the target gene, and double distilled water (ddH_2O). The final volume of mix solution was 20 µl.

2. Components were thoroughly mixed and tubes briefly centrifuged to collect the reaction mix at the bottom.

3. Set up of the RT-PCR plate:

A) RT-PCR reaction mix was dispensed into the appropriate wells of a 96-well PCR plate (Table 2.2). Note that detecting the expression level of a specific gene in the same sample requires at least three replicates to avoid the randomness introduced by pipetting.

B) Plates were sealed with an adhesive film (Table 2.2) to prevent evaporation.

4. Performance of RT-PCR:

A) Sealed PCR plates were placed in a thermal cycler machine.

B) The cycling parameters were defined based on the primer annealing temperature and the expected amplicon size. The typical PCR cycling steps were as follows:

Initial denaturation: 3-5 minutes at 94-95°C.

Denaturation: 15-30 seconds at 94-98°C.

Annealing: 15-30 seconds at the optimized primer annealing temperature (typically 55-65°C).

Extension: 30 seconds to 2 minutes at the recommended extension temperature (typically 68-72°C).

The denaturation, annealing, and extension steps were repeated for the specified number of cycles (usually 25-35 cycles). Final extension was done for 5-10 minutes at the extension temperature.

5. Data analysis:

A) Raw data collection: the raw qPCR data were obtained, which contained the quantification cycle (Cq) values for each sample. The Cq value represents the cycle number at which the fluorescence signal reaches a defined threshold.

B) Relative quantification: Use methods $2^{-\Delta\Delta CT}$ to compare target gene expression with reference genes or control conditions [158].

C) Statistical analysis: Analyze data using statistical methods ANOVA to determine significant differences.

2.2.5 Whole mount in situ hybridization

A. Synthesis and labeling of digoxigenin (DIG) RNA probes

The following antisense digoxigenin-labeled probes were used: *fabp10a* [159], *cdh17* [160], *podocin* [161], *nephrin* [162], *slc20a1a* [163] and *trpm7* [164]. Templates were amplified by PCR from zebrafish embryonic cDNA using the primer sequences indicated in Table 2.3. The templates obtained were inserted

into the pGEM-T Easy Vector System (Table 2.2) [157, 165], followed by transformation into XL1-Blue Competent Cells (Table 2.2), bacterial screening and amplification, plasmid extraction and purification through QIAGEN plasmid kits (Table 2.2) and subsequent sequencing. Purified circular plasmid vectors were cut with SacI or SacII the restriction enzymes according to the orientation of target gene insertion, purified by GeneJET gel extraction kit (Table 2.2), and collected as linearized plasmid DNA.

After successfully preparing the linearized plasmid DNA, the next step was to incubate them at 37°C for 30 minutes *in vitro* to synthesize antisense RNA using the following transcription mixture:

1 µg linearized plasmid DNA
4 µl 5x transcription buffer
1.5 µl ribonuclease inhibitor (Table 2.2)
2 µl DIG labelling mix (Table 2.2)
1.5 µl T7 or Sp6 RNA polymerase (Table 2.2)
Add DEPC water to 20 µl
total volume 20 µl

After the initial incubation, the DNA template underwent digestion by adding 2 µl of DNase and incubating for 15 minutes at 37°C. The digestion reaction was halted by adding 1 µl of 0.5M pH 8.0 EDTA. Synthesized RNA was purified by RNA purification kit (Table 2.2). Finally, purified RNA was diluted 1:1 with hybridization buffer for storage at -80°C.

B. Whole mount in situ hybridization

1. Fixation

- Zebrafish larvae were collected at the 3-4 dpf stage.
- Embryos or larvae were transferred into a 1.5 ml microcentrifuge tube containing 4% PFA solution (Table 2.1).
- Samples were fixed overnight at 4°C.

2. Dehydration

- Samples were washed three times with PTW (Table 2.1) for 10 minutes each to remove PFA.
- Samples were transferred into methanol and stored at -20°C until further use.

3. Rehydration

Embryos stored in 100% methanol are rehydrated by successive incubations in the following solutions:

- 75% methanol - 25% PTW for 5 min.
- 50% methanol - 50% PTW for 5 min.
- 25% methanol - 75% PTW for 5 min.
- 100% PTW for 4 x 5 min.

4. Pigment removal

- The PTW was removed and 0.5 ml bleaching buffer (Table 2.1) were added at RT for 30 min.
- The bleaching buffer was removed and 0.5 ml PTW were added to wash sample at RT for 10 min.

5. Proteinase K treatment

- The PTW was removed and 10 µg/ml proteinase K solution (Table 2.1) was added. The samples were incubated at RT for 40 minutes.
- Samples were rinsed twice with PTW for 5 minutes each to stop the proteinase K activity.

6. Prehybridization

- The PTW was removed and 400 µl hybridization buffer (Table 2.1) was added. The samples were incubated at 65°C for 1 hour.

7. Hybridization

- A hybridization solution containing a 1:250 dilution of the labeled RNA probe stock solution was prepared.
- The prehybridization solution was removed from the samples and replaced with the hybridization solution containing the RNA probe.
- Samples were incubated overnight in a metal heating bath at 65°C (hybridization temperature).

8. Post-hybridization washes

- The hybridization solution was removed. Two washes of 30 minutes each in wash buffer 1 (Table 2.1) at 65°C.

- The wash buffer 1 was removed. 15 minutes wash in wash buffer 2 (Table 2.1) at 65°C.

- The wash buffer 2 was removed. Two washes of 30 minutes each in wash buffer 3 (Table 2.1) at RT.

- The wash buffer 3 was removed. 15 minutes wash in wash buffer 4 (Table 2.1) at RT.

- The wash buffer 4 was removed. 15 minutes wash in wash buffer 5 (Table 2.1) at RT.

- The wash buffer 5 was removed. Two washes of 15 minutes wash in PTW at RT.

9. Antibody incubation

- The PTW was removed and samples were incubated overnight in secondary antibody solution (anti-digoxigenin-AP (alkaline phosphatase) antibody (Table 2.2) solution diluted at 1/1000 in blocking buffer (ISH)) at RT.

- Samples were incubated overnight at 4°C.

10. Washes

- The blocking buffer (ISH) with antibody was removed. Four washes of 30 minutes each in PTW at RT.

- The PTW was removed. Two washes of 5 minutes each in staining buffer (Table 2.1).

11. Chemical color development

- The staining buffer was removed and the color development solution was prepared using the following mixture:

225 µl NBT (50 mg/ml)

175 µl BCIP (50 mg/ml)

Add staining buffer to 50 ml
total volume 50 ml

The color development solution was stored in a dark space to keep it out of the light.

- Color development solution was added to the samples and incubated at RT (in the dark).
- The color development was monitored every 15 minutes.
- The color development was stopped by rinsing the samples with PTW.

12. Mounting

- Samples were transferred into glycerol and positioned in a suitable orientation.

13. Imaging and analysis

- Images of the stained samples were acquired by a fluorescence stereomicroscope SMZ645 (Leica, Germany).

2.2.6 Western blotting

The protocol for western blotting described in the zebrafish book was used [166], with some modifications to improve the detection of phosphorylated proteins.

1. Collection of samples

- 30 to 40 embryos at 3 dpf were transferred to 1.5 ml microcentrifuge tube.
- The egg water was removed and 500 ml Ringer's buffer was added to ensure proper preservation of the samples.

2. Preparation of samples

- The Ringer's buffer was removed and 200 µl of RIPA buffer (Table 2.1) was added.
- The samples were put on ice for 30 minutes.
- The samples were homogenized using an ultrasonic tip sonifier (frequency: 20kHz) for 30-60 seconds.

Notes:

A). The time interval between sonication was important for allowing the sample to cool during ultrasound steps. Based on personal experience, it was recommended to sonicate for 15 seconds, allow the sample to cool for 15 seconds, and to repeat this cycle 3-4 times.

B). The probe's tip was fully immersed in the solution while avoiding contact with the bottom of the test tube. Excessive sonication can result in visible foaming, indicating protein denaturation in the solution.

- The homogenized samples were put on ice for 30-60 min and 50 ul loading buffer (Table 2.1) were added to each tube.
- Samples were boiled 5 minutes in a 95°C metal bath.

Note: for proper detection of the phosphorylated protein, fresh samples were used to avoid repeated freezing and thawing. Best results were obtained when the sample was prepared and run on the gel at the same day.

3. Loading samples and running gels

- Prepare an SDS-PAGE gel using a 10% separating gel and a 5% stacking gel (Table 2.1). The specific gel preparation protocol refer to Mahmood et al. [167].
- Protein samples were loaded onto a polyacrylamide gel for electrophoresis, including a protein ladder (10 to 250 kilodalton (kDa)) as a molecular weight marker.
- The gel was run at a constant voltage of 150 V in running buffer (Table 2.1) until the protein bands sufficiently separated based on their molecular weights.

4. Transferring gels

Proteins were transferred from the gel to a 0.45 μm polyvinylidene difluoride (PVDF) membrane using a wet transfer system.

- A PVDF membrane was activated with methanol for 1 min and rinsed with transfer buffer before preparing the stack.
- The gel was immersed in transfer buffer (Table 2.2) and equilibrated for 10 minutes.
- A transfer sandwich was assembled as follows: sponge, three layers of filter

paper, gel, PVDF membrane, three layers of filter paper, sponge. After each layer was positioned, air bubbles were removed through a test tube. It was important that the gel was placed with the negative (black) side facing up.

- The transfer apparatus was placed in an ice bath, the sandwich was inserted (black side facing black side), transfer buffer was added, the electrodes were inserted, and the apparatus was run at 100 V for 1 hour.
- After the transfer was complete, the power source was disconnected and the hybridization membrane removed.

5. Immunoblotting

- The membrane was blocked with a blocking buffer (WB) (Table 2.1) at RT for 1 hour to prevent non-specific binding of antibodies.
- The membrane was incubated with primary antibodies directed against phospho-ERK (p-ERK), phospho-p53 (p-p53), phospho-p38 (p-p38), p53, phospho-H2AX (p-H2AX) (Table 2.2). Antibodies were diluted 1:2000 in blocking buffer (WB) and incubated overnight at 4°C with gentle agitation.
- The membrane was washed with TBST buffer (Table 2.1) 2 x 30 minutes at RT to remove unbound primary antibodies.
- The membrane was incubated with a secondary antibody (Table 2.1, the secondary antibody should match the host species of the primary antibody used for detection) conjugated to horseradish peroxidase (HRP) for detection. The secondary antibody was diluted 1:2000 in TBST buffer and incubated for 2 hours at RT with gentle agitation.
- The membrane was washed with TBST buffer 2 x 30 minutes at RT to remove unbound secondary antibodies.
- Detection and visualization were carried out using the chemiluminescence imaging system ChemiDoc^{TM} MP (Bio-Rad, USA) according to the manufacturer's instructions.
- Quantitative analysis of protein expression in western blotting bands was achieved through the analysis of optical density using the image processing

software ImageJ [168, 169].

2.2.7 Whole mount immunohistochemistry

1. Sample fixation

- 10 to 15 zebrafish larvae aged 4 or 5 dpf were selected and placed in a 1.5 ml microtube.
- The egg water was removed and 1 ml of Dent's fixative was added to fix the larvae overnight at RT.

Note: While previous studies commonly used 4% PFA solution for tissue fixation, it is not suitable for ATP1A1 (α6f) (Table 2.2) antibody detection. Therefore, Dent's solution (80% MeOH, 20% DMSO) was used for embryo fixation.

- Dent's fixative was replaced with 100% methanol and samples were stored at 4°C.

2. Rehydration

Embryos stored in 100% methanol are rehydrated by successive incubations in the following solutions:

- 75% methanol - 25% PTW for 5 min.
- 50% methanol - 50% PTW for 5 min.
- 25% methanol - 75% PTW for 5 min.
- 100% PTW for 4 x 5 min.

3. Removal of pigment

- PTW was removed and 0.5 ml bleaching solution (Table 2.1) was added at RT for 30 minutes.
- The bleaching solution was removed and samples were washed 2 x 5 minutes in PTW at RT.

4. Permeabilization

- PTW was removed and 0.5 ml PBT (Table 2.1) was added at RT for 10 min.
- Samples were washed 2 x 10 minutes in PTW at RT.

5. Primary antibody incubation

- Samples were incubated in blocking solution (IHC) (Table 2.1) for 1 hour at RT.

- A monoclonal Na+/K+ ATPase (Anti-ATP1A1) antibody (α6F) (Table 2.2) was used at a 1:25 dilution in blocking solution (IHC) and incubated overnight at 4°C.

6. Secondary antibody incubation

- Samples were washed 2 x 10 minutes in PTW at RT.

- The PTW was removed and samples were incubated for 2 hours in secondary antibody solution (anti-mouse-fluorescent 488 secondary antibody (Table 2.2) solution diluted at 1/1000 in blocking buffer (IHC)) at RT.

- Samples were washed 4 x 10 minutes.in PTW at RT.

7. Samples were detected and visualized using the confocal imaging system TCS SP8 confocal microscope (Leica, Germany).

2.2.8 Histopathology

According to the experimental methods by Takamiya et al. [170], 4 dpf zebrafish larvae were firstly fixed overnight at 4°C in 4% PFA solution facilitating optimal structural preservation. The embryos were progressively dehydrated using ascending ethanol concentrations (50%, 70%, 95%, 100% (v/v)), then incubated with 100% propylene oxide, and subsequently infiltrated with EPON 812 resin (Table 2.2) in propylene oxide at increasing concentrations (30%, 70%, 100% EPON/propylene oxide mixture). Polymerization was carried out at 65°C with a mixture containing 20.8% (w/w) dodecenylsuccinic acid anhydride (DDSA) (Table 2.2) and 23.3% (w/w) methylenacid anhydride (MNA) (Table 2.2), along with 1.8% (w/w) 2,4,6-tris(dimethyl-aminomethyl)phenol (DMP 30) (Table 2.2) as the accelerator. The polymerized block was trimmed and 5 µm semi-thin sections were cut with glass knives using an RM2065 microtome (Leica Microsystems). This process commenced from the anterior aspect of the otic vesicle and encompassed posterior structures until reaching the cloacal vent. The region

subjected to sectioning extended from the glomerulus to the cloaca, encompassing the entirety of the pronephros. Detection and visualization were carried out using the DM6 B Fluorescence LED Microscope (Leica, Germany). It's worth noting that my colleague Takamiya found limited penetration of hematoxylin and eosin (H&E) dye into the plastic sections (personal communication by Masanari Takamiya). Consequently, the adoption of toluidine blue emerged as a viable alternative for staining purposes [170, 171]. Toluidine blue is a basic thiazine-type metachromatic dye with a strong affinity for acidic tissue components. It stains nucleic acids blue, polysaccharides purple, and enhances the clarity of histological tissue section images [172]. Based on the imaging results of Sullivan-Brown et al. [173] and Takamiya et al. [170], similar to the results of H&E staining, toluidine blue staining of plastic sections does not hinder the differentiation of different tissue organs and even renders the boundaries between different tissues clearer. This substitution not only overcomes the penetration constraint but also effectively distinguishes various tissues and organs which were classified according to the ZFIN atlas of zebrafish anatomy (https://zfin.org/zf_info/anatomy.html) and previous studies [131, 178, 186].

2.2.9 Fluorescent clearance assay

The protocol of the fluorescent clearance assay was modified from Christou-Savina [174] and Bauer et al. [99]. This method primarily assesses whether the glomerular filtration function is normal. Theoretically, normal zebrafish larvae can excrete metabolites smaller than or equal to 10 kilodalton (kDa) effectively, while the excretion rate of metabolites larger than 10 kDa will significantly decrease. Initially, we prepared the injection solution by mixing 1 µl of 50 mg/ml 10 or 70 kDa FITC-dextran (Table 2.2) solution with 10 µl of 3.3 mM cisplatin solution or 140 mM NaCl solution. The solution was then injected into the 3 dpf zebrafish larvae. Utilizing the TCS SP8 confocal microscope (Leica, Germany), we conducted time-lapse imaging of specific arterial regions

in zebrafish, capturing fluorescence intensity changes from 0 to 24 hpi. The specific analysis method was published by Buckley et al. [175]. The first step involves using the image processing software ImageJ to measure the fluorescence intensity in the specific region of arteries in different zebrafish larvae. The next step is to plot the decay curves of fluorescence intensity in different zebrafish larvae, andthen utilizing the curve fitting toolbox in the spreadsheet's software Excel (Microsoft, USA) to identify the most appropriate curve model. The third step involves calculating the half-life of fluorescence intensity in different embryos. The half-life can serve as a parameter to reflect the metabolic duration of dextran in zebrafish larvae. Finally, statistical analyses of the fluorescence half-life among different injection groups were performed using the software GraphPad Prism 8 (La Jolla, CA).

2.2.10 SYTO-59 dye injection

The pronephric tubule were visualized in live embryos by intravenously injecting SYTO-59 (Table 2.2), a dye typically employed for nuclear and mitochondrial staining [176], which unexpectedly also specifically stained kidney structures (personal communication by Masanari Takamiya) (Figure 2.2 A). The specific workflow is as follows: 3 dpf zebrafish larvae, after being injected with cisplatin or 140 mM NaCl solution, were incubated in E3 medium for 24 hours. Larvae that still exhibited blood flow were then selected and placed in 1.2% UltraPure low melting point agarose to immobilize them. Subsequently, a second injection of 10 µl SYTO-59 Dye solution was administered. Time-lapse imaging was conducted using the confocal imaging system TCS SP8 confocal microscope (Leica, Germany), capturing images continuously over a 24 hours period.

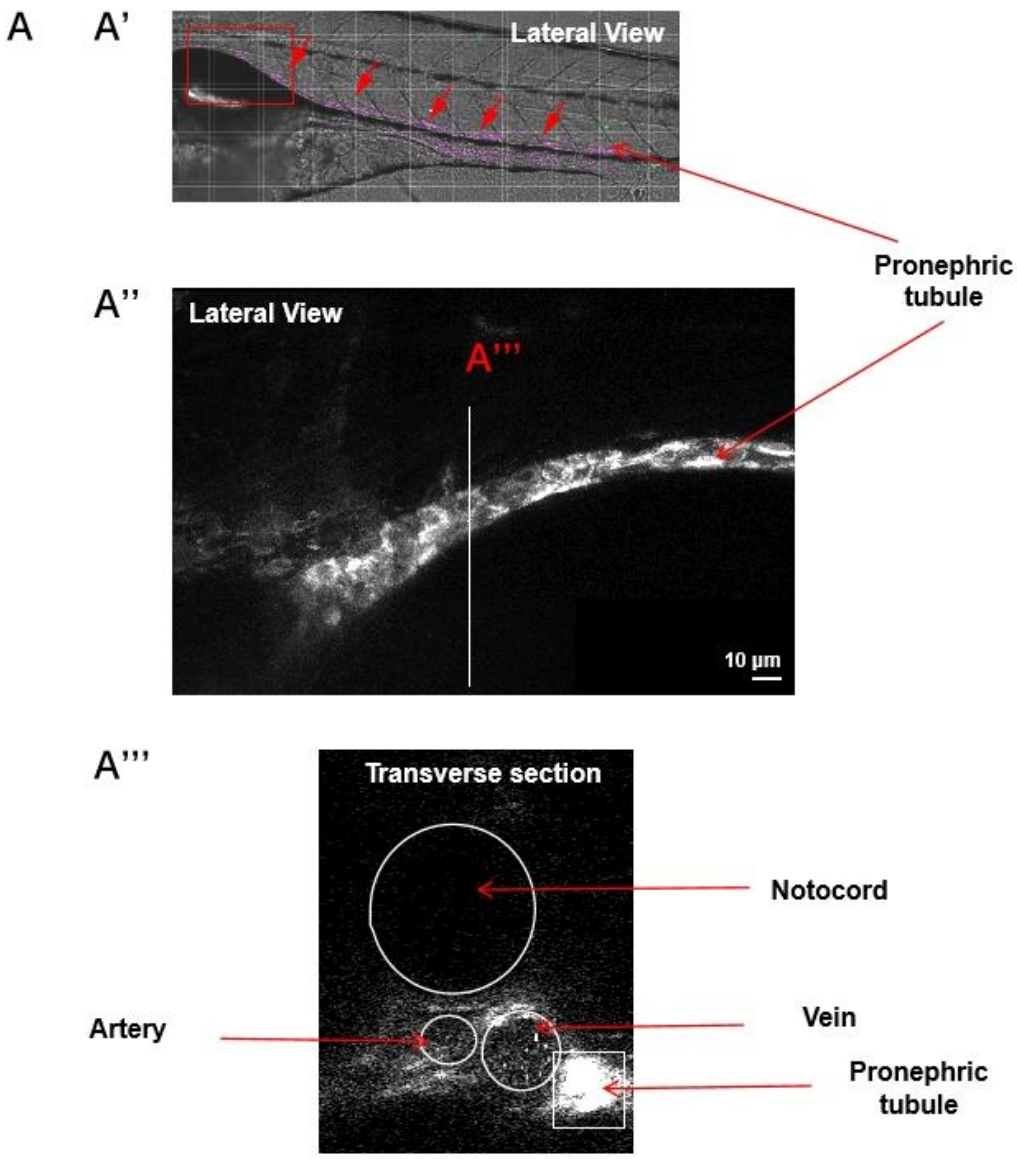

Figure 2.2 Visualization of pronephric tubules in live 5 dpf zebrafish larvae through SYTO-59 dye staining

(A) The SYTO-59 dye facilitates the visualization of the position and structure of the pronephric tubule in live zebrafish larvae. (A') Bright-field image taken 30 minutes after injecting SYTO-59 dye into 5 dpf zebrafish larvae. The white area indicated by the red arrow is the pronephric tubule. (A'') Confocal image (maximum projected view of z-stack) of the red box area in (A'), where the white area represents the pronephric tubule. (A''') Cross-section in (A'') depicting the anatomical positions of different organs or tissues.

3 Platinum drugs induce malformations and lethality in zebrafish larvae

3.1 Introduction

Previous studies have extensively investigated the physiological and pathological changes induced by various platinum drugs in different animal models, such as adult zebrafish [177, 178] and mouse models [179-181]. These different vertebrate animal models accurately replicate the clinical side effects of platinum-based drugs, including cisplatin-induced nephrotoxicity [179, 182], neurotoxicity [183] and ototoxicity [184], carboplatin-induced ototoxicity [185], and oxaliplatin-induced neurotoxicity [181]. However, due to ethical concerns related to experiments with rodents and adult zebrafish, stringent regulations are imposed by different countries or organizations. Therefore, many research groups or investigators want to use alternative models to explore the adverse effects of platinum drugs.

In recent years, zebrafish embryo has gained significant attention as an alternative animal model to study the adverse effects of platinum drugs [186, 187]. Previous sections discussed the advantages of utilizing zebrafish embryos as an alternative model, including their genetic similarity, experimental accessibility and conservation in nephron structure. Taking these factors into consideration, studying platinum drugs using zebrafish embryos is not only feasible but also a complement to existing research findings. However, previous studies did not establish specific methods for studying platinum-based drugs in zebrafish embryonic/larval model, and there is a lack of a standardized approach to assess the toxicity levels induced by these drugs in zebrafish larvae, especially regarding cisplatin-induced nephrotoxicity [125, 188]. Therefore, the first task of this project is to establish an effective method and standards for evaluating the toxicity of platinum drugs in the zebrafish embryonic/larval model.

Traditionally, toxicity studies involving zebrafish embryos have mainly relied on the addition of drugs to the medium in which the embryos or larvae are maintained. This method is convenient due to its simplicity, and standard operation procedures are well-developed [186, 189]. However, this method also exhibits significant limitations. Firstly, the internal dose is ill-defined and depends on the administered nominal dosage and exposure duration. Moreover, immersing the entire embryos in the exposure medium might not replicate the relevant exposure route in clinical setting, for instance, platinum drugs are administered via intravenous injection. Hence, this conventional method can impact zebrafish embryo physiology and development in ways that, occasionally, diverge entirely from those observed in other models such as rodents and humans.

Drawing on the earlier work of the laboratories of Joseph Bonventre [125] and John Kellum [125, 133] and our own research group [149], we established a research method utilizing zebrafish larvae to access the cisplatin-induced nephrotoxicity, involved selecting appropriate days for larval injection, improving injection techniques, and implementing phenotypic classification methods. Moreover, we compared the effects on zebrafish larval development at the same dosage and analyzed the toxicity levels of three different platinum drugs (cisplatin, carboplatin, and oxaliplatin).

3.2 Experimental design and procedures in brief

The experiments were conducted in three parts:

1) Establishment of a microinjection approach and determination of effective doses of cisplatin to induce malformations and mortality in zebrafish larvae

Previous research conducted by the laboratory of Joseph Bonventre has demonstrated that the injection of cisplatin can lead to the development of edema and increased mortality in zebrafish larvae [125]. However, this article does not provide specific details regarding the methodology and dosage used

to observe these phenotypes. Furthermore, it is unfortunate that there were no subsequent studies or data over the past two decades elucidating the effects of cisplatin on zebrafish larval development and edema formation.

Consequently, we conducted experiments to establish the injection of zebrafish embryos at 2 and 3 dpf with varying doses of cisplatin to observe and quantify the malformation and mortality rates in zebrafish larvae. The specific microinjection technique is described in chapter 2, section 2.2.2. Through a comprehensive analysis of the obtained results, the optimal cisplatin dose is determined for the subsequent mechanistic studies in zebrafish larvae.

2) Specific assays to detect nephrotoxicity in zebrafish larvae

After establishing the appropriate dosage and methodology for inducing abnormal embryonic development in zebrafish using cisplatin, it was essential to investigate whether the nephrotoxicity induced by cisplatin in a clinical setting could be replicated in the zebrafish larvae. Based on the previous researches conducted by the laboratories of John Kullum [133] and, more recently, of Angela Mally [99], our experiments were divided into three distinct parts: 1. Assessment of renal function through the utilization of dextran-based assays, with specific methodologies described in Chapter 2, Section 2.2.9; 2. Examination of renal histopathological changes, involving the utilization of in situ hybridization to detect kidney injury markers (outlined in Chapter 2, Section 2.2.5), histopathological analysis of kidney tissue sections (detailed in Chapter 2, Section 2.2.8); 3. Visualization of pronephric tubules in live zebrafish larvae through SYTO-59 dye staining (outlined in Chapter 2, Section 2.2.10).

3) Comparative studies on the toxicity of cisplatin, carboplatin and oxaliplatin in zebrafish larvae

Clinical data previously showed the enhanced nephrotoxicity of cisplatin in comparison to carboplatin and oxaliplatin. To investigate this differential toxicity in the zebrafish larval model, we administered equivalent doses of cisplatin, carboplatin, and oxaliplatin to 2 dpf zebrafish larvae. By comparing the

disparities in malformation and mortality, we aimed to verify the consistency of the clinically established data in the zebrafish model.

3.3 Results

3.3.1 Establishment of dose-response curves upon cisplatin injection into 2 and 3 dpf zebrafish larvae

In order to determine the appropriate dosage for the subsequent mechanistic experiments, 2 dpf zebrafish larvae were subjected to microinjections of 10 nl of 0.8 mM, 1.7 mM, and 3.3 mM cisplatin solution, respectively. The specific experimental procedure involves, 1). Injecting 10 nl of 140 mM NaCl solution and different concentrations (0.8 mM, 1.7 mM, and 3.3 mM) of cisplatin solution into the pericardiac space of 2 dpf zebrafish larvae as the control (CON) group and the cisplatin-injected (Cisplatin) group, respectively. 2). The cardiac edema and mortality rates were calculated from 3 to 5 dpf (Figure 3.1A). The cardiac edema rate is the ratio of the embryos with cardiac edema to the total number of embryos. The mortality rate is the ratio of the sum of disintegrated embryos and embryos without heartbeat to the total number of embryos.

Following the injection of 10 nl of 0.8 mM cisplatin solution, no cardiac edema and mortality rate change were observed in the zebrafish larvae from 1 dpi (3 dpf) to 3 dpi (5 dpf), indicating that this dosage did not exhibit toxicity (Figure 3.1B-C).

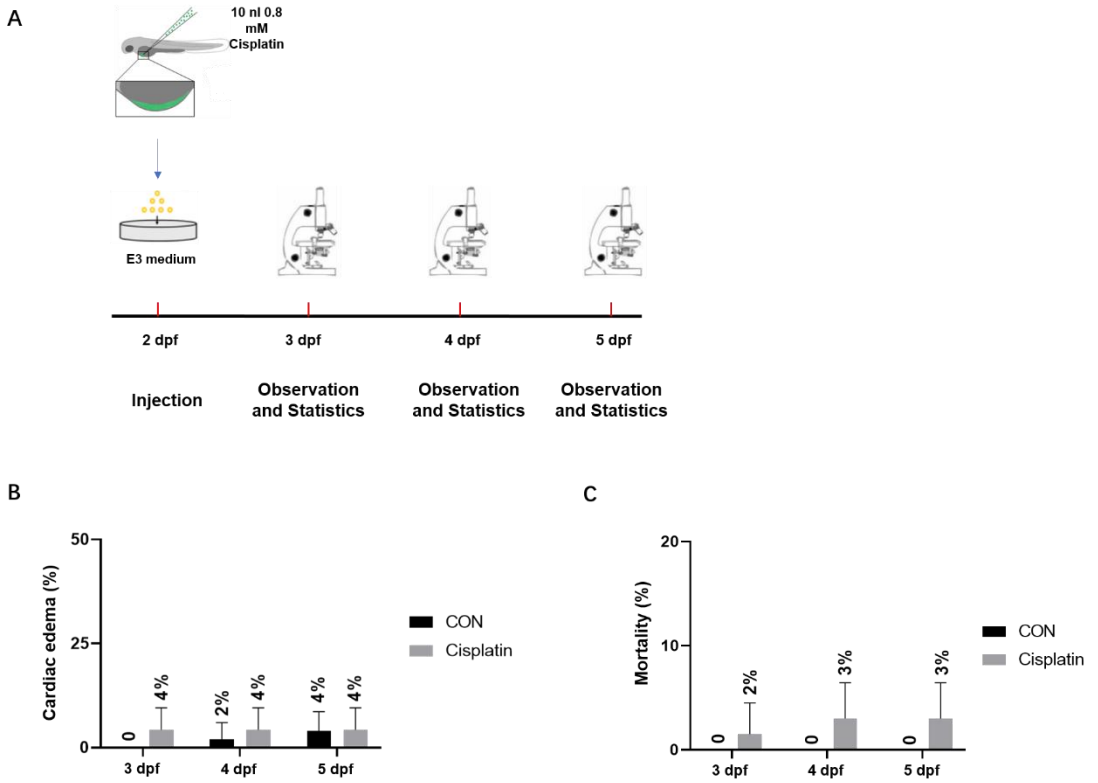

Figure 3.1 The cardiac edema and mortality rate of zebrafish larvae from 3 to 5 dpf after injection with 10 nl of 0.8 mM cisplatin solution

(A) Schematic outline of experimental timelines and set-up. Injecting 10 nl of 140 mM NaCl solution and 0.8 mM cisplatin solution into the pericardiac space of 2 dpf zebrafish larvae as the control (CON) group and the cisplatin-injected (Cisplatin) group, respectively. Then, the cardiac edema and mortality rates were calculated from 3 to 5 dpf.

(B) The change in cardiac edema rate from 3 dpf to 5 dpf in the CON and the Cisplatin group.

(C) The change in mortality rate from 3 dpf to 5 dpf in the CON and the Cisplatin group.

The CON group: 10 nl of 140 mM NaCl solution injected; The Cisplatin group: 10 nl of 0.8 mM cisplatin solution injected.

Data are expressed as mean ± standard deviation (SD) from four independent experiments. For each experiment, 12 and 18 embryos were used for the CON and the Cisplatin group, respectively (B-C).

However, after injecting 10 nl of 1.7 mM cisplatin solution, some zebrafish larvae showed obvious morphological changes, such as edema (Figure 3.2A-A'). The percentage of zebrafish with edema increased from 11% at 3 dpf to 35% at 5 dpf (Figure 3.2B), and the mortality rate increased from 5% at 3 dpf to 20% at 5 dpf (Figure 3.2C). These results indicate that this dosage exerted a certain level of toxicity and affected the normal development of zebrafish.

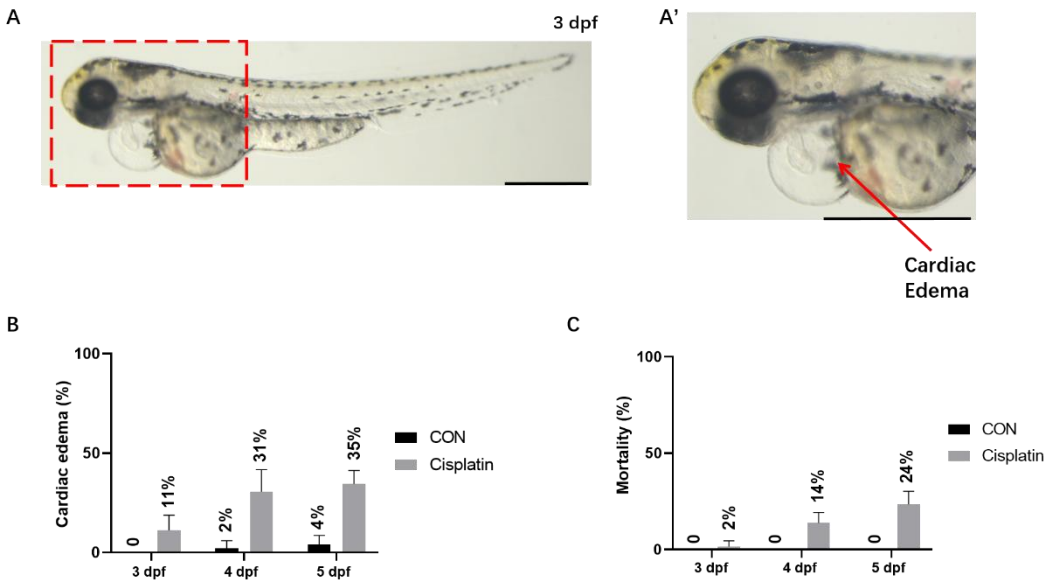

Figure 3.2 The cardiac edema and mortality rate of zebrafish larvae from 3 to 5 dpf after injection with 10 nl of 1.7 mM cisplatin solution

(A) Representative images: some zebrafish larvae at 1 dpi (3 dpf) exhibited edema, with a magnified view (A') highlighting significant fluid accumulation in the heart region of zebrafish (indicated by the red box with dotted arrows).

(B) The change in cardiac edema rate from 3 dpf to 5 dpf in the CON and the Cisplatin group.

(C) The change in mortality rate from 3 dpf to 5 dpf in the CON and the Cisplatin group.

The CON group: 10 nl of 140 mM NaCl solution injected; The Cisplatin group: 10 nl of 1.7 mM cisplatin solution injected.

The scale bar is 0.5 mm (A and A').

Data are expressed as mean ± SD from four independent experiments. For each experiment, 12 and 18 embryos were used for the CON and the Cisplatin group, respectively (B-C).

After injection of 10 nl of 3.3 mM cisplatin solution, the percentage of zebrafish larvae exhibiting edema (Figure 3.3A-A') increased even further from 35% at 3 dpf (1 dpi) to 92% at 5 dpf (3 dpi) (Figure 3.3B), and the mortality rate also increased from 15% at 3 dpf (1 dpi) to 52% at 5 dpf (3 dpi) (Figure 3.3C). These results indicate that this dosage already induces strong toxicity and essentially disrupts zebrafish development.

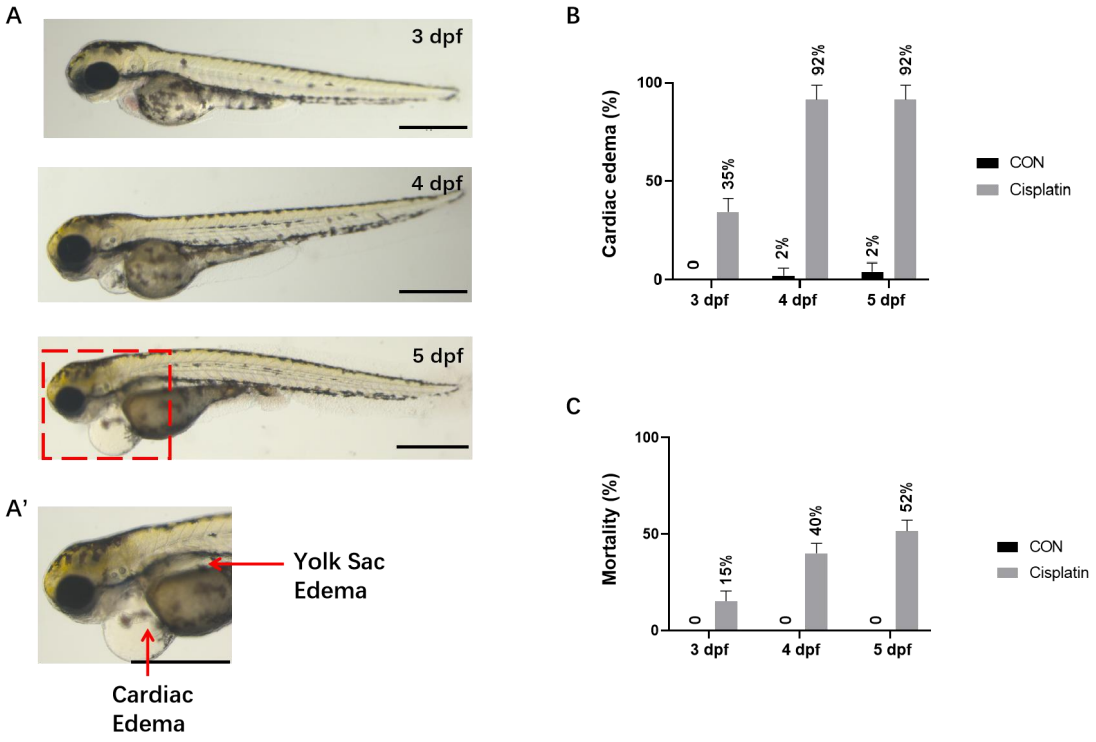

Figure 3.3 The cardiac edema and mortality rate of zebrafish larvae from 3 to 5 dpf after injection with 10 nl of 3.3 mM cisplatin solution

(A) The morphological changes in zebrafish from 1 dpi (3 dpf) to 3 dpi (5 dpf) following cisplatin injection, showing progressive cardiac edema and some zebrafish exhibiting yolk sac edema. (A') is a magnified image (indicated by the red box with dotted arrows) showing pronounced accumulation of fluid in the region of the zebrafish heart and above the yolk sac.

(B) The change in cardiac edema rate from 3 dpf to 5 dpf in the CON and the Cisplatin group.

(C) The change in mortality rate from 3 dpf to 5 dpf in the CON and the Cisplatin group.

The CON group: 10 nl of 140 mM NaCl solution injected; The Cisplatin group: 10 nl of 3.3 mM cisplatin solution injected.

The scale bar is 0.5 mm (A and A').

Data are expressed as mean ± SD from four independent experiments. For each experiment, 12 and 18 embryos were used for the CON and the Cisplatin group, respectively (B-C).

These results demonstrate that with the increasing dosage of cisplatin, there is a corresponding escalation in zebrafish morphological changes, manifested by the rise in edema and mortality rate, indicating an enhancement in toxicity. Based on the five phenotypes: cardiac edema, yolk sac edema, curved, motility, disintegrated, the zebrafish larvae injected with cisplatin can be classified into *Normal*, *Mild*, *Moderate*, *Severe*, *Disintegrated* categories (Table 3.1):

Normal — The zebrafish larvae did not show edema formation (Figure 3.4A);

Mild — The zebrafish larvae only showed cardiac edema formation (Figure 3.4B);

Moderate — The zebrafish larvae exhibited cardiac edema and yolk sac edema formation but show no body curvature and loss of motility (Figure 3.4C).

Severe — Most of the zebrafish larvae in this phenotype exhibited more severe cardiac edema and yolk sac edema formation, leading to body curvature and loss of motility (Figure 3.4D). A small subset within this phenotype underwent a faster toxic process, displaying body curvature and loss of motility even with only cardiac edema (Figure 3.4E).

Disintegrated — This phenotype is mainly divided into two types: one where partial tissues or organs of zebrafish larvae show disintegration (Figure 3.4F), another is completely dissolved in the medium (Figure 3.4G).

Importantly, during the phenotype classification process, even if the zebrafish no longer exhibited a heartbeat but haven't disintegrated, they would still be included in the statistical data for morphological changes.

Moreover, to better reflect the toxic changes induced by cisplatin, in addition to analyzing morphological changes, we also introduced the assessment of mortality rate, which is calculated as the ratio of the sum of disintegrated larvae and larvae without a heartbeat to the total number of embryos.

In subsequent studies, we will employ a dual criterion of phenotypic changes and mortality rate to reflect the degree of toxicity induced by cisplatin (The reasons for selecting these two parameters will be discussed in detail in Chapter 3, Section 3.4.).

Phenotype	Cardiac edema	Yolk sac edema	Curved	Motility	Disintegrated
Normal	-	-	-	+	-
Mild	+	-	-	+	-
Moderate	+	+	-	+	-
Severe	+	/	+	-	-

Disintegrated					+

Table 3.1 The criteria for phenotypic classification of zebrafish larvae
Based on the five phenotypes: cardiac edema, yolk sac edema, curved, motility, disintegrated, the zebrafish larvae injected with cisplatin can be classified into *Normal*, *Mild*, *Moderate*, *Severe*, *Disintegrated* categories. '+' indicates the presence, '-' indicates the absence, '/' implies a possible occurrence, and a blank space indicates uncertainty about the presence of the phenotype.

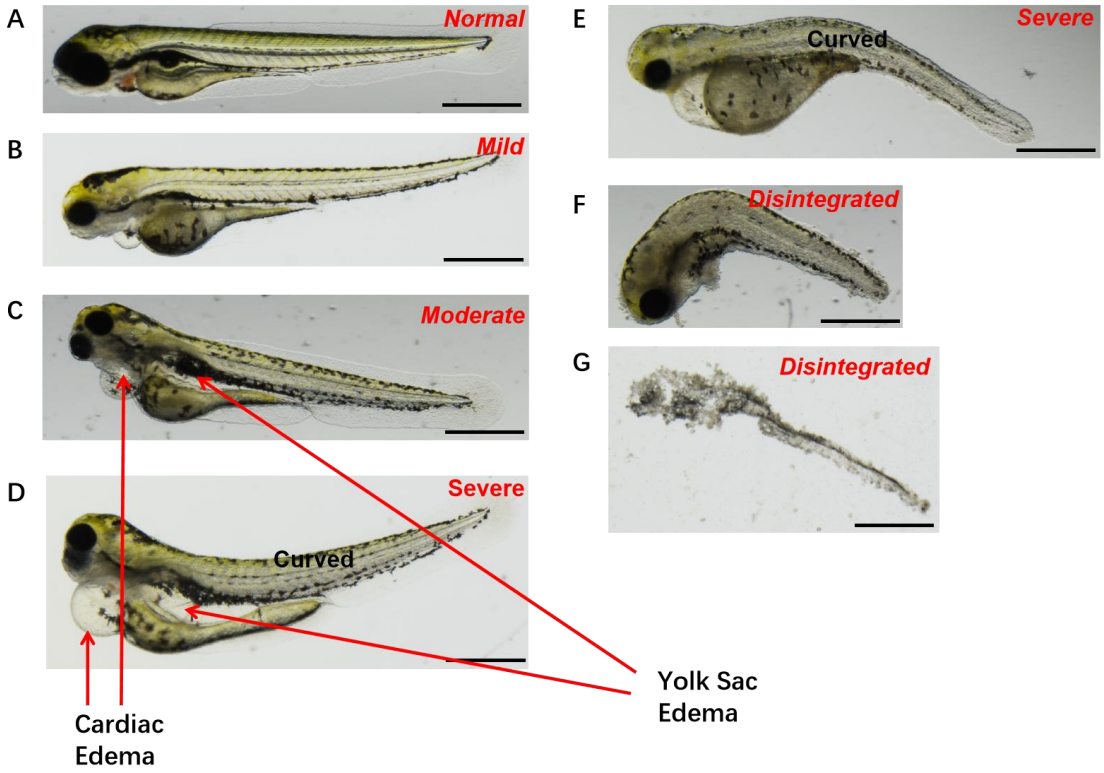

Figure 3.4 Zebrafish larvae exhibited different morphological changes after 10 nl of 3.3 mM cisplatin solution injected
Zebrafish phenotypes were classified based on the Table 3.1, resulting in the distinct categories: *Normal* (A), *Mild* (B), *Moderate* (C), *Severe* (D-E), and *Disintegrated* (F-G). The scale bar represents 0.5 mm for all panels.

To further determine the appropriate concentration, we performed morphological analysis for the two doses of cisplatin, 10 nl of 1.7 mM and 10 nl of 3.3 mM, respectively. The results showed that the phenotype changes induced by 10 nl of 1.7 mM cisplatin solution were not very pronounced. The *Moderate* phenotype increased from 1% at 3 dpf (1 dpi) to 10% at 5 dpf (3 dpi), the *Severe* phenotype increased from 2% at 3 dpf (1 dpi) to 17% at 5 dpf (3 dpi), and the *Disintegrated* phenotype increased from 0% at 3 dpf (1 dpi) to 5%

at 5 dpf (3 dpi) (Figure 3.5A). In contrast, the phenotype changes induced by 10 nl of 3.3 mM cisplatin solution were much more significant. The *Moderate* phenotype increased from 0% at 3 dpf (1 dpi) to 8% at 5 dpf (3 dpi), the *Severe* phenotype increased from 10% at 3 dpf (1 dpi) to 50% at 5 dpf (3 dpi), and the *Disintegrated* phenotype increased from 3% at 3 dpf (1 dpi) to 26% at 5 dpf (3 dpi) (Figure 3.5B). Considering that our subsequent experiments require the use of relevant inhibitors or gene knockdown/knockout tools for mechanistic studies, it is essential to have a greater dynamic range of phenotypic changes in zebrafish for easier observation and statistical analysis. Therefore, we selected 10 nl of 3.3 mM cisplatin solution as the appropriate dosage for subsequent toxicity studies in zebrafish larva model.

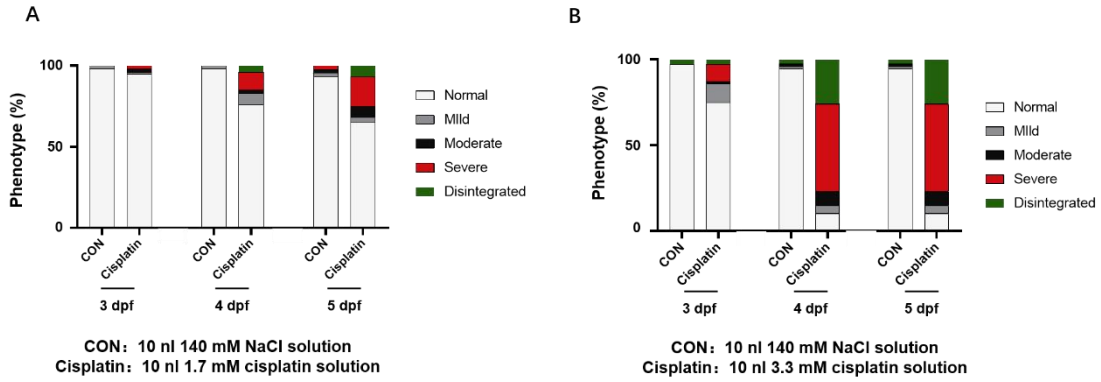

Figure 3.5 The morphological changes after different doses cisplatin solution injection
(A) The phenotypic changes from 1 dpi (3 dpf) to 3 dpi (5 dpf) in the CON and the Cisplatin group.
The CON group: 10 nl of 140 mM NaCl solution injected; The Cisplatin group: 10 nl of 1.7 mM cisplatin solution injected.
(B) The phenotypic changes from 1 dpi (3 dpf) to 3 dpi (5 dpf) in the CON and the Cisplatin group.
The CON group: 10 nl of 140 mM NaCl solution injected; The Cisplatin group: 10 nl of 3.3 mM cisplatin solution injected.
Data are obtained from four independent experiments. For each experiment, 12 and 18 embryos were used for the CON and the Cisplatin group, respectively (A-B).

Finally, I attempted to investigate the impact of developmental stage on the severity of cisplatin toxicity. Thus, 10 nl of 3.3 mM cisplatin solution was injected into 2 and 3 dpf zebrafish larvae for evaluating the morphological changes and mortality rates. The data showed that when zebrafish embryos

developed to 5 dpf, 97% of the larvae injected on Day 2 displayed edema, with 93% showing the *Severe* or *Disintegrated* phenotypes and a mortality rate of 42% (Figure 3.6A). Similarly, the larvae injected on Day 3 exhibited edema in 90% of cases, with 84% showing the *Severe* or *Disintegrated* phenotypes and a mortality rate of 39% (Figure 3.6B). The differences between the two groups were not significant. Considering the ongoing divergence in past studies regarding the choice of 2 [98, 118] or 3 [99, 190] dpf zebrafish for nephrotoxin evaluation, my results indicate that, at least for cisplatin, the choice between 2 or 3 dpf zebrafish embryos had minimal impact on the subsequent outcomes. Considering the higher efficiency and practicality of injections at 2 dpf compared to 3 dpf, I selected 2 dpf embryos for injection with 10 nl of 3.3 mM cisplatin solution as the standard procedure for future studies.

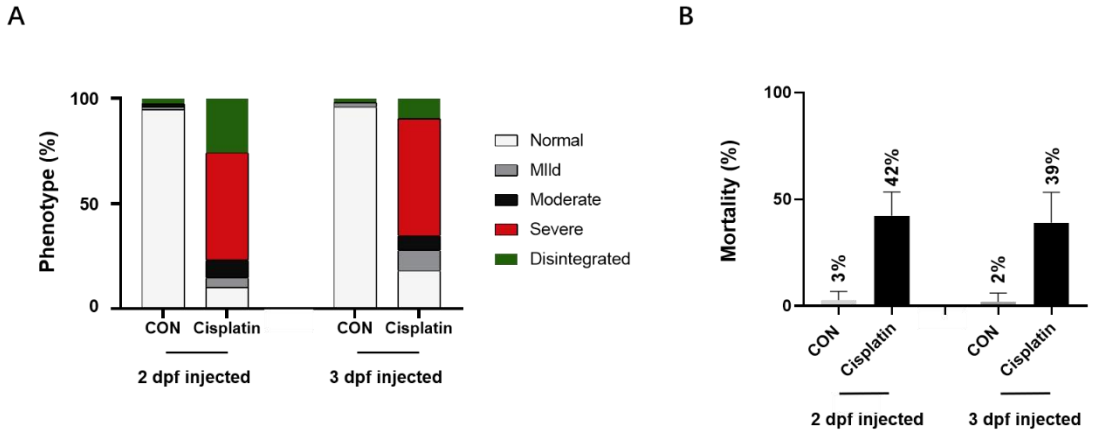

Figure 3.6 The changes in phenotype and mortality rate of zebrafish larvae at 2 and 3 dpf following cisplatin injection

(A) The phenotypic changes of 5 dpf larvae in the CON and the Cisplatin group.

(B) The change in mortality rate of 5 dpf larvae in the CON and the Cisplatin group.

The '2 dpf injected' refer to zebrafish larvae injected with 10 nl of 3.3 mM cisplatin solution or 140 mM NaCl solution (control) at 2 dpf. The '3 dpf injected' refer to zebrafish larvae injected with 10 nl of 3.3 mM cisplatin solution or 140 mM NaCl solution (control) at 3 dpf. The CON group: 10 nl of 140 mM NaCl solution injected; The Cisplatin group: 10 nl of 3.3 mM cisplatin solution injected.

Data are obtained from four independent experiments. For each experiment, 12 and 18 embryos were used for the CON and the Cisplatin group, respectively (A-B).

3.3.2 Cisplatin-induced kidney injury in zebrafish larvae

In order to validate the nephrotoxicity of cisplatin in zebrafish larvae, we

examined both the filtration function and histological changes of the kidney. Initially, the in situ hybridization technique was employed to detect the expression of relevant markers in the kidneys, including *cdh17* (pronephric tube) [160], *podocin* (glomerulus) [161], *nephrin* (glomerulus) [161], *slc20a1a* (proximal tube) [163], and *trpm7* (distal tube) [164]. For subsequent experiments, only *cdh17* and *podocin* probes were successfully used, as for the *nephrin*, *slc20a1a*, and *trpm7* probes a specific signal in the selected regions of the kidney could not be detected. In the control group, *cdh17* exhibited high expression in the distal tube region, while cisplatin injection significantly reduced *cdh17* expression in the distal tube region (Figure 3.7A). In the controls, the *podocin* probe demarcated the structure of the glomerulus, while cisplatin treatment led to the disruption of the glomerular structure, with cells showing a scattered pattern (Figure 3.7B).

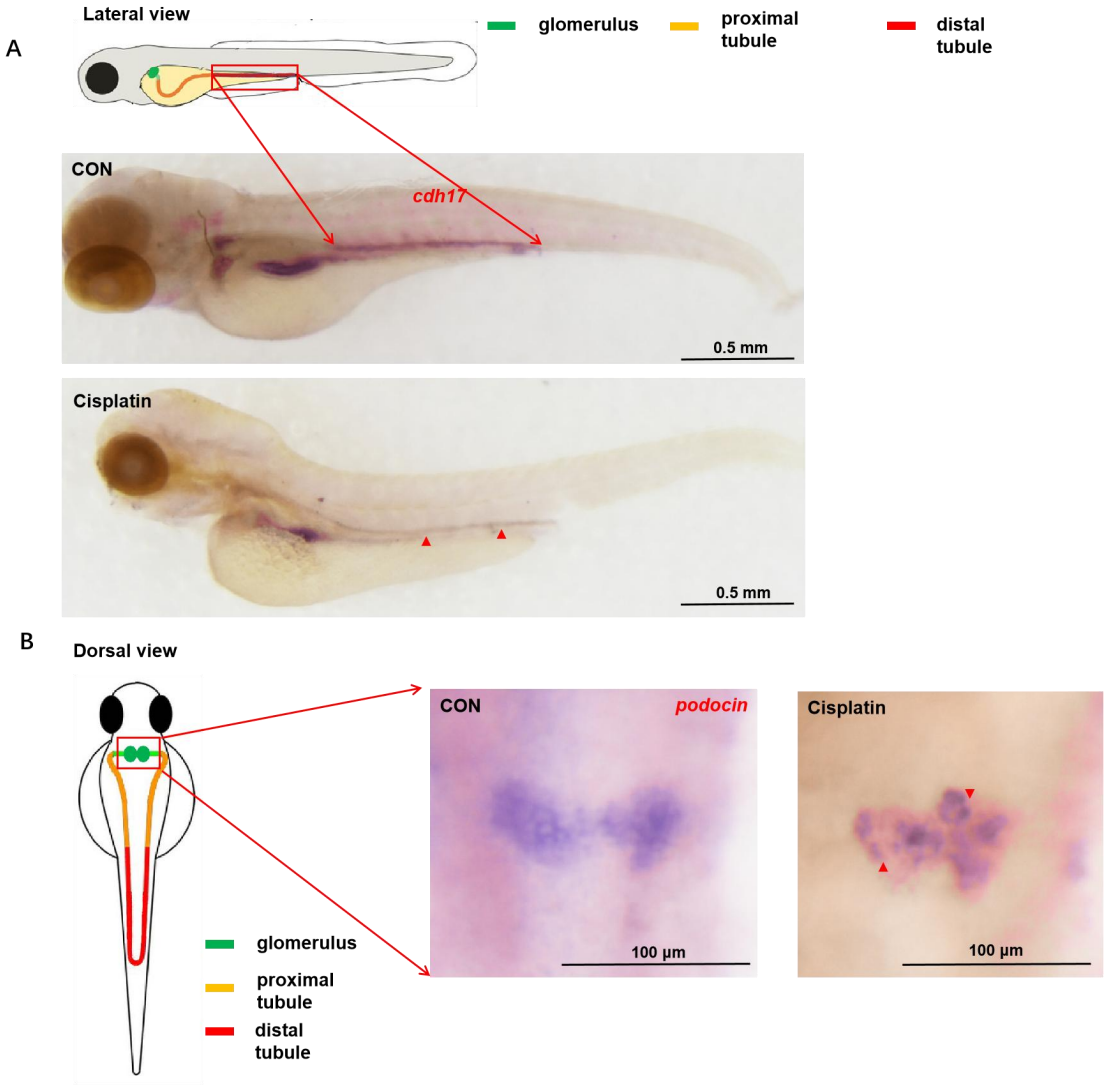

Figure 3.7 The expression changes of *cdh17* and *podocin* in zebrafish larvae at 2 dpi (4 dpf) following cisplatin injection

(A) The expression patterns of *cdh17* in the CON and the Cisplatin group.

(B) The expression patterns of *podocin* in the the CON and the Cisplatin group.

Figures A and B are accompanied by schematic representations of the 2 dpi (4 dpf) zebrafish pronephron as a reference for anatomical location. The red boxes and red arrows indicate the specific expression locations of the whole mount in situ hybridization (WISH) signal. The red triangles indicate regions with altered expression after cisplatin injection.

The CON group: 10 nl of 140 mM NaCl solution injected; The Cisplatin group: 10 nl of 3.3 mM cisplatin solution injected.

n=6 animals in each group (A-B).

The scale bar is shown in different panels.

In the absence of a zebrafish kidney reporter line, a method was sought to precisely determine the position of the pronephric duct in live zebrafish larvae. By injecting zebrafish with SYTO-59 dye, the specific location of the pronephric

duct could be observed in live zebrafish larvae (personal communication by Masanari Takamiya) (Figure 2.2 A). Upon injecting zebrafish larvae at 3 dpf with cisplatin or 140 mM NaCl solution and subsequently injecting the SYTO-59 dye 24 hours later (Figure 3.8A), we observed a reduction in the width of the pronephric tubule (Figure 3.8B-C). This phenomenon indicates that after cisplatin injection, the zebrafish pronephric tubules underwent abnormal physiological changes resulting in a change in diameter. Based on previous studies on cisplatin in other models, we speculated that the potential cause was due to tubule constriction [191-193] or collapse [125, 194, 195].

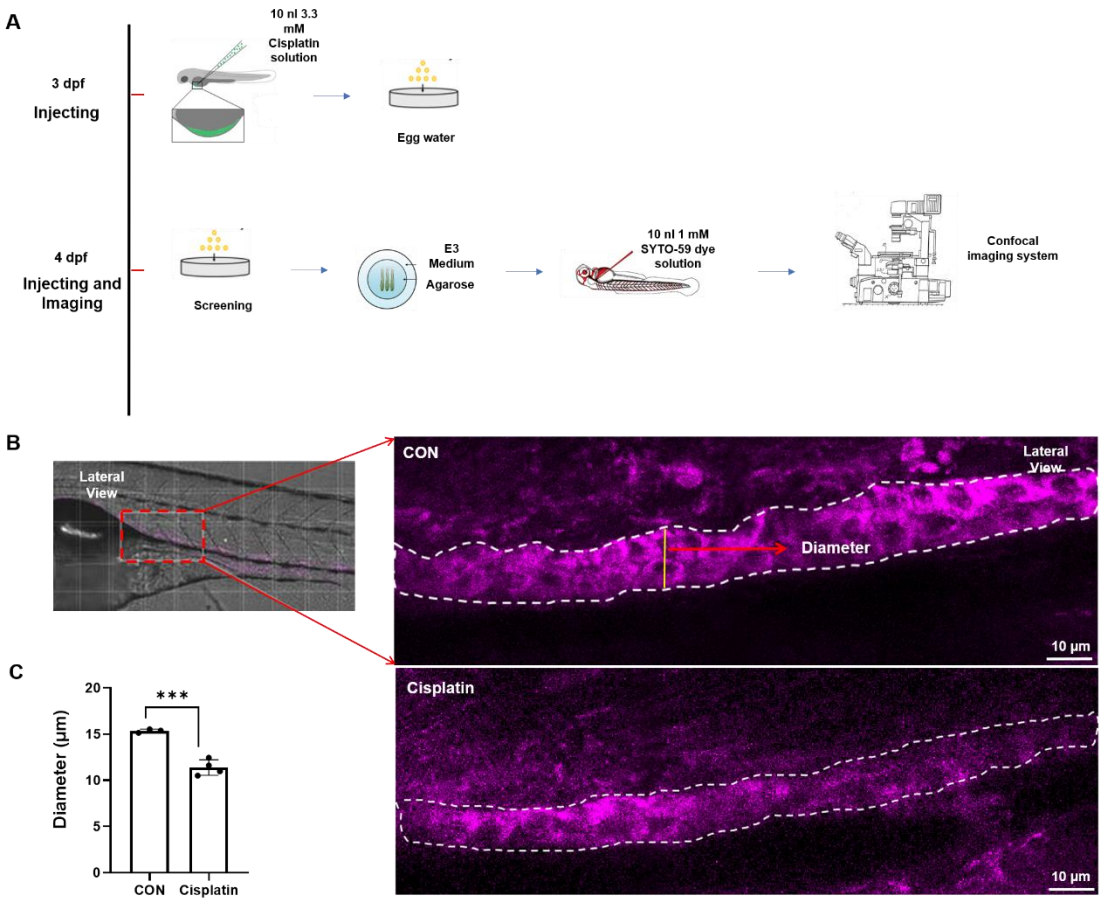

Figure 3.8 Cisplatin injection reduced the diameter of the pronephric tubule in 4 dpf zebrafish larvae

(A) Schematic outline of experimental timelines and set-up. The experimental procedure include: 1) At 3 dpf, injecting 10 nl of 3.3 mM cisplatin solution or 140 mM NaCl solution (control) separately into zebrafish larvae as the Cisplatin group and the CON group. 2) At 1 dpi (4 dpf), injecting 10 nl of 1 mM SYTO-59 dye into the Cisplatin group and the CON group, followed by immediate imaging using a Confocal imaging system.

(B) The Cisplatin group and the CON group stained with SYTO-59 dye. The confocal

image (maximum projected view of z-stack) shows the red-framed area in bright field. The magenta region represents the area stained by SYTO-59 dye, and the white dotted arrow indicates the boundary of the pronephric tubule.
(C) The changes in the diameter of the pronephric tubule in the CON and the Cisplatin group. The diameter of the pronephric tubule is indicated by the yellow vertical line in Figure B, and the individual diameter length used for statistics is the average taken from five different positions of the pronephric tubule.
The CON group: 10 nl of 140 mM NaCl solution injected; The Cisplatin group: 10 nl of 3.3 mM cisplatin solution injected.
The scale bar is shown in the figure.
Data are expressed as mean ± SD, using 3 and 4 embryos for the CON and the Cisplatin group respectively.
All significance values were determined using Student's t-tests. *, $0.01 \leq p < 0.05$; **, $p < 0.01$; ***, $p < 0.001$; ****, $p < 0.0001$.

To further analyze whether the reduced diameter of the zebrafish larval pronephric tubule caused by cisplatin is due to renal cell injury and death, we could study the accumulation of macrophages in the area of the pronephric duct after cisplatin injection by combined detection of GFP in the macrophage reporter line Tg(*mpeg1*:EGFP) and SYTO-59. Theoretically, cisplatin can cause apoptosis or necrosis of pronephric tubule epithelial cells, recruiting more macrophages to clear debris and dampen inflammation in the area [196, 197]. However, our results demonstrated that macrophages did not excessively migrate to the proximal tubules. Conversely, in the Cisplatin group, macrophages significantly accumulated in the region between arteries and veins (Figure 3.9). We will discuss and analyze the potential reasons for the abnormal macrophages recruitment in chapter 3, Section 3.4.

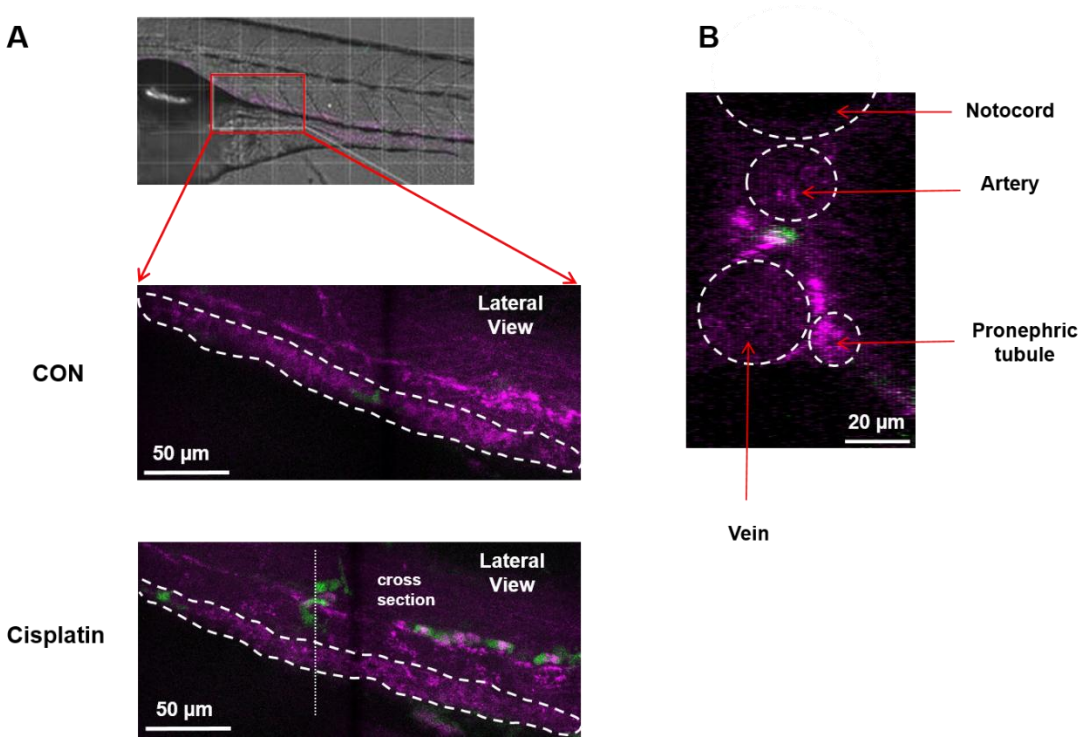

Figure 3.9 Cisplatin-induced significant accumulation of macrophages in the region between arteries and veins

(A) SYTO-59 dye staining and GFP signal in the CON and the Cisplatin group. The confocal image (maximum projected view of z-stack) shows the red-framed area in bright field. The magenta region represents the area stained by SYTO-59 dye, the GFP region represents macrophages, and the white dotted line indicates the boundary of the pronephric tubule.

(B) The cross-section in Figure A depicting the anatomical positions of different structures or cells.

The CON group: 10 nl of 140 mM NaCl solution injected; The Cisplatin group: 10 nl of 3.3 mM cisplatin solution injected.

The scale bar is shown in the figure.

In the third step, histochemistry was employed to examine the kidney sections of zebrafish larvae, where toluidine blue was used to distinguish specific organs and tissues [170, 171]. Based on the ZFIN Atlas of Zebrafish Anatomy and previous studies [99, 190, 198], we successfully identified the precise locations of the glomerulus and proximal tube (Figure 3.10). The results from the sections revealed that cisplatin injection led to the formation of noticeable cavities in the glomerular region, suggestive of internal edema (Figure 3.10). Although we also observed the structure of the proximal tube, no changes in tube morphology or lumen diameter were observed.

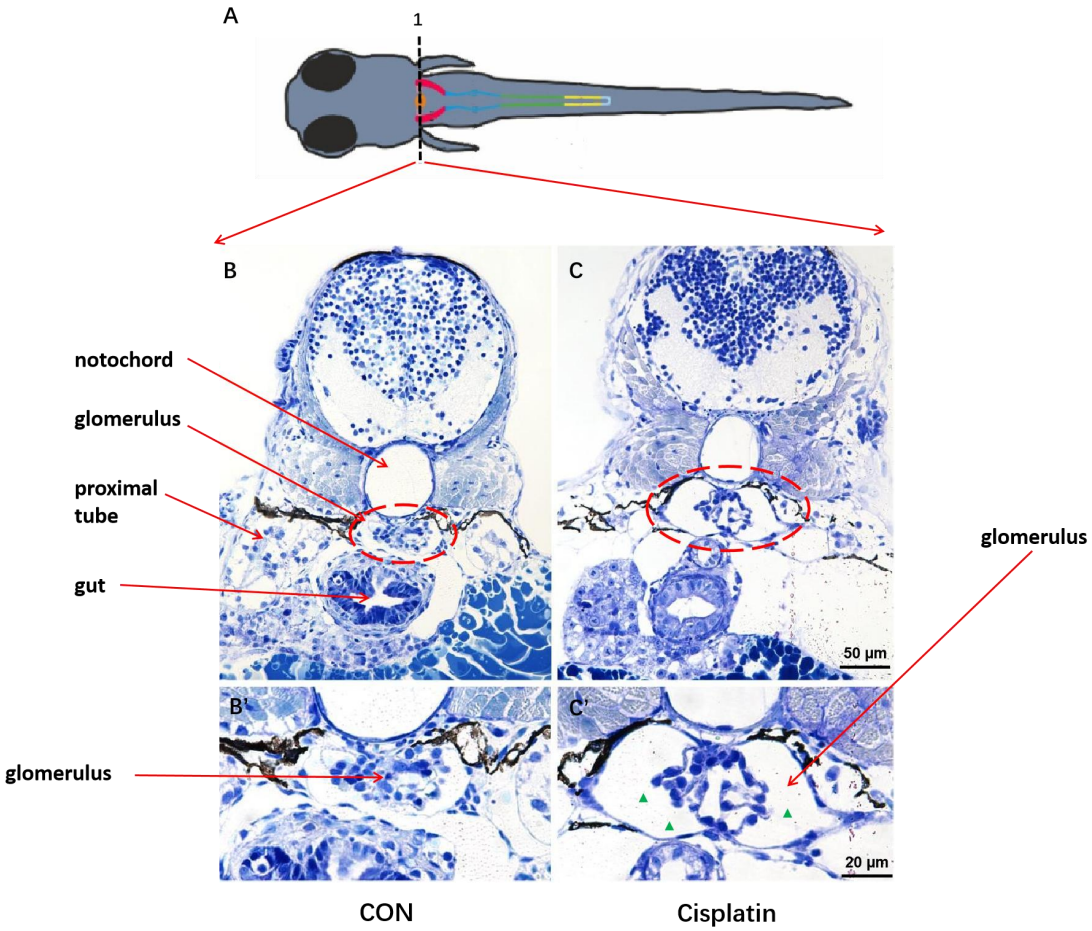

Figure 3.10 Cisplatin-induced significant edema formation in the glomerular region
(A) Schematic drawing to illustrate the position of transverse sections (5 µm) of the glomerulus and proximal convoluted tubule (1). The schematic is modified from Bauer et al. [99]. Orange region: glomerulus, red region: proximal convoluted tubule, blue region: proximal straight tubule, green region: distal convoluted tubule, yellow region: distal straight tubule.
(B) A toluidine blue staining section (cross section 1 as depicted in panel A above) of a 2 dpi (4 dpf) larva from the CON group, with a magnified view (B') of the area indicated by the red dotted circle.
(C) A toluidine blue staining section (cross section 1 as depicted in panel A above) of a 2 dpi (4 dpf) larva from the Cisplatin group, with a magnified view (C') of the area indicated by the red dotted circle. The green triangles indicate the formation of cavities due to internal edema (C').
The CON group: 10 nl of 140 mM NaCl solution injected; The Cisplatin group: 10 nl of 3.3 mM cisplatin solution injected.
The scale bar is shown in the figure.
n=4 animals in each group (B-C).

In the fourth step, to evaluate kidney function, we employed fluorescently labeled dextran as a marker. Christou-Savina et al. demonstrated that normally developing 3 dpf zebrafish larvae excrete approximately 85% of 10 kDa

dextran within 24 hours post-injection (hpi) [174]. However, in cases of impaired kidney function, the excretion of 10 kDa dextran is reduced. We selected a confined arterial region for time-lapse imaging, measured fluorescence intensity, and plotted decay curves to compare the half-life of dextran retention in the vasculature (Figure 3.11A-B). Our results indicated that, compared to normal zebrafish, 3 dpf larvae injected with cisplatin exhibited shorter retention time of dextran (Figure 3.11C). This finding contradicts some previous studies [99, 174], prompting us to validate our experiments further. To address this discrepancy, we repeated the experiments using 70 kDa dextran instead of 10 kDa dextran. In normal zebrafish embryos, the glomerular barrier restricts the excretion of 70 kDa dextran. However, in cases of kidney dysfunction, the excretion of 70 kDa dextran increases. Our experimental results with 70 kDa dextran reaffirmed that cisplatin-injected 3 dpf zebrafish larvae exhibit enhanced release of 70 kDa dextran in line with an impaired glomerular function (Figure 3.11C). We will discuss and analyze the potential reasons for the size-difference in dextran clearance in chapter 3, Section 3.4.

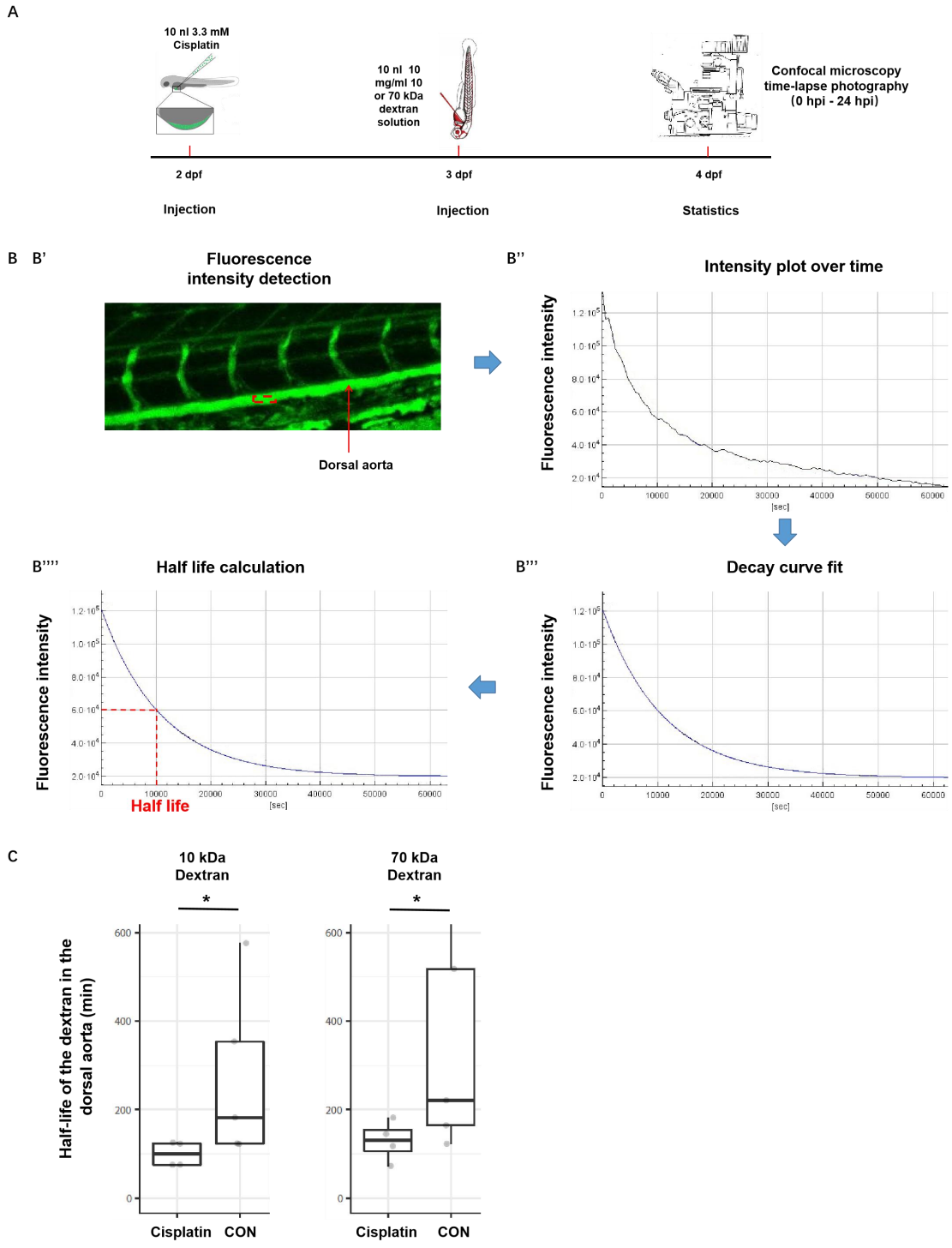

Figure 3.11 The clearance analysis of 10 and 70 kDa dextran in 3 dpf zebrafish larvae

(A) Schematic to illustrate the experimental timeline for the dextran clearance assays. The experimental procedure include: 1) At 3 dpf, injecting 10 nl of 3.3 mM cisplatin solution or 140 mM NaCl solution (control) separately into zebrafish larvae as the Cisplatin group and the CON group. 2) At 1 dpi (4 dpf), injecting 10 nl of 10 mg/ml 10 kDa or 70 kDa dextran solution into the Cisplatin group and CON group. Subsequently, time-lapse imaging was conducted using a confocal microscope for a duration of 24 hours.

(B) Dextran clearance assay: 1) The fluorescence intensity was measured within a confined region (red box) in the dorsal aorta (B'). 2) The fluorescence intensity versus

time curve, with the black line representing the raw data curve (B''). 3) The fluorescence intensity versus time curve, with the blue line representing the fitted curve. Specific curve fitting methods refer to Chapter 2, Section 2.2.9 (B'''). 4) The time taken for the fluorescence intensity to decay to half of the initial fluorescence, calculated based on the fitted curve, represents the half-life of dextran retention in the vasculature (B'''').
(C) The half-life of injected 10 and 70 kDa dextran in the dorsal aorta in the CON and the Cisplatin group.
The CON group: 10 nl of 140 mM NaCl solution injected; The Cisplatin group: 10 nl of 3.3 mM cisplatin solution injected.
Data are expressed as mean ± SD (n=4 embryos in each group) (C).
All significance values were determined using Student's t-tests. *, $0.01 \leq p < 0.05$; **, $p < 0.01$; ***, $p < 0.001$; ****, $p < 0.0001$.

Overall, our histopathological experiments, including in situ hybridization and histochemical analysis, confirmed the disruption of glomerular and distal tube structures in the zebrafish pronephros following cisplatin injection. While some aspects of the renal filtration function assays and SYTO-59 dye staining yielded results not entirely aligned with our expectations, they still indicated aberrations in renal filtration function induced by cisplatin injection.

3.3.3 Cisplatin exhibits stronger toxicity compared to carboplatin and oxaliplatin in zebrafish larval model

Following the injection of the same dose of 10 nl of 3.3 mM cisplatin, carboplatin, and oxaliplatin solution into 2 dpf zebrafish larvae, we observed changes in phenotype from 3 to 5 dpf. Unlike the 94% of zebrafish larvae in the cisplatin group at 5 dpf that exhibited edema, only 4% and 6% of larvae in the carboplatin and oxaliplatin groups, respectively, displayed mild edema formation (Figure 3.12B). Similarly, the mortality rate of 5 dpf zebrafish larvae in the cisplatin group is as high as 31%, while the carboplatin and oxaliplatin groups have rates of only 4% and 2%, respectively (Figure 3.12C). Notably, at this dosage, carboplatin had minimal impact on zebrafish larval development, but 34% of larvae showed reduced length (Figure 3.12A). The present study does not suggest a correlation between the appearance of this phenotype with developmental delay or nephrotoxicity.

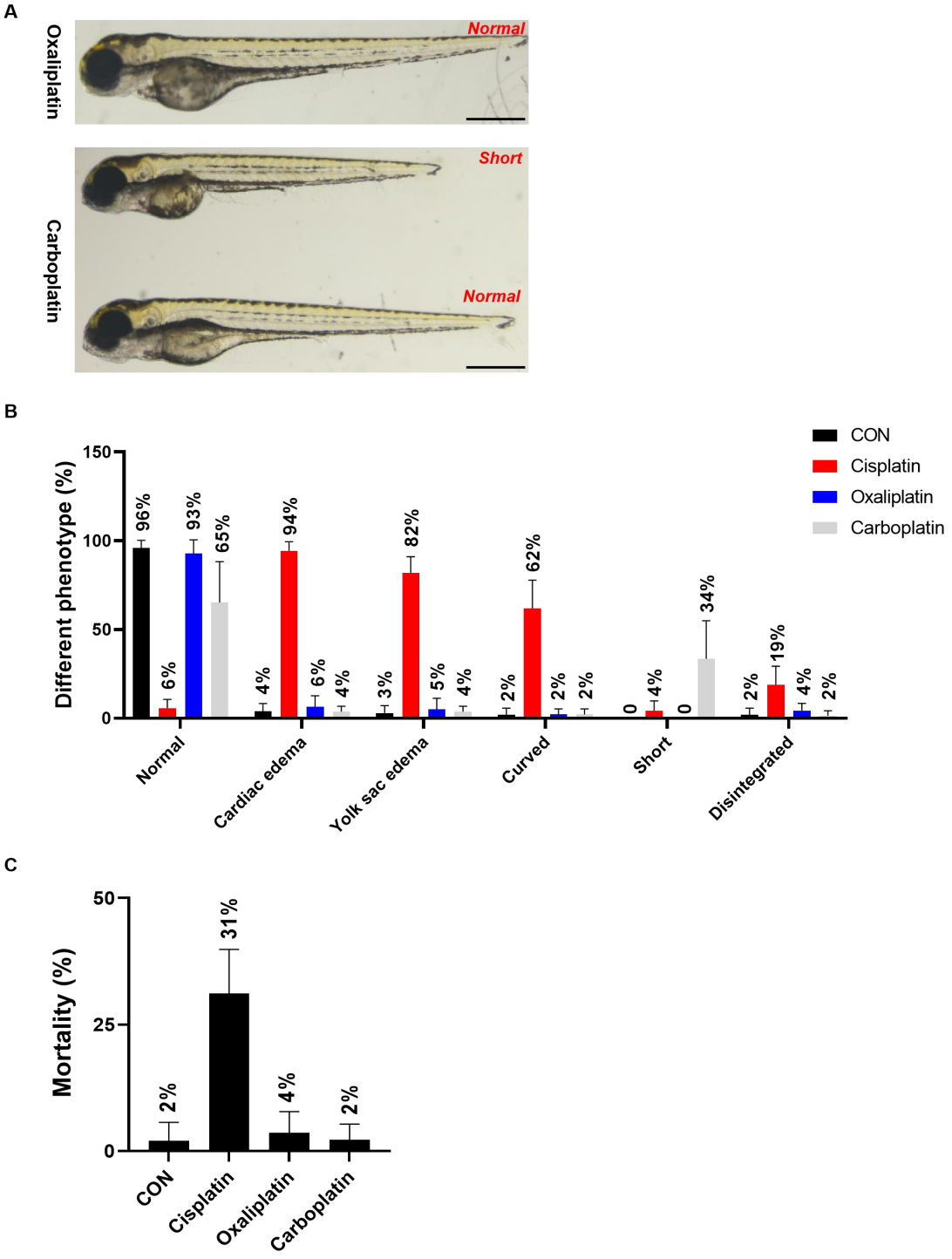

Figure 3.12 The phenotypic changes in 2 dpf zebrafish larvae following injection of the same dose of cisplatin, carboplatin, and oxaliplatin

(A) The phenotypic changes of 3 dpi (5 dpf) zebrafish larvae in the carboplatin or oxaliplatin-injected larvae. No changes were observed in the oxaliplatin group, while some larvae in the carboplatin group exhibited reduced body length.

(B) The percentage of different phenotypes of 5 dpf larvae in the control (CON), the cisplatin-injected (Cisplatin), the carboplatin-injected (Carboplatin), and the

oxaliplatin-injected (Oxaliplatin) injected groups, including the categories Normal, Cardiac edema, Yolk sac edema, Curved, Short, Disintegrated. The ‘Short’ phenotype represents zebrafish showing a reduction in body length without additional abnormal phenotypes like edema, as depicted in the carboplatin group of zebrafish in Figure A.
The CON group: 10 nl of 140 mM NaCl solution injected; The Cisplatin group: 10 nl of 3.3 mM cisplatin solution injected; The Carboplatin group: 10 nl of 3.3 mM carboplatin solution injected; The Oxaliplatin group: 10 nl of 3.3 mM oxaliplatin solution injected.
The scale bar is 0.5 mm (A).
Data are expressed as mean ± SD from eight independent experiments. For each experiment, 12 and 18 embryos were used for the CON and the Cisplatin/Carboplatin/Oxaliplatin group, respectively (A-B).

In conclusion, our study validated in zebrafish larval model that cisplatin exhibited stronger toxicity compared to carboplatin and oxaliplatin, a finding consistent with clinical outcomes [199].

3.4 Discussion

The subsequent discussion will primarily revolve around two main sections:

3.4.1 Assessment of cisplatin-induced nephrotoxicity based on phenotype alterations and mortality rate in zebrafish larvae

Previous studies on zebrafish embryo toxicity primarily involved adding drugs to the embryo medium. Similarly, in our laboratory we showed that incubating zebrafish larvae at 2 dpf with different concentrations of cisplatin resulted in malformations and mortality in larvae at 3-5 dpf. Lower concentrations of cisplatin (below 0.5 mg/ml) did not significantly affect zebrafish larval development or mortality. Yet, higher concentrations (above 1 mg/ml) caused substantial mortality at 4-5 dpf accompanied by disintegration of larvae, although without noticeable morphological abnormalities. These findings suggested that high concentrations of cisplatin administered via the embryo medium induce overall systemic failure in zebrafish rather than organ-specific toxicity leading to morphological abnormalities. However, the work of Wen et al. [133] and McCampbell et al. [118], has demonstrated that injection of nephrotoxic drugs such as gentamicin into zebrafish larvae can induce edema

formation. Similarly, although specific injection methods and dosages were not provided, Haentschel et al. demonstrated that cisplatin injection into 2 dpf zebrafish could induce varying degrees of edema formation [125]. These results prompted our consideration to improve the experimental method by replacing the previous microinjection targeting the cardinal vein region within the yolk sac with injections into the pericardiac space. This significantly improved injection efficiency and minimized the occurrence of blood cell clotting associated with cardinal vein injections. However, it should be noted that this method requires caution as the microinjection needle needs to pass through the yolk sac, increasing the risk of injection solution leaking into the yolk.

After injecting different concentrations of cisplatin, we determined that 10 nl of 3.3 mM cisplatin solution was the optimal dosage for drug injection. We observed that upon injection of this cisplatin dose, over 95% of the zebrafish embryos developed cardiac edema. Considering the subsequent experiments that involved the addition of inhibitors to restore the abnormal phenotypes induced by cisplatin, relying solely on cardiac edema as a single phenotype makes it challenging to classify the toxicity caused by cisplatin. Drawing from previous zebrafish embryo toxicity-related studies, we introduced multiple phenotypes or parameters for toxicity classification, including heart beat [200, 201], heart size [202], kidney edema [128], cardiac edema, yolk sac edema [203], cerebral edema [204], motility [205], and body curvature [206]. We observed that zebrafish injected with cisplatin initially developed cardiac edema, which gradually progressed to yolk sac edema. In more severe instances, the larvae displayed increased body curvature and lost motility leading to the eventual disintegration of zebrafish larvae. Combining the subsequent inhibitor-induced restoration of cisplatin-induced abnormal phenotypes, we ultimately selected five phenotypes for toxicity classification including cardiac edema, yolk sac edema, curved, motility, and disintegrated. Choosing these five phenotypes for toxicity classification was not only because

they could be rapidly screened using microscopy but also because other phenotypes or parameters had significant limitations. For instance, kidney edema (Cisplatin injection failed to induce bubble formation in the glomerulus region after *bbip1* morpholino injected as observed in Scheidecker et al. [128]), cerebral edema (Cisplatin injection did not cause brain edema after *samhd1* morpholino injected as seen in Kasher et al. [204]), heart beat (statistical complexities; substantial individual differences post-injection; inhibitors did not aid in restoring heartbeat affected by cisplatin), and heart size (limited reference value in toxicity classification based on heart size changes).

This phenotypic classification method, by combining multiple phenotypes, circumvents the limitations of using single criteria in many studies, effectively reflecting the toxicity induced by cisplatin. Additionally, we introduced the mortality rate as a secondary criterion to manifest the level of toxicity induced by cisplatin, calculated as the ratio of disintegrated larvae and larvae without a heartbeat to the total number of embryos. This inclusion of mortality rate, combined with phenotype classification, not only helps avoid controversies regarding lethal endpoints (such as no heartbeat [207] or disintegrated [208]) but also systematically demonstrates the toxicity caused by cisplatin.

It is worth noting that this study performed injections of the same cisplatin dosage in zebrafish embryos at both 2 and 3 dpf. The results confirmed that, regardless of whether the zebrafish embryos were at 2 or 3 dpf, upon reaching 5 dpf after injection with 10 nl of 3.3 mM cisplatin solution, over 95% of the embryos exhibited cardiac edema. Previous studies have debated whether zebrafish larvae at 2 or 3 dpf should be chosen for kidney research [125]. The key point of contention is that the development of the glomerulus and proximal tubules in zebrafish embryos at 2 dpf is not yet complete, and their functions are not fully mature. However, compared to zebrafish larvae at 3 dpf, those at 2 dpf have a larger pericardiac space, which facilitates embryo injection and reduces the likelihood of the injection fluid entering the yolk sac, thereby decreasing the possibility of injection failure. Overall, through a series of

experiments, we have demonstrated the advantages of using 2 dpf zebrafish larvae for cisplatin toxicity studies: they exhibit higher injection efficiency compared to zebrafish larvae at 3 dpf, while producing similar results.

Last but not least, we administered the same dosage of cisplatin, carboplatin, and oxaliplatin to 2 dpf zebrafish larvae. The results demonstrated that only cisplatin-induced edema and a higher mortality rate in zebrafish larvae. This finding not only confirmed the greater toxicity of cisplatin as observed in clinical data but also represented the first investigation on the relative toxicity of different platinum-based drugs upon injection into zebrafish larvae. It further validated the advantages and potential of zebrafish larvae as a model for studying platinum-based drug toxicity with relevance to human pathology.

3.4.2 Cisplatin-induced nephrotoxicity in zebrafish larvae

In the introduction, it was mentioned that drug-induced nephrotoxicity can ultimately lead to edema in zebrafish larvae. However, it is important to consider that nephrotoxicity is just one potential factor contributing to the occurrence of edema in zebrafish larvae, along with factors such as cardiac injury and abnormal vascular development. Although cisplatin is known to induce nephrotoxicity in clinical and mouse models, further verification is required in zebrafish larvae to link the occurrence of edema to kidney damage. To address this, we conducted three separate experiments focusing on renal function and tissue pathology. Indeed, some experimental results align with expectations and match previous research findings. On the other hand, some results do not align with expectations but still provide valuable reference for subsequent studies.

1 Dextran clearance analysis limitation

To assess renal function, we performed a co-injection of fluorescently labelled 10 kDa dextran and cisplatin, andthen observed the decay in fluorescence signal in a specific region of the dorsal aorta within 24 hours. In unperturbed zebrafish larval pronephron, 10 kDa dextran, due to its small size, can pass

through the podocyte barrier within the glomerulus and be excreted slowly [174]. Cisplatin can lead to a decrease in renal blood flow [136] and a reduction in glomerular filtration rate, and thus the excretion of 10 kDa dextran would be slow, resulting in increased retention within the blood vessels. However, quantifying the fluorescence decay in the blood vessels did not yield the expected results. The injection of cisplatin resulted in a significant reduction in the retention time of 10 kDa dextran. Previous studies reported the feasibility of this method for detecting kidney clearance in zebrafish larvae [209]. Yet, in our case, the injected dose of cisplatin might have disrupted the filtration barrier leading to uncontrolled, enhanced leakage of 10 kDa dextran.

Therefore, in addition to using 10 kDa dextran, we also injected 70 kDa dextran. In normal zebrafish larvae, 70 kDa dextran cannot pass through the podocyte barrier within the glomerulus due to its larger size, leading to its retention within the body [136]. Theoretically, due to the malfunctioning podocyte barrier within the glomerulus, the excretion of 70 kDa dextran would be accelerated, resulting in reduced retention time within the blood vessels [136]. We obtained the expected results when quantifying the fluorescence decay in the blood vessels. These results aligned with our expectations of a damaged glomerular barrier, which fits with the results obtained upon injection of 10 kDa dextran. In addition, the unexpected decrease in fluorescence intensity could also be a result of the loss of blood vessel barrier function, leading to the diffusion of 10 kDa dextran into other tissues.

2 SYTO-59 dye staining in live zebrafish

In order to study kidney injury at the tissue level, it is theoretically possible to use suitable kidney reporter lines for further research. In Chapter 1, Section 1.4.3, we have discussed the limitations of the available kidney reporter lines from the European Zebrafish Resource Center (EZRC). Fortunately, my colleague Masanari Takamiya discovered, in a serendipitous moment, that by injecting the SYTO-59 dye into zebrafish larvae, the positioning and architecture of the pronephric tubule can be observed within live zebrafish

larvae. This method still has some limitations, especially after injecting cisplatin or gentamicin. Some zebrafish larvae with yolk sac edema display an overly strong staining due to water accumulation in the kidney area, which might overshadow the signal of the pronephric tubule. However, this staining technique could visualize the position of the pronephric tubule in live zebrafish larva, serving as a complement to existing research, especially in the absence of appropriate kidney reporters.

Upon administering cisplatin to 3 dpf zebrafish larvae, we observed a reduction in the external diameter of the pronephric tubule, indicating an abnormal physiological state of the pronephric tubule, potentially interpreted as tubule constriction or tubule collapse. Numerous studies in other models have demonstrated that cisplatin can induce constriction of the pronephric tubule [191-193], with the primary cause being the decrease in glomerular filtration rate induced by cisplatin leading to reduced regional blood flow. We observed an overall decrease in blood flow after cisplatin injection, possibly causing this constriction to be more widespread, occurring not only in the pronephric tubule region. Additionally, in the analysis of potential pronephric tubule constriction, the term ‘luminal diameter’ is often used as a parameter in previous studies [210, 211]. However, accurately determining this parameter with our existing techniques has proven challenging, including difficulties in precisely determining the position of the proximal tubule in histologic sections and unclear lumen contours in confocal images.

In comparison to the analysis of potential pronephric tubule constriction, the term ‘tubule collapse’ can more intuitively reflect the abnormal physiological state of the pronephric tubule, indicating renal cell death. Previous studies demonstrated in other models that cisplatin can lead to the death of pronephric tubule epithelial cells, disrupting polarity and affecting reabsorption function [125, 194, 195]. Theoretically, zebrafish larvae would also experience the death of pronephric tubule epithelial cells after cisplatin injection, triggering the recruitment of more macrophages to eliminate potential inflammation in this

area. Interestingly, based on experiments with the macrophage reporter line, we did not observe a large number of macrophages in the pronephric tubule region of the cisplatin group. Regarding this phenomenon, two potential explanations are proposed:

a) Our study indicates that at the experimental dose of cisplatin injection, a large number of macrophages might undergo cell death, explaining the possibility of an insufficient number of macrophages recruited to this pronephric tubule area;

b) Compared to macrophages, other leukocytes may play a more critical role, such as neutrophils. Although no studies yet suggested the role of neutrophils in cisplatin-induced nephrotoxicity in zebrafish larval model, studies in other animal models have shown that the infiltration of neutrophils into the kidneys could exacerbate cisplatin-induced nephrotoxicity [212]. Subsequent experiments may consider further exploration by employing a neutrophil reporter line.

3 Histopathological accessment of nephrotoxicity in zebrafish model

In contrast to the functional analysis of the kidney, the histopathological changes in the tissues were more evident. Various renal markers were employed to investigate these changes, revealing alterations in the patterning of glomerular cells following cisplatin injection. Further examination of tissue sections unveiled the presence of cavities within the glomerulus, attributed to edema. Clinical studies have already confirmed that cisplatin not only disrupts the structure and function of the glomerulus but also affects the proximal tubule [125]. Unfortunately, our study could not replicate the use of all markers employed in other studies to detect proximal tubule abnormalities, possibly due to the relative depth of the proximal tubule in zebrafish larvae, making it difficult for the ISH probes to penetrate. Although the distal tubule is not the primary region for cisplatin-induced structural damage to the nephron, the *cdh17* ISH staining results indicate abnormal development of the distal tubule following cisplatin injection, which aligns with some clinical [213] and murine

[214, 215] model findings. Overall, cisplatin-induced kidney damage and led to the occurrence of tissue edema in zebrafish larvae.

To summarize, this part of the study took a whole year to complete and involved the collaboration of multiple research groups. It systematically summarized the methods for studying cisplatin toxicity in zebrafish larvae, including injection techniques and concentrations. It also encompassed the quantification of different phenotypes through morphological analysis and the assessment of nephrotoxicity. These findings lay the foundation for future mechanistic research.

4 GPER-ERK signaling regulates cisplatin-induced nephrotoxicity

4.1 Introduction

In chapter 1, the progress of research on cisplatin-induced nephrotoxicity has been illustrated, emphasizing the activation of MAPK and p53 as downstream signals, although its specific regulatory mechanisms are not fully understood. However, in the recent work in our laboratory, GPER has been introduced as a novel potential regulatory factor for cisplatin-induced apoptosis in several cancer cell lines [65].

GPER (G protein-coupled estrogen receptor), also known as GPR30, is a G protein-coupled receptor associated with estrogen signaling [66]. It belongs to the G protein-coupled receptor family and interacts with estrogens both inside and outside of cells, regulating various physiological and pathological processes.

No previous studies demonstrated the involvement of GPER in the regulation of cisplatin-induced nephrotoxicity, let alone the function of GPER in the kidney. Although there is no direct evidence to demonstrate that GPER can regulate renal cell apoptosis, it has been confirmed in distinct cells that GPER, as an upstream receptor, can activate MAPK [90, 95] or p53 [216] to promote apoptosis. Therefore, investigating GPER and subsequent signaling cascade such as MAPK or p53 could provide a new insight to understand the cisplatin induced nephrotoxicity.

This chapter, based on the morphological and mortality assessment of cisplatin-induced embryonic toxicity in Chapter 3, aims to explore the potential involvement of GPER-MAPK/p53 signaling in the regulation of cisplatin-induced nephrotoxicity using the zebrafish larval model.

4.2 Experimental design and procedures in brief

The experiments were conducted in four parts:

1) Examination whether chemical inhibition or knockdown of GPER rescues cisplatin-induced zebrafish larval malformation and mortality

This section utilizes two chemical inhibitors against GPER and knockdown of GPER by an anti-sense morpholino oligonucleotide.

A) Examination of the effect of GPER inhibitor G36 and G15 on the cisplatin-induced zebrafish larval malformation and mortality.

The experiments primarily involve the use of two different GPER inhibitors, G36 and G15 [217], replicating Iris Hansjosten's work on human cancer cells [65]. Schematic representation of the specific experimental timelines and set-up ispresented in the Chapter 4, Section 4.3.1.

B) Examination of the effect of GPER knockdown on cisplatin-induced zebrafish larval malformation and mortality

The morphological effects of morpholino-mediated GPER knockdown are assessed according to the criteria shown in Table 3.1 and Figure 3.4. The morpholino sequences (described in Chapter 2, Section 2.2.3) are derived from previous studies which established the GPER ATG-blocking morpholino (GPER ATG-MO) [145], GPER splice site morpholino (GPER SP-MO) [145], and control morpholino (CON MO) [146]. The dosage of injection was adjusted in this study, and the effectiveness of gene knockdown was validated. Schematic representation of the experimental timelines and set-up is presented in the Chapter 4, Section 4.3.3.

2) Examination whether inhibition of GPER function by GPER inhibitor G36 reverses cisplatin-induced zebrafish nephrotoxicity

This section focuses on nephrotoxicity, utilizing known kidney injury markers and a kidney pronephric duct marker to assess the effect of GPER inhibitor G36 after the injection of cisplatin. Two main approaches were employed:

A) Quantification of kidney injury markers using quantitative real-time PCR

This study employed quantitative real-time PCR to assess the expression of kidney injury-related genes, including kidney injury molecule 1 (*kim1*) [141,

142], clusterin (*clu*) [143], connective tissue growth factor (*ctgf*) [144].

After pre-treatment at 1 dpf with or without GPER inhibitor G36, zebrafish embryos were injected with or without cisplatin at 2 dpf. Zebrafish at 1 dpi (3 dpf) were collected for subsequent RNA extraction. The specific method of quantitative real-time PCR is outlined in Section 2.2.4 of Chapter 2. β-actin was chosen as a house keeping gene, because earlier study confirmed that this gene expression level was unchanged in various chemical treatments [218].

B) Kidney injury detection using whole mount immunohistochemistry (IHC)

In order to label the pronephric duct and examine morphological changes in the proximal tubule after cisplatin injection, ATP1A1 (α6f) antibody was used [198, 219]. The specific method for whole mount IHC is outlined in Chapter 2, Section 2.2.7. It is important to note that different fixation methods are employed for zebrafish embryos. Once again and emphasized here, while previous studies commonly used 4% PFA for tissue fixation, it is not suitable for ATP1A1 (α6f) antibody detection. Therefore, Dent's fixative (80% MeOH, 20% DMSO) was used for embryo fixation.

3) Examination whether inhibition of potential GPER downstream proteins reverses cisplatin-induced zebrafish larval malformation and mortality

After establishing GPER as a potential modulator of cisplatin-induced renal toxicity, further investigations are needed to identify the downstream proteins involved in this process. Considering Chapter 1, Sections 1.2 to 1.3, the MAPK family and p53 are potential GPER downstream proteins associated with the entire process. This section focuses on the use of various chemical inhibitors and genetic (morpholinos and mutant zebrafish line) methods to inhibit the functions of ERK and p53, caspases:

A) Examination of the effect of MEK inhibitors PD98059 or U0126 on cisplatin-induced zebrafish larval malformation and mortality

Two distinct MEK inhibitors, PD98059 [220] and U0126 [221], which prevent

activation of the downstream kinases ERK1 and 2 by MEK, were utilized in the experiment. Schematic representation of the specific experimental timelines and set-up is presented in the Chapter 4, Section 4.3.7.

B) Examination of the effect of pan-caspase inhibitor Q-VD-OPh on cisplatin-induced zebrafish larval malformation and mortality

Pan-caspase inhibitor Q-VD-OPh [222] was utilized in the experiment. Schematic representation of the specific experimental timelines and set-up ispresented in the Chapter 4, Section 4.3.8.

C) Examination of the effect of p53 morpholinos on cisplatin-induced zebrafish larval malformation and mortality

To knockdown p53, p53 ATG-blocking morpholino (p53 ATG-MO) [146], and control morpholino (CON MO) [146] were injected into one-cell stage zebrafish embryos. Schematic representation of the specific experimental timelines and set-up is presented in the Chapter 4, Section 4.3.9.

D) Examination of the effect of p53 knock-out on cisplatin-induced zebrafish larval malformation and mortality

A p53 knockout line previously published by the laboratory of Christine Blattner [150] was employed. Schematic representation of the specific experimental timelines and set-up is presented in the Chapter 4, Section 4.3.10.

4) Detection of signaling events through western blotting in response to cisplatin treatment and GPER functional inhibition

This section primarily utilizes western blotting to examine changes in the expression and post-translational modifications of downstream proteins, including three members of the MAPK family (ERK, p38, JNK) and their phosphorylated (activated) forms (phospho-ERK, phospho-p38, phospho-JNK), as well as p53 and its phosphorylated (activated) form (p-p53). The investigation is divided into three main parts:

a. Changes in downstream protein expression and phosphorylation after cisplatin injection.

b. Changes in downstream protein expression and phosphorylation after

GPER functional inhibition.

c. Changes in downstream protein expression and phosphorylation after the combination of GPER functional inhibition and cisplatin injection.

The specific method for western blotting is outlined in chapter 2, section 2.2.6. Vinculin will serve as loading control in the experiments [150]. It is important to note that compared to cell models derived from mice or humans, the availability of antibodies for specific detection of zebrafish proteins is limited. Therefore, during the experiment, different primary antibodies from various companies and sources were tested for their effectiveness.

4.3 Results

4.3.1 GPER is a potential modulator in cisplatin-induced nephrotoxicity

As mentioned earlier, GPER could be as a potential modulator in cisplatin-induced nephrotoxicity. As outlined in Chapter 3, the morphological changes and mortality assessment of zebrafish larvae could rapidly determine whether the functional inhibition of GPER affects cisplatin-induced nephrotoxicity. Moreover, by integrating parameters associated with renal injury, including various markers of kidney injury and pronephron morphological alterations, the impact of GPER on cisplatin-induced nephrotoxicity can be further delineated.

4.3.1.1 The GPER inhibitor G36 rescued cisplatin-induced abnormal phenotypes formation and high mortality

Two different GPER inhibitors, G36 and G15 [217], were employed in the experiments to investigate whether inhibition of GPER function could mitigate cisplatin-induced morphologic change and high mortality in zebrafish larvae. The experimental procedure involved inhibitors pre-treatment at 1 dpf, 3.3 mM cisplatin solution injection at 2 dpf, and phenotype and mortality analysis at 5

dpf (Figure 4.1A). The results revealed that, following pre-treatment with G36 solution either at 5, 10 or 20 μM, the abnormal phenotypes became less evident and the percentage of *Normal* embryos increased up to 33% in a G36 concentration dependent manner (Figure 4.1B). Accordingly, it accompanied by a dose-dependent and significantly reduced mortality caused by cisplatin-injection down to 9% upon 20 μM G36 pre-treatment, otherwise cisplatin mortality was as high as 42% without G36 pre-treated (Figure 4.1C). In contrast, G15 did not exhibit significant changes. The abnormal phenotypes in zebrafish did not show noticeable recovery with G15 pre-treatment (Figure 4.1D), and mortality remained high (Figure 4.1E). This outcome mirrors our findings in human cancer cells, demonstrating that G36, as opposed to G15, effectively attenuates the toxicity of cisplatin [65].

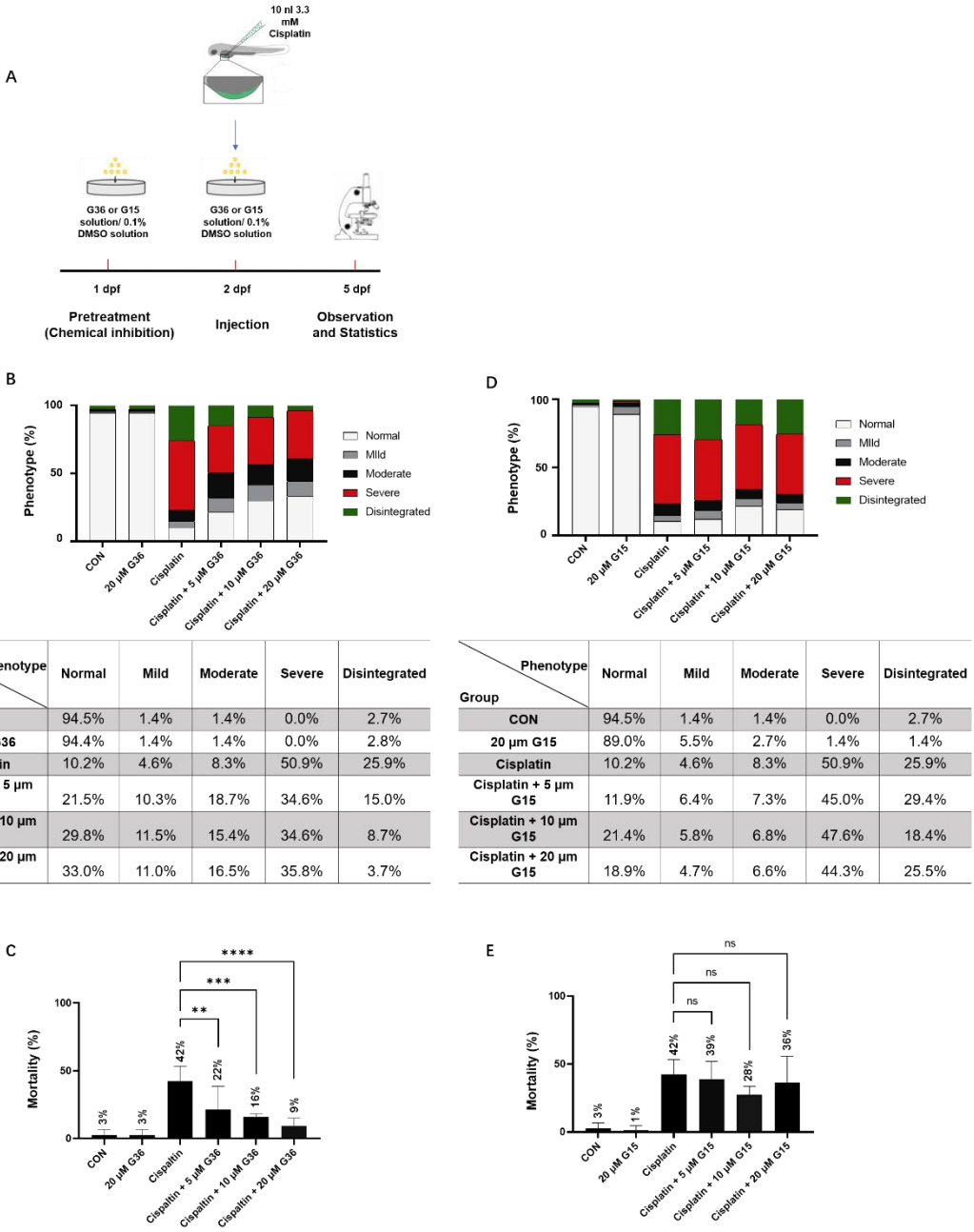

Group \ Phenotype	Normal	Mild	Moderate	Severe	Disintegrated
CON	94.5%	1.4%	1.4%	0.0%	2.7%
20 μm G36	94.4%	1.4%	1.4%	0.0%	2.8%
Cisplatin	10.2%	4.6%	8.3%	50.9%	25.9%
Cisplatin + 5 μm G36	21.5%	10.3%	18.7%	34.6%	15.0%
Cisplatin + 10 μm G36	29.8%	11.5%	15.4%	34.6%	8.7%
Cisplatin + 20 μm G36	33.0%	11.0%	16.5%	35.8%	3.7%

Group \ Phenotype	Normal	Mild	Moderate	Severe	Disintegrated
CON	94.5%	1.4%	1.4%	0.0%	2.7%
20 μm G15	89.0%	5.5%	2.7%	1.4%	1.4%
Cisplatin	10.2%	4.6%	8.3%	50.9%	25.9%
Cisplatin + 5 μm G15	11.9%	6.4%	7.3%	45.0%	29.4%
Cisplatin + 10 μm G15	21.4%	5.8%	6.8%	47.6%	18.4%
Cisplatin + 20 μm G15	18.9%	4.7%	6.6%	44.3%	25.5%

Figure 4.1 The GPER inhibitor G36 can alleviate cisplatin-induced abnormal phenotypes and high mortality, while G15 has no effect

(A) Schematic outline of experimental timelines and set-up. The inhibitors are all stored in 100% DMSO and diluted to working concentrations using E3 medium. Embryos without inhibitor treatment are placed in a 0.1% DMSO solution (diluted in E3 medium), equivalent to the DMSO content in a 20 μM G36/G15 solution. The experimental procedure involves the following steps: 1) Pre-treatment: Pre-treatment of G36/G15 solution or 0.1% DMSO solution (control) at 1 dpf. 2) Drug administration: Injection of 10 nl of 3.3 mM cisplatin solution or 10 nl of 140 mM NaCl solution (control) at 2 dpf. 3) Statistical analysis: Evaluation of phenotypic changes and mortality at 5 dpf.

Following annotations in the figure, the example of 'Cisplatin + 20 μM G36' is used for illustration that larvae were pretreated with 20 μM G36 solution at 1 dpf and 10 nl of 3.3

mM cisplatin solution were injected at 2 dpf.
(B) The phenotypic changes, following the phenotype classification shown in Table 3.1 and Figure 3.4, of 5 dpf zebrafish larvae across different groups to examine the effect of G36 pre-treatment on cisplatin-induced malformation.
(C) The mortality rates of 5 dpf zebrafish larvae across different groups to examine the effect of G36 pre-treatment on cisplatin-induced mortality.
(D) The phenotypic changes of 5 dpf zebrafish larvae across different groups to examine the effect of G15 pre-treatment on cisplatin-induced malformation.
(E) The mortality rates of 5 dpf zebrafish larvae among different groups to examine the effect of G15 pre-treatment on cisplatin-induced mortality.
The table below the bar chart represents the percentage distribution of five different phenotypes in different experimental groups as depicted in the bar chart (B and D).
Data are expressed as mean ± SD from six independent experiments. For each experiment, the non-cisplatin injected groups consisted of 12 embryos per group, while all cisplatin-injected groups contained 18 embryos per group.
All significance values were determined using Dunnett's test following one-way ANOVA. ns, $p \geq 0.05$; *, $0.01 \leq p < 0.05$; **, $p < 0.01$; ***, $p < 0.001$; ****, $p < 0.0001$.

4.3.1.2 GPER knockdown alleviated the formation of cisplatin-induced abnormal phenotypes and reduced high mortality

Although G36, a GPER inhibitor, mitigated the severity of cisplatin-induced abnormal phenotypes and mortality, as demonstrated in the previous section 4.3.2, considering the potential nonspecific effects of G36, the use of GPER gene knockdown tools, such as morpholinos, can further validate whether reducing GPER protein levels attenuates cisplatin-induced abnormal phenotypic formation and high mortality rates in zebrafish.

In the morpholinos effectiveness experiment, two distinct morpholinos previously validated for GPER knockdown were employed: GPER ATG-blocking MO (GPER ATG-MO) [145] and GPER splice site MO (GPER SP-MO) [145]. As a control for sequence-unspecific effects of morpholino, a mixture of morpholinos [146] with random targeting sequences ("CON MO") was injected into a separate group of embryos.

Chaturantabut et al. demonstrated that both GPER ATG-MO and GPER SP-MO effectively led to a reduction in liver size [145]. Using in situ hybridization (ISH) to assess the expression of *fabp10a* (a liver marker), the results indicated that compared to the CON MO injected group, the GPER

ATG-MO group exhibited a significant reduction in liver area among zebrafish larvae (Figure 4.2A-B). This aligns with the anticipated outcome, confirming the efficacy of GPER ATG-MO. However, after injection of the GPER SP-MO, no decrease in zebrafish larval liver size could be detected (Figure 4.2A-B), indicating the inefficacy of the GPER SP-MO.

To further analyze the effectiveness of the GPER SP-MO, three different primers were designed for subsequent detection of splicing: Ex1-F, Int-F, and Ex2-R (Figure 4.2C'), which correspond to forward primers targeting the Exon 1 and Intron 1, and a reverse primer targeting the Exon 2 of the GPER pre-mRNA, respectively. If the GPER SP-MO is effective, no splicing of the Intron 1 should be detected [223, 224]. Therefore, the cDNA obtained through reverse transcription should include also the sequence of Intron 1, and not just the spliced Exon 1 and Exon 2. By using PCR to amplify the DNA fragment between Ex1-F and Ex2-R, as well as between Int-F and Ex2-R, it was expected that in the CON MO group, only the DNA fragment between Ex1-F and Ex2-R is present, while the GPER SP-MO group would retain the DNA fragment between Int-F and Ex2-R, and a small amount or none of the DNA fragment between Ex1-F and Ex2-R. Conversely, if the splice site blocking MO is ineffective, in both the CON MO and GPER SP-MO groups only the DNA fragment between Ex1-F and Ex2-R is amplified, whereas the DNA fragment between Int-F and Ex2-R is not detectable due to efficient splicing of the pre-mRNA. Gel electrophoresis revealed that both the CON MO and GPER SP-MO group exhibited the DNA fragment between Ex1-F and Ex2-R, and only a very weak band of the DNA fragment between Int-F and Ex2-R in the GPER SP-MO group (Figure 4.2C''). This result further confirmed the ineffectiveness of the GPER SP-MO.

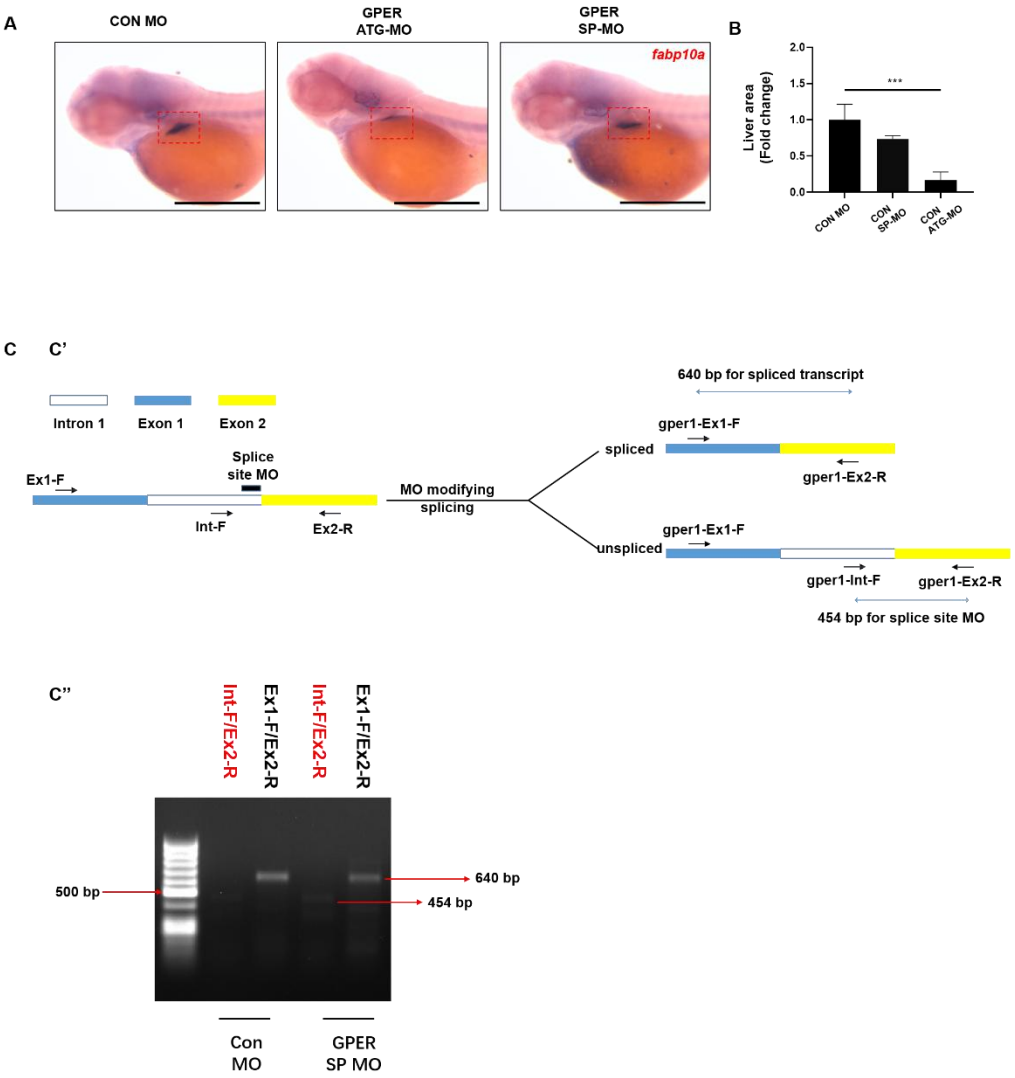

Figure 4.2 Validation of GPER morpholinos effectiveness

(A) Expression patterns of *fabp10a* in the CON MO-injected (CON MO), the GPER ATG-MO-injected (GPER ATG-MO) and the GPER SP-MO-injected (GPER SP-MO) group (4 dpf). The red box represents the liver-specific expression of *fabp10a*.

(B) Liver area (fold change from the CON MO) in the CON MO, the GPER ATG-MO and the GPER SP-MO group (4 dpf).

(C) Assessing the effectiveness of GPER SP-MO.

(C') The mechanism of GPER SP-MO and schematic diagram for designing primers to validate effectiveness.

(C'') Detecting PCR products in the the CON MO and the GPER SP-MO group by Gel electrophoresis.

The scale bar represents 0.5 mm for all panels (A).

Data are expressed as mean ± SD (n≥4 animals in each group). All significance values were determined using Dunnett's test following one-way ANOVA. ns, $p \geq 0.05$; *, $0.01 \leq p < 0.05$; **, $p < 0.01$; ***, $p < 0.001$; ****, $p < 0.0001$ (B).

Based on the efficacy test results of GPER morpholinos, the GPER ATG-MO

was employed in the experiment to investigate whether GPER knockdown could reduce cisplatin-induced edema formation and mortality in zebrafish larvae. The GPER ATG-MO could specifically target the start codon of GPER transcripts and block GPER translation. CON MO was injected into embryos as a control for sequence-unspecific effects of morpholino. The experimental procedure involves the following steps: CON MO or GPER ATG-MO injection at 1-4 cell stage embryos, cisplatin administration at 2 dpf, phenotype and mortality assessment at 5 dpf (Figure 4.3A). The results revealed that zebrafish larvae exhibited a certain degree of recovery in abnormal phenotypes following GPER knockdown by GPER ATG-MO, accompanied by a decrease in mortality rate (Figure 4.3B-C).

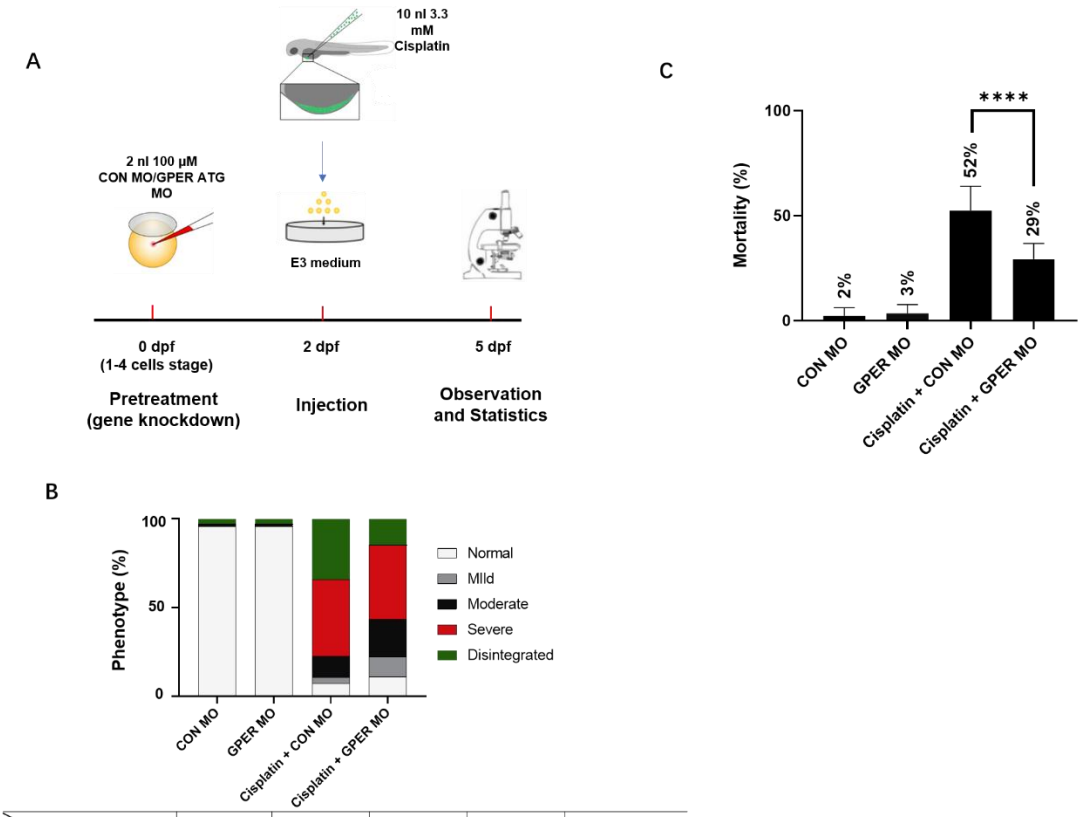

Group \ Phenotype	Normal	Mild	Moderate	Severe	Disintegrated
CON MO	95.8%	0.0%	1.4%	0.0%	2.8%
GPER MO	95.8%	0.0%	1.4%	0.0%	2.8%
Cisplatin + CON MO	7.2%	3.6%	11.7%	43.2%	34.2%
Cisplatin + GPER MO	11.1%	11.1%	21.3%	41.7%	14.8%

Figure 4.3 GPER knockdown alleviated the formation of cisplatin-induced abnormal phenotypes and reduced high mortality

(A) Schematic outline of experimental timelines and set-up. The experimental procedure involves the following steps: 1) Pre-treatment: Injection of GPER ATG-MO or CON MO (control) at 1-4 cell stage. 2) Drug administration: Injection of 10 nl of 3.3 mM cisplatin solution or 10 nl of 140 mM NaCl solution (control) at 2 dpf. 3) Statistical analysis: Evaluation of phenotypic changes and mortality at 5 dpf.
Following annotations in the figure, the example of 'Cisplatin + GPER MO' is used for illustration that zebrafish larvae were injected with 2 nl 100 μM GPER ATG-MO solution at 1-4 cell stage and injected with 10 nl of 3.3 mM cisplatin solution at 2 dpf.
(B) The phenotypic changes, following the phenotype classification shown in Table 3.1 and Figure 3.4, of 5 dpf zebrafish larvae across different groups to examine the effect of GPER knockdown by GPER ATG-MO on cisplatin-induced malformation.
(C) The mortality rates of 5 dpf zebrafish larvae among different groups to examine the effect of GPER knockdown by GPER ATG-MO on cisplatin-induced mortality.
The table below the bar chart represents the percentage distribution of five different phenotypes in each experimental group as depicted in the bar chart (B).
Data are expressed as mean ± SD from seven independent experiments. For each experiment, the non-cisplatin injected groups consisted of 12 embryos per group, while all cisplatin-injected groups contained 18 embryos per group (B-C).
All significance values were determined using Dunnett's test following one-way ANOVA. ns, $p \geq 0.05$; *, $0.01 \leq p < 0.05$; **, $p < 0.01$; ***, $p < 0.001$; ****, $p < 0.0001$.

4.3.1.3 The GPER inhibitor G36 or GPER knockdown do not rescue gentamicin-induced malformation

To ascertain that GPER inhibition specifically counters malformation and high mortality induced by cisplatin rather than exerting a general renoprotective effect, the impact of GPER inhibition on the effects of an alternate nephrotoxic drug, gentamicin, was assessed.

The experimental setup remained consistent with the aforementioned procedure for investigating the role of GPER in cisplatin toxicity, with the exception of replacing the 3.3 mM cisplatin solution with a 10 mg/ml gentamicin solution for injection (Figure 4.4A). The results indicate that pre-treatment with ATG-MO had no effect on the abnormal phenotypes or mortality rates induced by gentamicin (Figure 4.4D-E). Conversely, pre-treatment with G36 slightly exacerbated the abnormal phenotypes and mortality rates caused by gentamicin. *Normal* embryos decreased from 6.9% to 4.2%, while mortality rates increased from 17% to 20% (Figure 4.4B-C).

This observation indicated that the functional inhibition or knockdown of GPER

specifically suppressed cisplatin-induced edema, rather than having a general inhibitory effect on edema induced by other nephrotoxins, just like gentamicin. We will discuss and analyze in Chapter 4, Section 4.4, the reasons for choosing gentamicin instead of cisplatin to study the function of GPER, along with potential subsequent mechanism investigations.

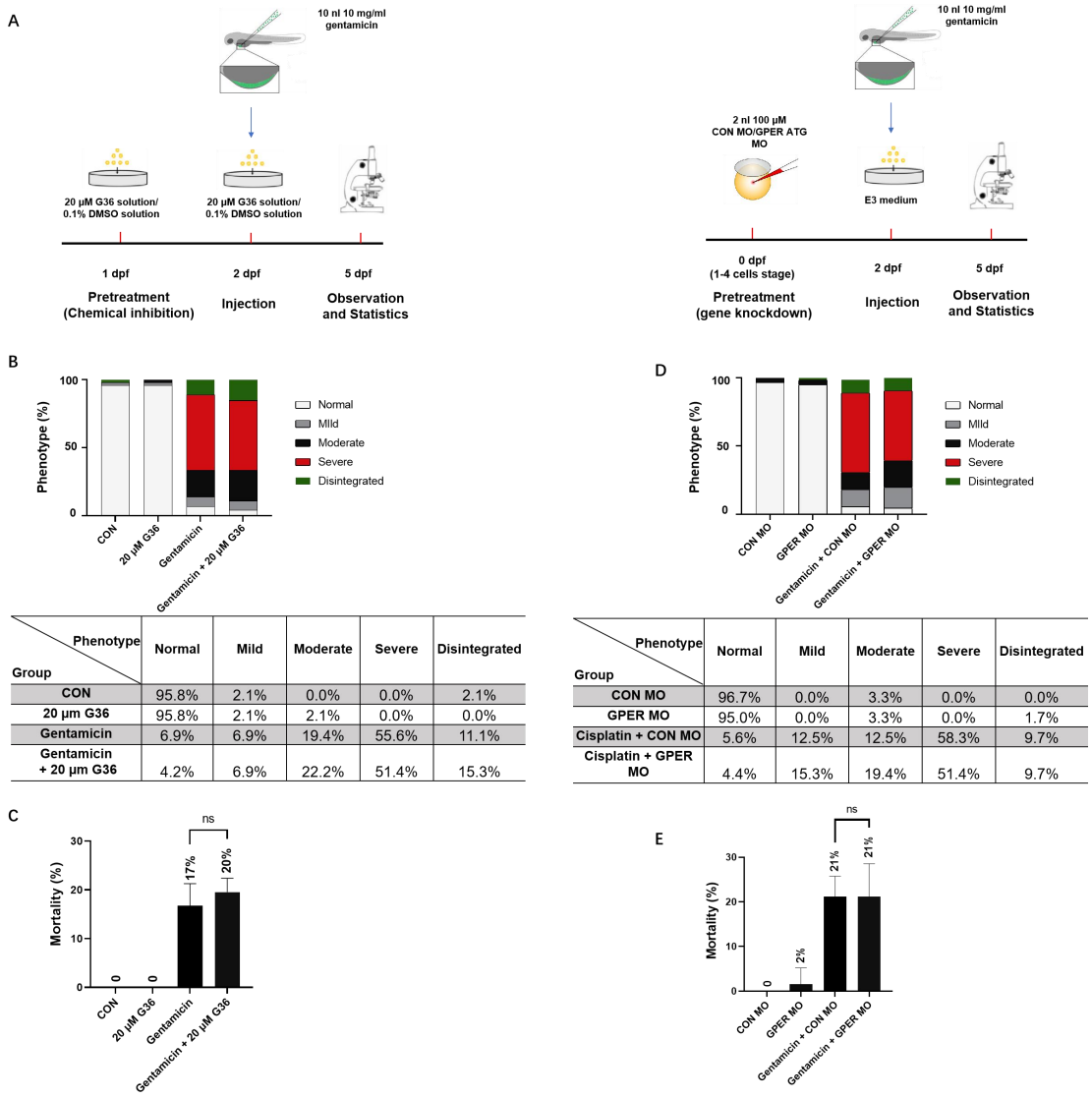

Group \ Phenotype	Normal	Mild	Moderate	Severe	Disintegrated
CON	95.8%	2.1%	0.0%	0.0%	2.1%
20 μm G36	95.8%	2.1%	2.1%	0.0%	0.0%
Gentamicin	6.9%	6.9%	19.4%	55.6%	11.1%
Gentamicin + 20 μm G36	4.2%	6.9%	22.2%	51.4%	15.3%

Group \ Phenotype	Normal	Mild	Moderate	Severe	Disintegrated
CON MO	96.7%	0.0%	3.3%	0.0%	0.0%
GPER MO	95.0%	0.0%	3.3%	0.0%	1.7%
Cisplatin + CON MO	5.6%	12.5%	12.5%	58.3%	9.7%
Cisplatin + GPER MO	4.4%	15.3%	19.4%	51.4%	9.7%

Figure 4.4 The GPER inhibitor G36 or GPER knockdown do not rescue gentamicin-induced mortality

(A) Schematic outline of experimental timelines and set-up. Left panel for GPER inhibitor G36 pre-treatment, right panel for GPER knockdown by GPER ATG-MO. The experimental procedure for Day 0 to 2 can be referred to in Figure 4.1A and 4.3A, including: 1) Pre-treatment: Gene knockdown tool - GPER ATG-MO or CON MO (control) injection at 1-4 cell stages embryos / Chemical inhibition - G36 solution or 0.1% DMSO solution (control) pre-treatment at 1 dpf. 2) Drug administration: Injection of 10 nl of 10 mg/ml gentamicin solution or 10 nl of 140 mM NaCl solution (control) at 2 dpf. 3) Statistical

analysis: Evaluation of phenotypic changes and mortality at 5 dpf.
Following annotations in the figure, the example of 'Gentamicin + 20 μM G36' is used for illustration that larvae were pretreated with 20 μM G36 solution at 1 dpf and 10 nl of 10 mg/ml gentamicin solution were injected at 2 dpf.
(B) The phenotypic changes, following the phenotype classification shown in Table 3.1 and Figure 3.4, of 5 dpf zebrafish larvae across different groups to examine the effect of G36 pre-treatment to gentamicin-induced abnormal phenotypes.
(C) The mortality rates of 5 dpf zebrafish larvae among different groups to examine the effect of G36 pre-treatment to gentamicin-induced mortality.
(D) The phenotypic changes of 5 dpf zebrafish larvae across different groups to examine the effect of GPER knockdown by GPER ATG-MO to gentamicin-induced abnormal phenotypes.
(E) The mortality rates of 5 dpf zebrafish larvae among different groups to examine the effect of GPER knockdown by GPER ATG-MO to gentamicin-induced mortality.
The table below the bar chart represents the percentage distribution of five different phenotypes in various experimental groups as depicted in the bar chart (B and D).
Data are expressed as mean ± SD from five independent experiments. For each experiment, the non-gentamicin injected groups consisted of 12 embryos per group, while all gentamicin-injected groups contained 18 embryos per group (B-E).
All significance values were determined using Dunnett's test following one-way ANOVA. ns, $p \geq 0.05$; *, $0.01 \leq p < 0.05$; **, $p < 0.01$; ***, $p < 0.001$; ****, $p < 0.0001$.

4.3.1.4 The GPER inhibitor G36 decreases the expression of cisplatin-induced kidney injury genes

It was determined that inhibition of GPER function reverses cisplatin-induced toxicity through changes in zebrafish phenotype and mortality rate. Considering nephrotoxicity as a potential significant factor leading to phenotype changes and mortality, subsequent experiments are required to validate the restorative effect of GPER functional inhibition on cisplatin-induced nephrotoxicity.

Quantitative real-time PCR (qPCR) was employed in the experiment to assess the expression of kidney injury-related genes across different groups, including kidney injury molecule 1 (*kim1*) [141, 142], clusterin (*clu*) [143], and connective tissue growth factor (*ctgf*) [144]. These genes show high expression in zebrafish larval models after exposure to different nephrotoxic agents [99]. Particularly, for *kim1*, the mRNA expression levels can increase by 2-3 times after treatment with gentamicin [99] and bacterial infection [133] in zebrafish

larvae. The qPCR results revealed that the mRNA levels of *kim1*, *clu* and *ctgf* were significantly increased in response to cisplatin stimulation. The use of the GPER inhibitor G36 reduced the elevated expression induced by cisplatin (Figure 4.5). These findings underscored the protective effect of G36 against cisplatin-induced nephrotoxicity.

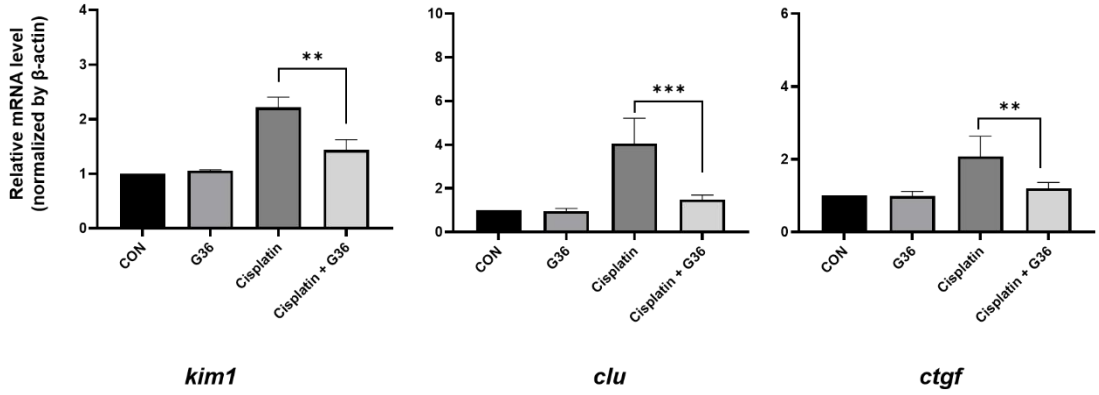

Figure 4.5 The GPER inhibitor G36 decreases the expression of cisplatin-induced kidney injury genes in mRNA level

Expression of *kim1, clu* and *ctgf* in 3 dpf zebrafish larvae across different groups to examine the effect of G36 pre-treatment to cisplatin-induced kidney injury. β-actin was used as the house keeping gene.

The experimental procedure for Day 0 to 2 can be referred to in Figure 4.3A. The experimental procedure involves the following steps: 1) Pre-treatment: Pre-treatment of 20 μM G36 solution or 0.1% DMSO solution (control) at 1 dpf. 2) Drug administration: Injection of 10 nl of 3.3 mM cisplatin solution or 10 nl of 140 mM NaCl solution (control) at 2 dpf. 3) RNA extraction: RNA extraction was done at 3 dpf.

Following annotations in the figure, the example of 'Cisplatin + G36' is used for illustration that larvae were pretreated with 20 μM G36 solution at 1 dpf and 10 nl of 3.3 mM cisplatin solution were injected at 2 dpf.

Data are expressed as mean ± SD from four independent experiments. Each experiment involved RNA extraction from over 30 embryos per group.

All significance values were determined using Dunnett's test following one-way ANOVA. ns, $p \geq 0.05$; *, $0.01 \leq p < 0.05$; **, $p < 0.01$; ***, $p < 0.001$; ****, $p < 0.0001$.

4.3.1.5 The GPER inhibitor G36 restores the reduced diameter of the proximal tubule induced by cisplatin

Previous research established that by monitoring the ATP1A1 protein [198, 219], morphological changes in the pronephric duct can be detected at the whole mount level. While IHC results may not display overt morphological

changes, such as tubule bending due to potential edema (Figure 4.6 A), the width of the proximal tubule in the cisplatin group noticeably diminished compared to the control group (Figure 4.6 B) which is similar to the SYTO-59 dye staining in living zebrafish larvae (Figure 3.7). These results indicated the abnormal constriction or collapse of the proximal tubule under cisplatin stimulation. Upon pre-treatment with the GPER inhibitor G36, the width of the proximal tubule in the Cisplatin + G36 group significantly increased compared to the cisplatin group (Figure 4.6 B). We will discuss and analyze the potential reasons for cisplatin-induced reduction in proximal tubule diameter and the restoration by G36 in the Chapter 4, Section 4.4.

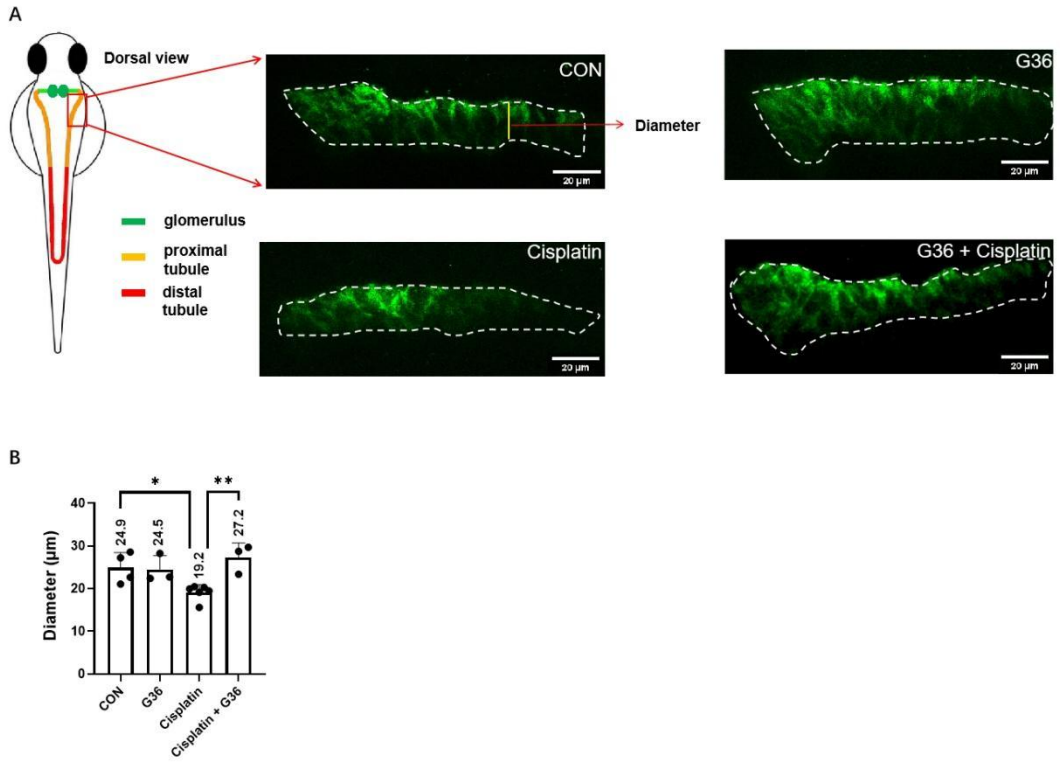

Figure 4.6 The GPER inhibitor G36 restore the reduced diameter of the proximal tubule induced by cisplatin

(A) ATP1A1 antibody staining in the 3 dpf zebrafish larvae. The confocal image (maximum projected view of z-stack) shows the red-framed area depicted in the schematic. The fluorescence signal represents the pronephric area which was stained by ATP1A1 antibody and the white dotted line indicates the boundary of the pronephric tubule.

(B) Changes in the diameter of the pronephric tubule in the different groups with/without 20 μM G36 pre-treatment. The diameter of the pronephric tubule is indicated by the yellow vertical line in Figure A, and the individual diameter length used for statistics is the

average taken from five different positions of the pronephric tubule.
The experimental procedure for Day 0 to 2 can be referred to in Figure 4.3A. The experimental procedure involves the following steps: 1) Pre-treatment: Pre-treatment of G36 solution or 0.1% DMSO solution (control) at 1 dpf. 2) Drug administration: Injection of 10 nl of 3.3 mM cisplatin solution or 10 nl of 140 mM NaCl solution (control) at 2 dpf. 3) IHC: IHC was done at 3 dpf.
In the figure, the example of 'Cisplatin + G36' is used for illustration that larvae were pretreated with 20 μM G36 solution at 1 dpf and 10 nl of 3.3 mM cisplatin solution were injected at 2 dpf.
The scale bar is shown in the figure (A).
Data are expressed as mean ± SD (n≥3 animals in each group) (B).
All significance values were determined using Dunnett's test following one-way ANOVA. ns, p≥0.05; *, 0.01≤p<0.05; **, p<0.01; ***, p<0.001; ****, p<0.0001.

4.3.1.6 Summary

The significant attenuation of abnormal phenotypes and reduced mortality rates induced by cisplatin post-GPER inhibition using GPER inhibitor G36 and GPER ATG MO suggests a potential reparative effect of GPER functional inhibition against cisplatin-induced nephrotoxicity. By introducing gentamicin, a nephrotoxin with a completely different mechanism of inducing nephrotoxicity, the specific role of GPER in cisplatin-induced nephrotoxicity was established, indicating that inhibition of GPER function is not solely associated with widespread renal protection. Finally, the substantial reduction of high expression of cisplatin-induced kidney injury markers and restoration of the diminished diameter of proximal tubules post-GPER inhibition highlights the potential role of GPER as a modulator in cisplatin-induced nephrotoxicity.

4.3.2 GPER-ERK signaling regulates cisplatin-induced nephrotoxicity

Previous studies demonstrated that cisplatin can stimulate elevated expression of MAPK in renal cells [57-61]. MAPK, as an important downstream protein of GPER, participates in regulating various physiological responses, especially apoptosis [90, 95]. Hence, the GPER-MAPK signaling might serve as a potential regulatory pathway involved in cisplatin-induced nephrotoxicity.

The MAPK family primarily includes ERK, p38, and JNK. It is essential to initially determine, at the protein level, the impact of cisplatin and GPER functional inhibition on the expression of these three downstream proteins to ascertain whether MAPK is regulated by GPER. Subsequently, through zebrafish phenotype and mortality rate experiments, it is necessary to establish whether MAPK inhibition affects cisplatin-induced toxicity, thereby determining if GPER-MAPK regulates cisplatin-induced zebrafish nephrotoxicity.

4.3.2.1 Cisplatin-induced ERK activation is blocked by the GPER inhibitor G36 and GPER knockdown

To further substantiate this hypothesis (GPER-MAPK signaling in cisplatin induced nephrotoxicity), western blotting was employed to assess the changes in phosphorylated ERK (p-ERK), an indicator of ERK activation, at the protein level. The Cisplatin group exhibited an increase in p-ERK levels compared to the CON group. However, upon inhibiting GPER function (by G36 or GPER ATG-MO), the elevated p-ERK level induced by cisplatin was decreased (Figure 4.7A-B). These results indicate that ERK, as a potential downstream protein of GPER, is involved in the process of cisplatin-induced nephrotoxicity in zebrafish larval model (Figure 4.7C).

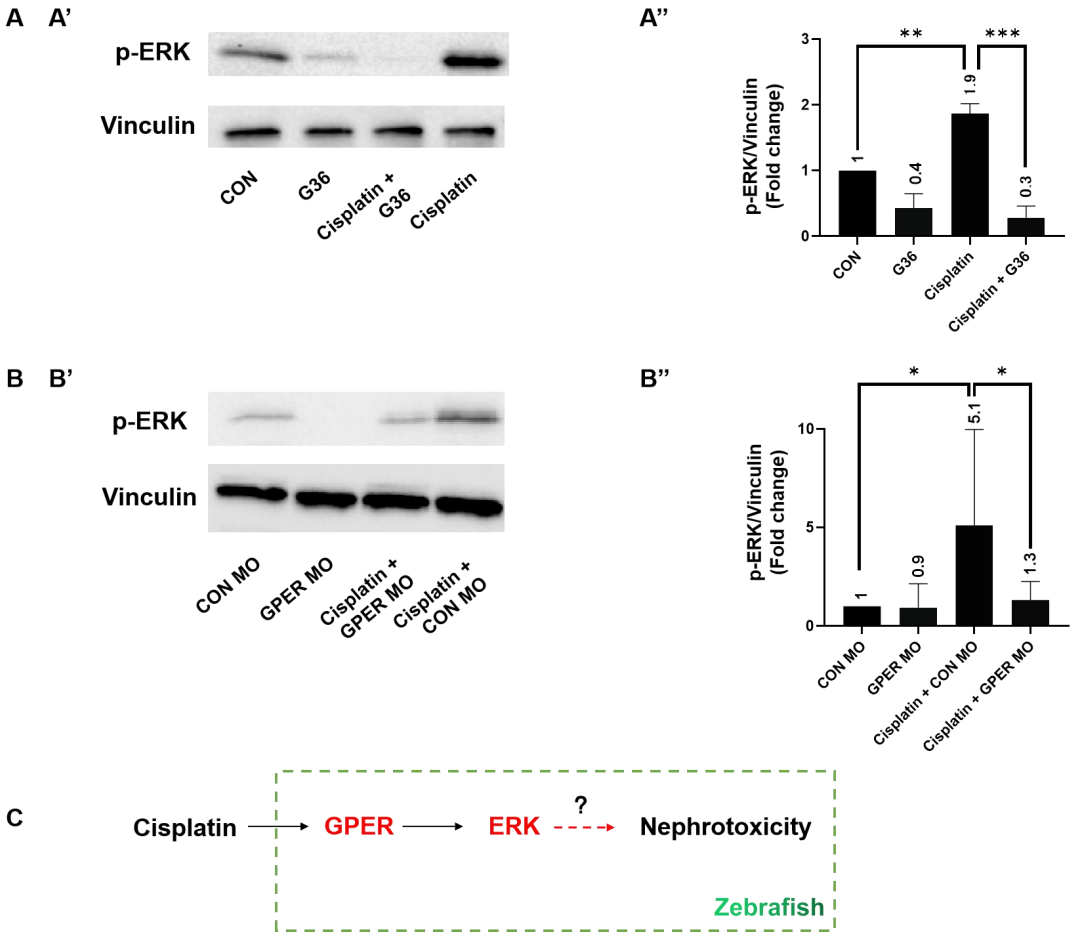

Figure 4.7 Inhibition of GPER using G36 and GPER ATG-MO blocks cisplatin-induced ERK activation

(A) Amount of phosphorylated ERK (p-ERK) in 3 dpf zebrafish larvae across different groups with/without G36 pre-treatment.

(B) Amount of phosphorylated ERK (p-ERK) in 3 dpf zebrafish larvae across different groups with/without GPER knockdown by GPER ATG-MO.

Left panel shows a representative result (A' and B'), while the right panel presents the quantification of relative p-ERK levels normalized to the intensity of the loading control Vinculin for the different conditions (A'' and B'').

(C) Based on protein detection results, ERK could be a potential downstream protein of GPER to regulate the process of cisplatin-induced nephrotoxicity in zebrafish larval model.

G36 are all stored in 100% DMSO and diluted to working concentrations using E3 medium. Embryos without inhibitor treatment are placed in a 0.1% DMSO solution (diluted in E3 medium), equivalent to the DMSO content in a 20 μM G36 solution. The experimental procedure for Day 0 to 2 can be referred to in Figure 4.1A and 4.3A, including: 1) Pre-treatment: Gene knockdown tool - GPER ATG-MO or CON MO (control) injection at 1-4 cell stages embryos / Chemical inhibition – 20 μM G36 solution or 0.1% DMSO solution (control) pre-treatment at 1 dpf. 2) Drug administration: Injection of 10 nl of 3.3 mM cisplatin solution or 10 nl of 140 mM NaCl solution (control) at 2 dpf. 3) Protein extraction: whole amount proteins were extracted at 3 dpf.

In the figure, the example of ‘Cisplatin + G36’ is used for illustration that larvae were pretreated with 20 μM G36 solution at 1 dpf and 10 nl of 3.3 mM cisplatin solution were injected at 2 dpf.
p-ERK levels are quantified from multiple densitometry scans based on the signals obtained for p-ERK and Vinculin, which was used as a loading control. The relative intensity ratios of p-ERK/Vinculin are plotted and have been set to 1 for the controls (A’’ and B’’).
Black solid arrows (—) represent signal transduction experimentally confirmed in this thesis. Red dotted arrows (— — —) with a question mark (?) represent potential signal transduction requiring additional experimental investigations (C).
Data are expressed as mean ± SD from three independent experiments. Each experiment involved protein extraction from 30 embryos per group (A’’ and B’’).
All significance values were determined using Dunnett’s test following one-way ANOVA. ns, $p \geq 0.05$; *, $0.01 \leq p < 0.05$; **, $p < 0.01$; ***, $p < 0.001$; ****, $p < 0.0001$.

4.3.2.2 p38 activation was not influenced by cisplatin and GPER knockdown

In addition to ERK, previous studies have confirmed that p38 [59], as another member of the MAPK family, is also involved in cisplatin-induced nephrotoxicity. Western blotting was employed to assess alterations in the phosphorylation of p38 (p-p38), indicative of p38 activation, across different experimental groups. The findings revealed that, compared to the control (CON) group, there were no discernible changes in p-p38 levels within the cisplatin-treated group. Similarly, upon functional inhibition of GPER using GPER ATG-MO, there were no observable changes in the phosphorylation of p38 (Figure 4.8A-B). These results indicate that p38 could not serve as a potential downstream protein of GPER to regulate the process of cisplatin-induced nephrotoxicity in zebrafish larval model (Figure 4.8B).

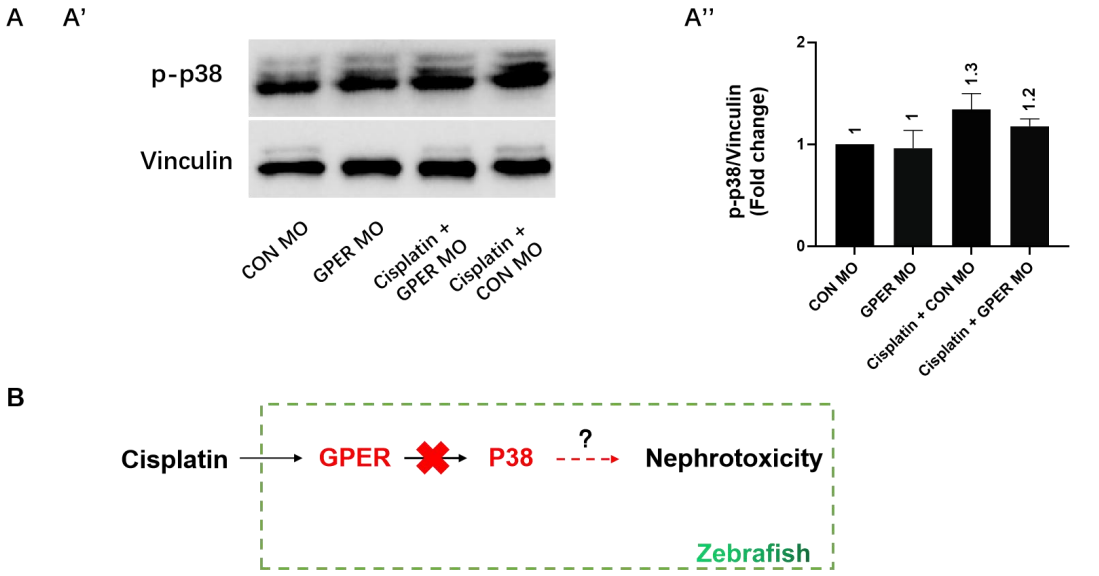

Figure 4.8 p38 activation was not influenced by cisplatin and GPER knockdown

(A) Amount of phosphorylated p38 (p-p38) in 3 dpf zebrafish larvae across different groups with/without GPER knockdown by GPER ATG-MO. Left panel shows a representative result (A'), while the right panel presents the quantification of relative p-p38 levels normalized to the intensity of the loading control Vinculin for the different conditions (A'').

(B) Based on protein detection results, p38 could not serve as a potential downstream protein of GPER to regulate the process of cisplatin-induced nephrotoxicity in zebrafish larval model.

The experimental procedure for Day 0 to 2 can be referred to in Figure 4.3A, including: 1) Pre-treatment: Injection of GPER ATG-MO or CON MO (control) at 1-4 cell stage. 2) Drug administration: Injection of 10 nl of 3.3 mM cisplatin solution or 10 nl of 140 mM NaCl solution (control) at 2 dpf. 3) Protein extraction: whole amount proteins were extracted at 3 dpf.

In the figure, the example of 'Cisplatin + GPER MO' is used for illustration that larvae were pretreated with 2 nl 100 μM GPER ATG-MO solution at 0-2 hpf and 10 nl of 3.3 mM cisplatin solution were injected at 2 dpf.

p-p38 levels are quantified from multiple densitometry scans based on the signals obtained for p-p38 and Vinculin, which was used as a loading control. The relative intensity ratios of p-p38/Vinculin are plotted and have been set to 1 for the controls (A'').

Black solid arrows (—) represent signal transduction experimentally confirmed in this thesis. Red dotted arrows (— — —) with a question mark (**?**) represent potential signal transduction requiring additional experimental investigations. Black solid arrows (—) with a red cross mark (**X**) represent signal transduction identified to be false in this thesis (B).

Data are expressed as mean ± SD from two independent experiments. Each experiment involved protein extraction from 30 embryos per group (A'').

All significance values were determined using Dunnett's test following one-way ANOVA. ns, $p \geq 0.05$; *, $0.01 \leq p < 0.05$; **, $p < 0.01$; ***, $p < 0.001$; ****, $p < 0.0001$.

4.3.2.3 Inhibition of ERK by PD98059 and U0126 rescued cisplatin-induced abnormal phenotypes formation and high mortality

To investigate whether inhibiting ERK function could mitigate cisplatin-induced abnormal phenotypes and high mortality in zebrafish larvae, two distinct MEK inhibitors, PD98059 [220] and U0126 [221], which prevent activation of the downstream kinases ERK1 and 2 by MEK, were utilized. The experimental procedure involved inhibitors pre-treatment at 1 dpf, 3.3 mM cisplatin solution injection at 2 dpf, and phenotype and mortality analysis at 5 dpf (Figure 4.9A). The results revealed that, following pre-treatment with PD98059 or U0126 either at 10 or 20 μM, the abnormal phenotypes became less evident and the percentage of *Normal* embryos increased up to approximately 20% in a PD98059/U0126 concentration dependent manner (Figure 4.9B). Accordingly, it accompanied by a dose-dependent and significantly reduced mortality caused by cisplatin-injection down to approximately 10% upon 20 μM PD98059 or U0126 pre-treatment, otherwise cisplatin mortality was as high as 54% without PD98059 or U0126 pre-treatment (Figure 4.9C). Combining with protein detection results in Section 4.3.2.1, these results confirmed that GPER-ERK signaling regulates cisplatin-induced nephrotoxicity.

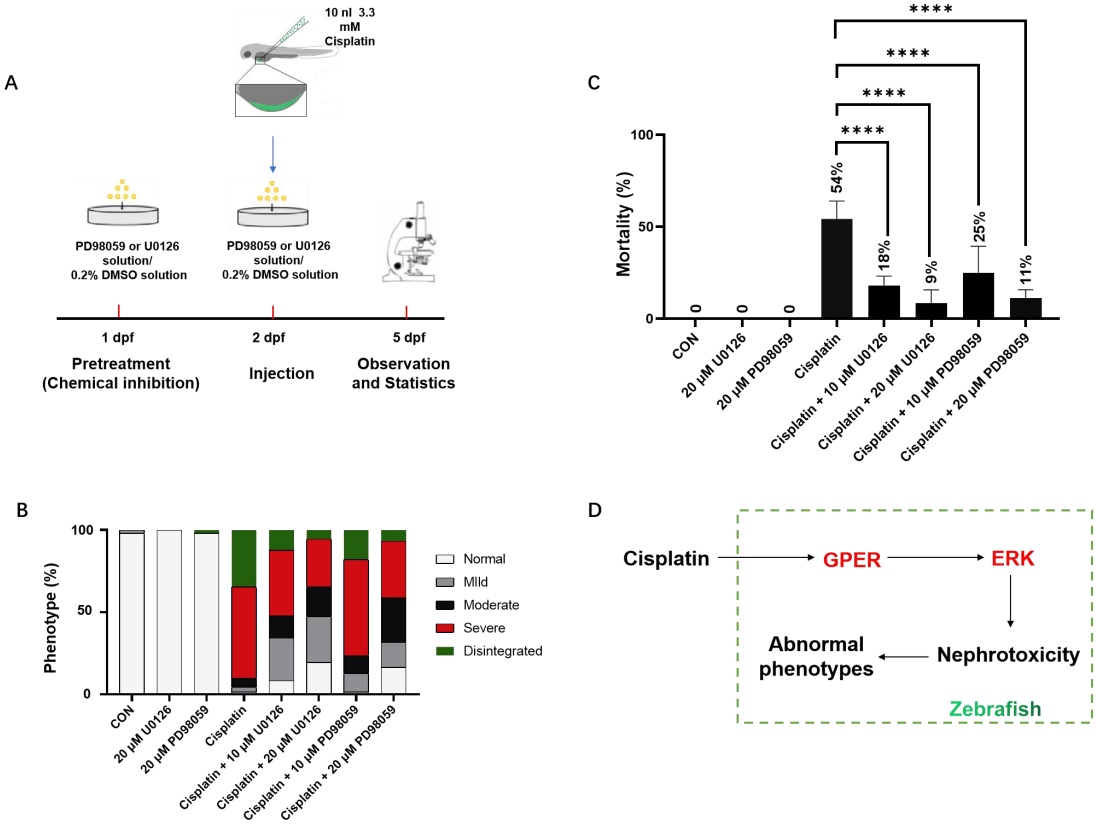

Group \ Phenotype	Normal	Mild	Moderate	Severe	Disintegrated
CON	97.9%	2.1%	0.0%	0.0%	0.0%
20 μM U0126	100.0%	0.0%	0.0%	0.0%	0.0%
20 μM PD98059	97.9%	0.0%	0.0%	0.0%	2.1%
Cisplatin	1.4%	2.8%	5.6%	55.6%	34.7%
Cisplatin + 10 μM U0126	8.2%	26.0%	13.7%	39.7%	12.3%
Cisplatin + 20 μM U0126	19.4%	27.8%	18.1%	29.2%	5.6%
Cisplatin + 10 μM PD98059	1.4%	11.1%	11.1%	58.3%	18.1%
Cisplatin + 20 μM PD98059	16.4%	15.1%	27.4%	34.2%	6.8%

Figure 4.9 Inhibition of ERK by PD98059 and U0126 rescued cisplatin-induced abnormal phenotypes formation and high mortality

(A) Schematic outline of experimental timelines and set-up. The inhibitors are all stored in 100% DMSO and diluted to working concentrations using E3 medium. Embryos without inhibitor treatment are placed in a 0.2% DMSO solution (diluted in E3 medium), equivalent to the DMSO content in a 20 μM PD98059/U0126 solution. The experimental procedure involves the following steps: 1) Pre-treatment: Pre-treatment of PD98059/U0126 solution or 0.2% DMSO solution (control) at 1 dpf. 2) Drug administration: Injection of 10 nl of 3.3 mM cisplatin solution or 10 nl of 140 mM NaCl solution (control) at 2 dpf. 3) Statistical analysis: Evaluation of phenotypic changes and mortality at 5 dpf.

Following annotations in the figure, the example of 'Cisplatin + 20 μM PD98059' is used for illustration that larvae were pretreated with 20 μM PD98059 solution at 1 dpf and 10 nl of 3.3 mM cisplatin solution were injected at 2 dpf.

(B) The phenotypic changes, following the phenotype classification shown in Table 3.1 and Figure 3.4, of 5 dpf zebrafish larvae across different groups to examine the effect of

PD98059 or U0126 pre-treatment on cisplatin-induced malformation.
(C) The mortality rates of 5 dpf zebrafish larvae among different groups to examine the effect of PD98059 or U0126 pre-treatment to cisplatin-induced mortality.
(D) GPER-ERK signaling regulates cisplatin-induced nephrotoxicity.
The table below the bar chart represents the percentage distribution of five different phenotypes in various experimental groups as depicted in the bar chart (B).
Black solid arrows (—) represent signal transduction experimentally confirmed in this thesis (D).
Data are expressed as mean ± SD from four independent experiments. For each experiment, the non-cisplatin injected groups consisted of 12 embryos per group, while all cisplatin-injected groups contained 18 embryos per group (B-C).
All significance values were determined using Dunnett's test following one-way ANOVA. ns, $p \geq 0.05$; *, $0.01 \leq p < 0.05$; **, $p < 0.01$; ***, $p < 0.001$; ****, $p < 0.0001$.

4.3.2.4 The pan-caspase inhibitor Q-VD-OPh alleviated the formation of cisplatin-induced abnormal phenotypes and reduced high mortality

In these experiments, the pan-caspase inhibitor Q-VD-OPh [222] was employed to assess whether inhibiting caspases could mitigate cisplatin-induced edema formation and mortality in zebrafish larvae. The experimental procedure involved inhibitor pre-treatment at 1 dpf, 3.3 mM cisplatin solution injection at 2 dpf, and phenotype and mortality analysis at 5 dpf (Figure 4.10A). The results revealed that, following pre-treatment with Q-VD-OPh at 50 μM, the abnormal phenotypes became less evident and the percentage of *Normal* embryos increased up to 11% (Figure 4.10B). Accordingly, it accompanied by a significantly reduced mortality caused by cisplatin-injection down to approximately 19% upon 50 μM Q-VD-OPh pre-treatment, otherwise cisplatin mortality was as high as 45% without Q-VD-OPh pre-treatment (Figure 4.10C). Considering previous studies that have confirmed cisplatin could activate caspases following ERK activation to trigger apoptosis of renal cells [60, 63], GPER-ERK-caspases is a potential signaling regulating cisplatin-induced nephrotoxicity.

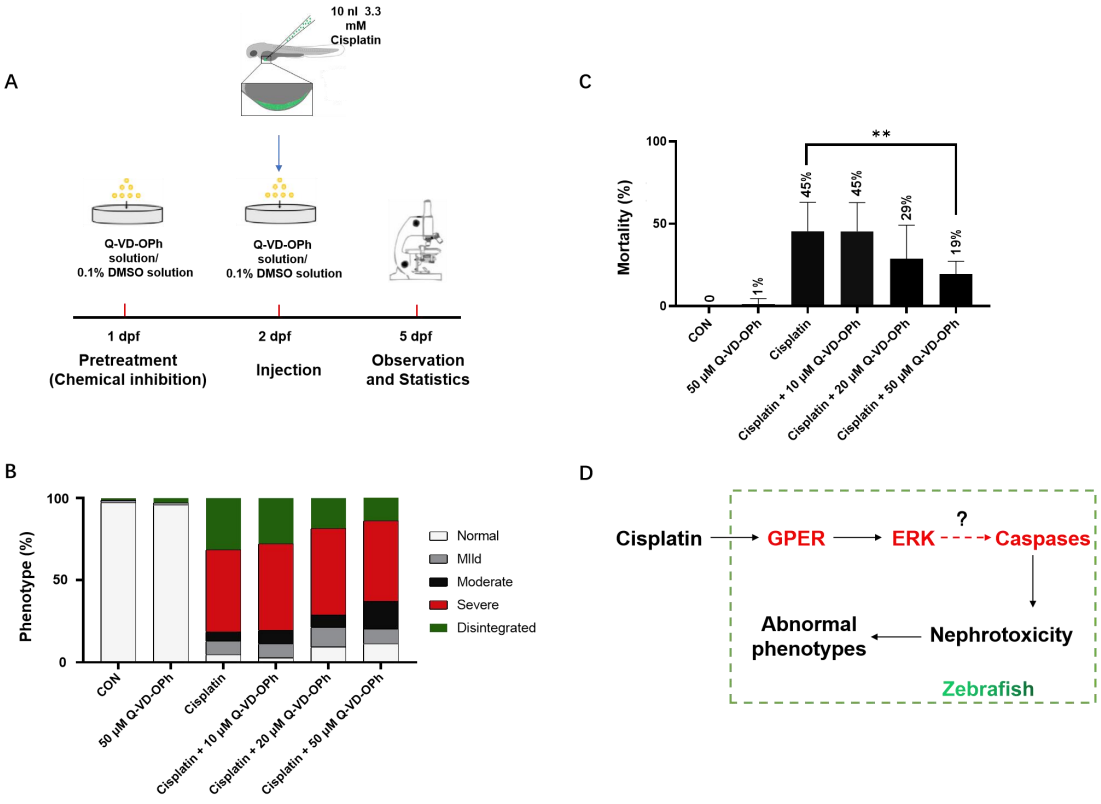

Group \ Phenotype	Normal	Mild	Moderate	Severe	Disintegrated
CON	97.2%	1.4%	0.0%	0.0%	1.4%
50 μM Q-VD-OPh	95.8%	1.4%	0.0%	0.0%	2.8%
Cisplatin	4.6%	8.3%	5.6%	50.0%	31.5%
Cisplatin + 10 μM Q-VD-OPh	2.8%	8.3%	8.3%	52.8%	27.8%
Cisplatin + 20 μM Q-VD-OPh	9.3%	12.0%	7.4%	52.8%	18.5%
Cisplatin + 50 μM Q-VD-OPh	11.1%	9.3%	16.7%	49.1%	13.9%

Figure 4.10 The pan-caspase inhibitor (Q-VD-OPh) alleviated the formation of cisplatin-induced abnormal phenotypes and reduced high mortality

(A) Schematic outline of experimental timelines and set-up. Q-VD-OPh is stored in 100% DMSO and diluted to working concentrations using E3 medium. Embryos without inhibitor treatment are placed in a 0.1% DMSO solution (diluted in E3 medium), equivalent to the DMSO content in a 50 μM Q-VD-OPh solution. The experimental procedure involves the following steps: 1) Pre-treatment: Pre-treatment of Q-VD-OPh solution or 0.2% DMSO solution (control) at 1 dpf. 2) Drug administration: Injection of 10 nl of 3.3 mM cisplatin solution or 10 nl of 140 mM NaCl solution (control) at 2 dpf. 3) Statistical analysis: Evaluation of phenotypic changes and mortality at 5 dpf.

Following annotations in the figure, the example of 'Cisplatin + 50 μM Q-VD-OPh' is used for illustration that larvae were pretreated with 50 μM Q-VD-OPh solution at 1 dpf and 10 nl of 3.3 mM cisplatin solution were injected 24 hour later at 2 dpf.

(B) The phenotypic changes, following the phenotype classification shown in Table 3.1 and Figure 3.4, of 5 dpf zebrafish larvae across different groups to examine the effect of Q-VD-OPh pre-treatment on cisplatin-induced malformation.

(C) The mortality rates of 5 dpf zebrafish larvae among different groups to examine the effect of Q-VD-OPh pre-treatment to cisplatin-induced mortality.

(D) GPER-ERK-caspases is a potential signal casade regulating cisplatin-induced nephrotoxicity.
The table below the bar chart represents the percentage distribution of five different phenotypes in various experimental groups as depicted in the bar chart (B).
Black solid arrows (—) represent signal transduction experimentally confirmed in this thesis. Red dotted arrows (— — —) with a question mark (**?**) represent potential signal transduction requiring additional experimental investigations (C).
Data are expressed as mean ± SD from six independent experiments. For each experiment, the non-cisplatin injected groups consisted of 12 embryos per group, while all cisplatin-injected groups contained 18 embryos per group (B-C).
All significance values were determined using Dunnett's test following one-way ANOVA. ns, $p \geq 0.05$; *, $0.01 \leq p < 0.05$; **, $p < 0.01$; ***, $p < 0.001$; ****, $p < 0.0001$.

4.3.2.5 Summary

We initially confirmed the involvement of the GPER-ERK signaling at the protein level in cisplatin-induced toxicity. Additionally, upon the utilization of MEK inhibitor and pan-caspase inhibitor, a significant reduction in abnormal phenotypes and mortality rates induced by cisplatin was observed. This highlights the pivotal roles of ERK and caspases in cisplatin-induced nephrotoxicity, suggesting the potential regulation of cisplatin-induced nephrotoxicity through the GPER-MAPK-caspases cascade.

4.3.3 The role of the GPER-p53 signaling in cisplatin-induced nephrotoxicity is unclear

The involvement of p53 in regulating cisplatin-induced nephrotoxicity has been confirmed in various *in vivo* [46] and *in vitro* [47] studies. Considering the GPER-p53 signaling regulates apoptosis in different cell types, our study aims to confirm whether the GPER-p53 signaling can also modulate cisplatin-induced nephrotoxicity. It is essential to initially determine, at the protein level, the impact of cisplatin and GPER functional inhibition on the expression of these three downstream proteins to ascertain whether p53 is regulated by GPER. Subsequently, through zebrafish phenotype and mortality rate experiments, it is necessary to establish whether p53 inhibition affects cisplatin-induced toxicity, thereby determining if GPER-p53 regulates

cisplatin-induced zebrafish nephrotoxicity.

4.3.3.1 Cisplatin-induced levels of p53 were not influenced by GPER knockdown

To analyze the correlation between GPER and p53 at the protein level, western blotting was employed to investigate alterations in the expression and phosphorylation of p53 by either an antibody detecting total p53 or a phospho-p53 (Ser15) antibody to recognize phosphorylated p53 (p-p53) across various treatment groups. The results indicated that compared to the control group, the cisplatin-injected group exhibited an elevated expression and phosphorylation of p53. Following the functional inhibition of GPER (using GPER ATG-MO), the elevated expression of p53 induced by cisplatin remained unaltered, while the elevated levels of p-p53 were decreased (Figure 4.11A-B).

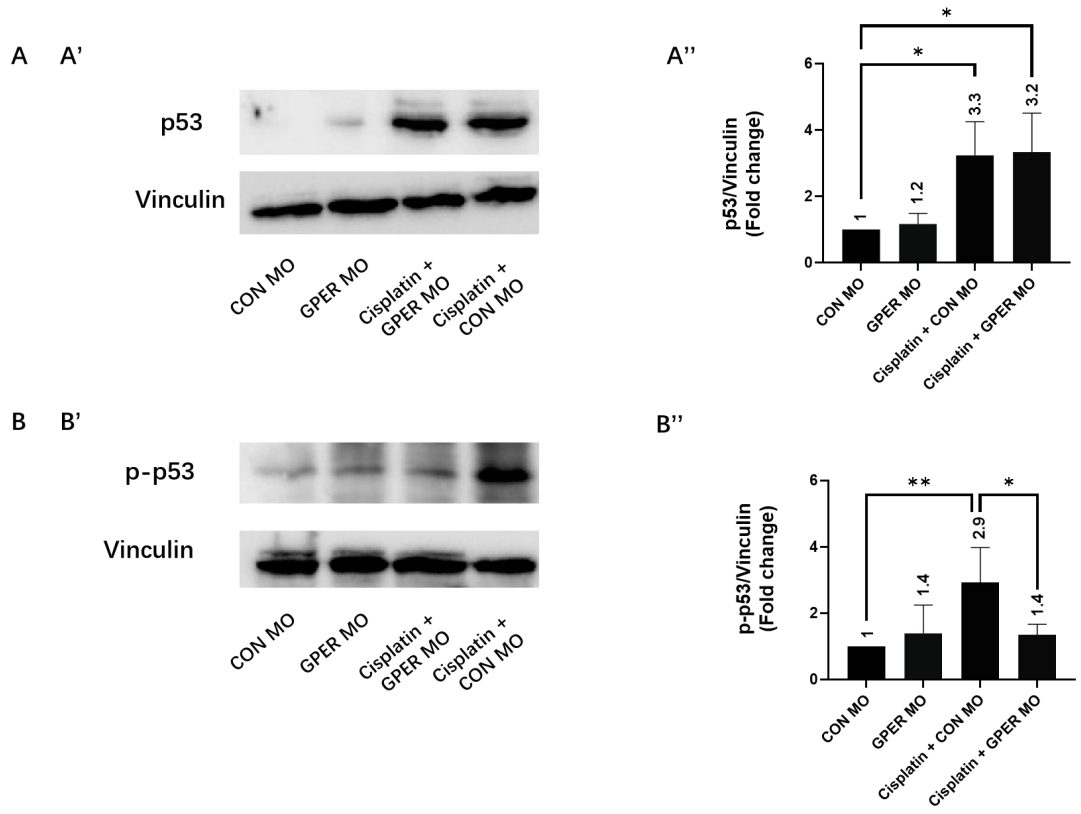

Figure 4.11 Cisplatin-induced phosphorylation of p53, but not its total levels, were influenced by GPER knockdown

(A) Amount of p53 in 3 dpf zebrafish larvae across different groups with/without GPER

knockdown by GPER ATG-MO. Left panel shows a representative result (A'), while the right panel presents the quantification of relative p53 levels normalized to the intensity of the loading control Vinculin for the different conditions (A'').
(B) Amount of phosphorylated p53 (p-p53) in 3 dpf zebrafish larvae across different groups with/without GPER knockdown by GPER ATG-MO. Left panel shows a representative result (B'), while the right panel presents the quantification of relative p-p53 levels normalized to the intensity of the loading control Vinculin for the different conditions (B'').
The experimental procedure for Day 0 to 2 can be referred to in Figure 4.3A, including: 1) Pre-treatment: Injection of GPER ATG-MO or CON MO (control) at 1-4 cell stage. 2) Drug administration: Injection of 10 nl of 3.3 mM cisplatin solution or 10 nl of 140 mM NaCl solution (control) at 2 dpf. 3) Protein extraction: whole amount proteins were extracted at 3 dpf.
In the figure, the example of 'Cisplatin + GPER MO' is used for illustration that larvae were pretreated with 2 nl 100 μM GPER ATG-MO solution at 0-2 hpf and 10 nl of 3.3 mM cisplatin solution were injected at 2 dpf.
p53 or p-p53 levels are quantified from multiple densitometry scans based on the signals obtained for p53 (p-p53) and Vinculin, which was used as a loading control. The relative intensity ratios of p53 (p-p53)/ Vinculin are plotted and have been set to 1 for the controls (A'').
Data are expressed as mean ± SD from three independent experiments. Each experiment involved protein extraction from 30 embryos per group (A'' and B'').
All significance values were determined using Dunnett's test following one-way ANOVA. ns, $p \geq 0.05$; *, $0.01 \leq p < 0.05$; **, $p < 0.01$; ***, $p < 0.001$; ****, $p < 0.0001$.

4.3.3.2 p53 knockdown does not influence cisplatin-induced abnormal phenotypes formation and mortality

The p53 ATG-MO [146] was utilized to examine whether inhibiting p53 function could mitigate cisplatin-induced edema formation and mortality in zebrafish larvae. The p53 ATG-MO could specifically target the start codon of p53 transcripts and block p53 translation. CON MO was injected into embryos as a control for sequence-unspecific effects of morpholino. Firstly, it's essential to assess the effectiveness of p53 ATG-MO. Utilize Western blotting technique to examine whether injecting p53 ATG-MO results in a reduction of p53 protein expression. The results indicated that the p53 ATG-MO group displayed a noticeable decrease in p53 protein expression compared to the Con MO injected group, confirming the successful knockdown of p53 and aligning with the expected outcome (Figure 4.12A).

The experimental procedure included CON MO or p53 ATG-MO injection at 1-4 cell stage embryos, cisplatin administration at 2 dpf, phenotype and mortality assessment at 5 dpf (Figure 4.12A). The experimental procedure involved inhibitor pre-treatment at 1 dpf, 3.3 mM cisplatin solution injection at 2 dpf, and phenotype and mortality analysis at 5 dpf (Figure 4.12B). The results indicated that the edema phenotype and mortality rates in zebrafish larvae did not exhibit any changes due to p53 knockdown by p53 ATG-MO (Figure 4.12C-D).

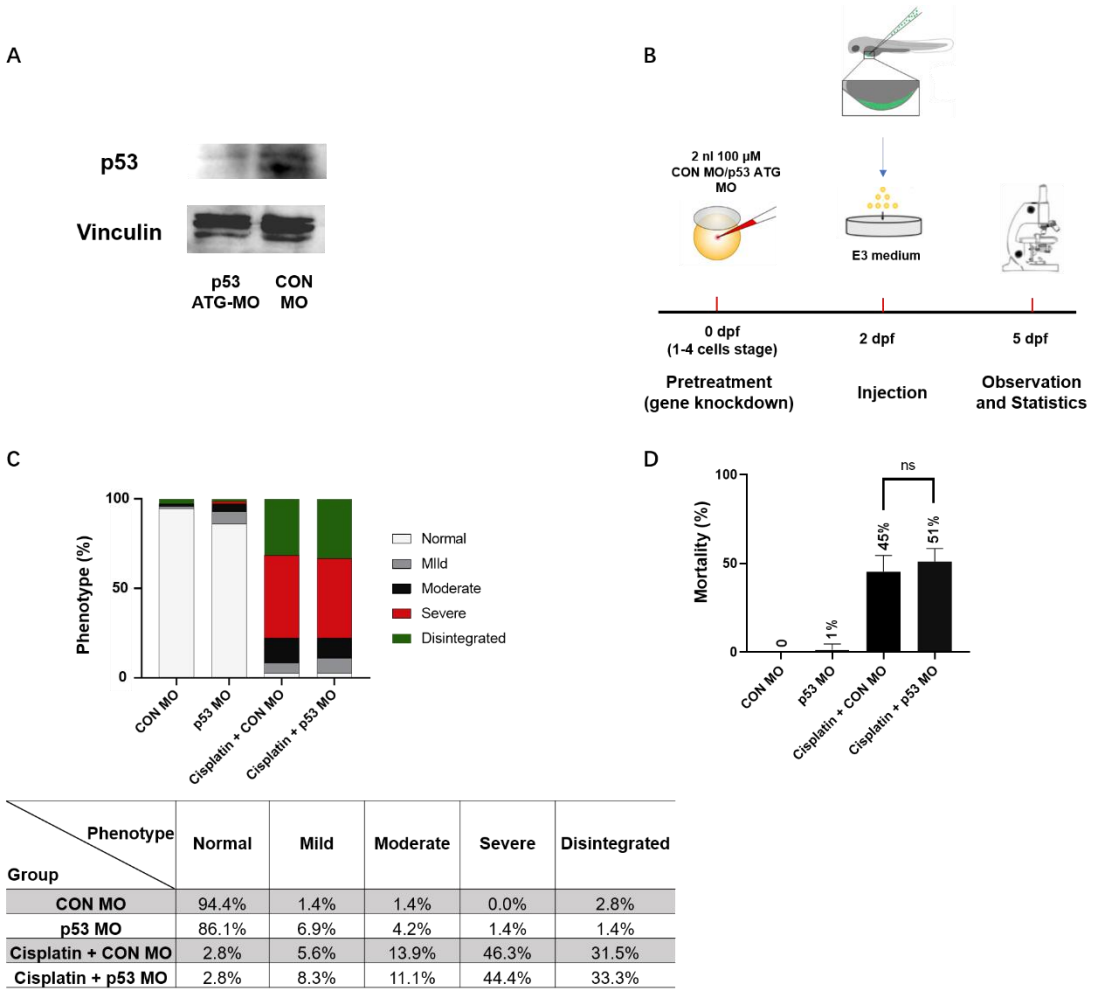

Phenotype / Group	Normal	Mild	Moderate	Severe	Disintegrated
CON MO	94.4%	1.4%	1.4%	0.0%	2.8%
p53 MO	86.1%	6.9%	4.2%	1.4%	1.4%
Cisplatin + CON MO	2.8%	5.6%	13.9%	46.3%	31.5%
Cisplatin + p53 MO	2.8%	8.3%	11.1%	44.4%	33.3%

Figure 4.12 p53 knockdown has no impact on cisplatin-induced abnormal phenotypes formation and mortality

(A) Western blotting to detect the expression of p53 in 9 hpf zebrafish embryos injected with CON MO and p53 ATG-MO.

(B) Experimental timeline schematic for experiments. The experimental procedure involves the following steps: 1) Pre-treatment: Injection of p53 ATG-MO or CON MO (control) at 1-4 cell stage. 2) Drug administration: Injection of 10 nl of 3.3 mM cisplatin solution or 10 nl of 140 mM NaCl solution (control) at 2 dpf. 3) Statistical analysis:

Evaluation of phenotypic changes and mortality at 5 dpf.
Following annotations in the figure, the example of 'Cisplatin + p53 MO' is used for illustration that larvae were injected with 2 nl 100 μM p53 ATG-MO solution at 1-4 cell stage and 10 nl of 3.3 mM cisplatin solution were injected at 2 dpf.
(C) The phenotypic changes, following the phenotype classification shown in Table 3.1 and Figure 3.4, of 5 dpf zebrafish larvae across different groups to examine the effect of p53 knockdown by p53 ATG-MO on cisplatin-induced malformation.
(D) The mortality rates of 5 dpf zebrafish larvae among different groups to examine the effect of p53 knockdown by p53 ATG-MO on cisplatin-induced mortality.
The table below the bar chart represents the percentage distribution of five different phenotypes in various experimental groups as depicted in the bar chart (C).
Data are expressed as mean ± SD from six independent experiments. For each experiment, the non-cisplatin injected groups consisted of 12 embryos per group, while all cisplatin-injected groups contained 18 embryos per group (C-D).
All significance values were determined using Dunnett's test following one-way ANOVA. ns, $p \geq 0.05$; *, $0.01 \leq p < 0.05$; **, $p < 0.01$; ***, $p < 0.001$; ****, $p < 0.0001$.

4.3.3.3 p53 knock-out increase cisplatin-induced abnormal phenotypes formation and mortality

A p53 knock-out line previously published by the laboratory of Christine Blattner [150] was employed to investigate whether the absence of the p53 protein could attenuate cisplatin-induced edema formation and mortality in zebrafish larvae. The experimental procedure involved inhibitors 3.3 mM cisplatin solution injection at 2 dpf, and phenotype and mortality analysis at 5 dpf (Figure 4.13A). It's worth noting that the $p53^{-/-}$ embryos used in the experiment were obtained from an incross of homozygous mutant adults [150], which are maternal zygotic homozygous p53 mutants lacking all functional p53. The embryos derived from WT zebrafish were used as control.

The results revealed that cisplatin-induced abnormal phenotypes became more severe and the percentage of *Disintegrated* embryos increased up to 72% when p53 knockout (Figure 4.13B). Accordingly, it accompanied by a significantly increased mortality caused by cisplatin-injection down to approximately 67% when p53 knockout, otherwise cisplatin mortality was as high as 49% without p53 knockout (Figure 4.13C).

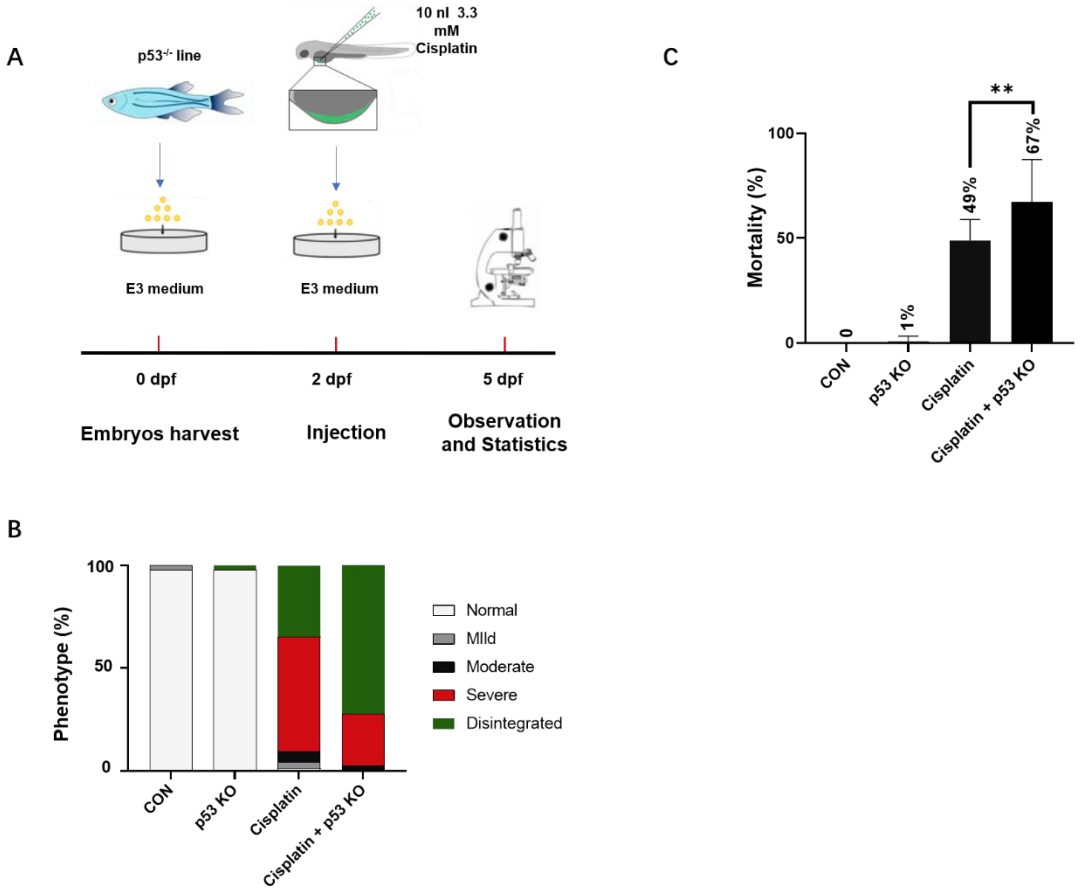

Group \ Phenotype	Normal	Mild	Moderate	Severe	Disintegrated
CON	97.9%	2.1%	0.0%	0.0%	0.0%
p53 KO	97.9%	0.0%	0.0%	0.0%	2.1%
Cisplatin	1.4%	2.8%	5.6%	55.6%	34.7%
Cisplatin + p53 KO	0.0%	0.0%	2.8%	25.0%	72.2%

Figure 4.13 p53 knock-out increase cisplatin-induced abnormal phenotypes formation and mortality

(A) Experimental timeline schematic for experiments. Embryos in p53 KO group were derived from an incross of homozygous mutant adults [150], which are maternal zygotic homozygous p53 mutants and lack all functional p53. Embryos in CON group were derived from WT adults. The experimental procedure involved $p53^{-/-}$ and WT (control) embryos harvest at 0 dpf, 10 nl of 3.3 mM cisplatin solution or 10 nl of 140 mM NaCl solution (control) injection at 2 dpf, and phenotype and mortality analysis at 5 dpf.

Following annotations in the figure, the example of 'Cisplatin + p53 KO' is used for illustration that $p53^{-/-}$ zebrafish larvae were injected with 10 nl of 3.3 mM cisplatin solution at 2 dpf.

(B) The phenotypic changes, following the phenotype classification shown in Table 3.1 and Figure 3.4, of 5 dpf zebrafish larvae across different groups to examine the effect of p53 knock-out on cisplatin-induced malformation.

(C) The mortality rates of 5 dpf zebrafish larvae among different groups to examine the effect of p53 knock-out on cisplatin-induced mortality.

The table below the bar chart represents the percentage distribution of five different phenotypes in various experimental groups as depicted in the bar chart (B).
Data are expressed as mean ± SD from ten independent experiments. For each experiment, the non-cisplatin injected groups consisted of 12 embryos per group, while all cisplatin-injected groups contained 18 embryos per group (B-C).
All significance values were determined using Dunnett's test following one-way ANOVA. ns, $p \geq 0.05$; *, $0.01 \leq p < 0.05$; **, $p < 0.01$; ***, $p < 0.001$; ****, $p < 0.0001$.

4.3.3.4 Summary

The results in this section showed some unexpected disparities. Firstly, protein detection results indicated that GPER knockdown does not affect the overall upregulation of p53 induced by cisplatin, suggesting that the GPER-p53 signaling might not be involved in cisplatin-induced toxicity. Secondly, the use of p53 ATG-MO did not impact the abnormal phenotypes and mortality rates induced by cisplatin, whereas p53 knockout exacerbated the abnormal phenotypes and mortality rates induced by cisplatin. Based on the current results, we cannot determine whether the GPER-p53 signaling is involved in regulating cisplatin-induced nephrotoxicity.

4.3.3 Inhibiting GPER does not affect the DNA damage caused by cisplatin

4.3.4.1 Cisplatin-induced levels of p-H2AX were not influenced by GPER inhibitor G36 and GPER knockdown

To evaluate whether GPER is involved in cisplatin-induced DNA damage, western blotting was employed to assess the changes in phosphorylated H2AX (p-H2AX) [225], an indicator of DNA damage, across different experimental groups. The results indicated that compared to the CON group, the cisplatin-treated group exhibited an increase in p-H2AX levels. However, upon inhibiting GPER function (by G36 or GPER ATG-MO), the elevated p-H2AX level induced by cisplatin was not influenced (Figure 4.14A-B). This outcome mirrors our findings in human cancer cells that G36 don't influence cisplatin-induced levels of p-H2AX [65].

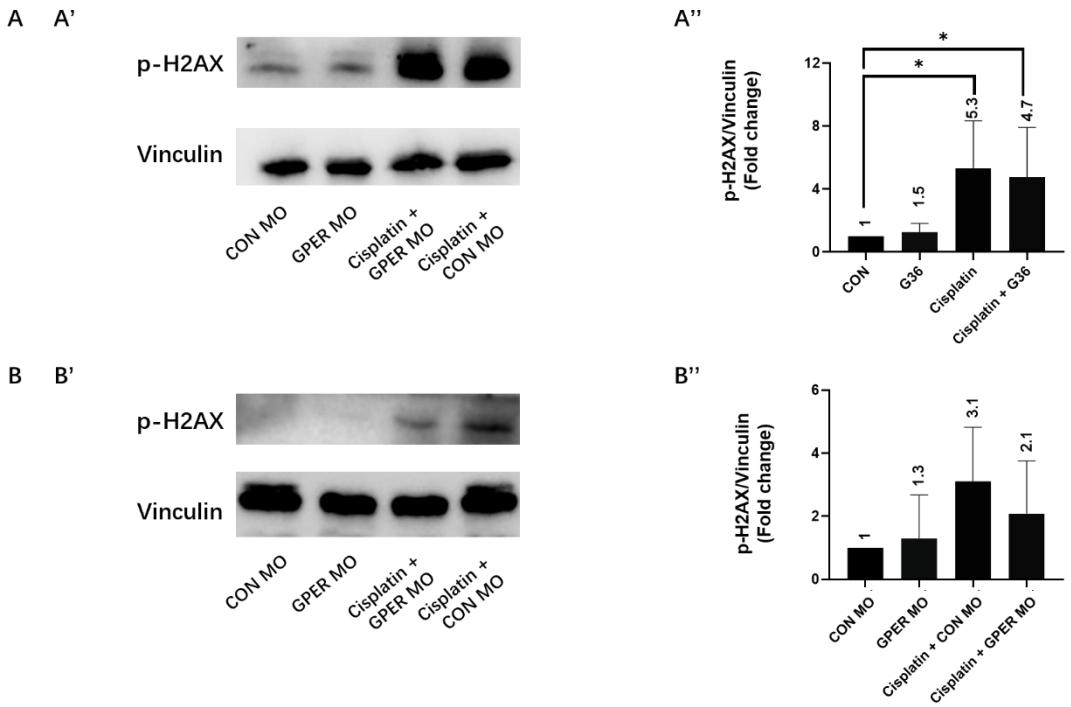

Figure 4.14 Cisplatin-induced levels of p-H2AX were not influenced by GPER inhibitor G36 and GPER knockdown

(A) Amount of phosphorylated H2AX (p-H2AX) in 3 dpf zebrafish larvae across different groups with/without G36 pre-treatment.

(B) Amount of phosphorylated H2AX (p-H2AX) in 3 dpf zebrafish larvae across different groups with/without GPER knockdown by GPER ATG-MO.

Left panel shows a representative result (A' and B'), while the right panel presents the quantification of relative p-H2AX levels normalized to the intensity of the loading control Vinculin for the different conditions (A'' and B'').

The inhibitors are all stored in 100% DMSO and diluted to working concentrations using E3 medium. Embryos without inhibitor treatment are placed in a 0.1% DMSO solution (diluted in E3 medium), equivalent to the DMSO content in a 20 μM G36 solution. The experimental procedure for Day 0 to 2 can be referred to in Figure 4.1A and 4.3A, including: 1) Pre-treatment: Gene knockdown tool - GPER ATG-MO or CON MO (control) injection at 1-4 cell stages embryos / Chemical inhibition - G36 solution or 0.1% DMSO solution (control) pre-treatment at 1 dpf. 2) Drug administration: Injection of 10 nl of 3.3 mM cisplatin solution or 10 nl of 140 mM NaCl solution (control) at 2 dpf. 3). Protein extraction: whole amount proteins were extracted at 3 dpf.

In the figure, the example of 'Cisplatin + G36' is used for illustration that larvae were pretreated with 20 μM G36 solution at 1 dpf and 10 nl of 3.3 mM cisplatin solution were injected at 2 dpf.

p-H2AX levels are quantified from multiple densitometry scans based on the signals obtained for p-H2AX and Vinculin, which was used as a loading control. The relative intensity ratios of p-H2AX/Vinculin are plotted and have been set to 1 for the controls (A'' and B'').

Data are expressed as mean ± SD from three independent experiments. Each experiment

involved protein extraction from 30 embryos per group (A'' and B'').
All significance values were determined using Dunnett's test following one-way ANOVA. ns, $p \geq 0.05$; *, $0.01 \leq p < 0.05$; **, $p < 0.01$; ***, $p < 0.001$; ****, $p < 0.0001$.

4.4 Discussion

Previous studies have attempted to unravel the mechanisms underlying cisplatin-induced nephrotoxicity through various *in vivo* and *in vitro* models. Yet, a comprehensive understanding of the main regulatory factors involved in this process is still lacking [125]. Building upon the preliminary work conducted in our laboratory on cancer cells and the similarity between cisplatin-induced nephrotoxicity and anticancer effects, our research proposes for the first time the potential involvement of GPER as an upstream regulator in the process of cisplatin-induced nephrotoxicity.

GPER, the G protein-coupled estrogen receptor, is a member of the G protein-coupled receptor family associated with estrogen signaling, regulating a wide range of physiological and pathological processes. While there are no studies reporting any connection between GPER or the other GPCR family members with cisplatin-induced nephrotoxicity, the fact that GPER can modulate the functions of MAPK [226] and p53 [227] in various intracellular contexts raises the possibility of its involvement in regulating cisplatin-induced nephrotoxicity. Thus, the potential role of the GPER-MAPK/p53 pathway as a regulatory mechanism was investigated here.

The subsequent discussion will primarily revolve around three main sections:

4.4.1 GPER is a potential modulator in cisplatin-induced nephrotoxicity

Chapter 3 elucidates, through a series of experiments, that cisplatin administration induces abnormal morphologic changes and renal structural damage in zebrafish larvae. Notably, upon employing the GPER inhibitor G36 or GPER-targeted morpholinos, a pronounced reduction in edema severity and

mortality in zebrafish larvae was observed. This revelation substantiates the plausible involvement of GPER in modulating cisplatin-induced nephrotoxicity.

1 GPER inhibition does not exerting a general renoprotective effect

To further confirm the specificity of GPER's functional inhibition on cisplatin-induced nephrotoxicity, as opposed to a general protective effect on the kidney, we employed gentamicin as a replacement for cisplatin. Gentamicin is a well-validated nephrotoxin extensively studied in zebrafish embryos [99, 118], yet it exhibits a completely different toxicity profile compared to cisplatin in other models. The main differences including (Figure 6.1 in Appendices), 1). Gentamicin primarily accumulates in the proximal tubules through reabsorption [228], while cisplatin accumulation occurs through basolateral-to-apical secretion [229]. 2) Although both toxins eventually trigger ROS and inflammatory responses, gentamicin primarily causes protein synthesis inhibition and lysosome disruption [228] upon entering renal cells. Conversely, cisplatin induction mainly leads to DNA damage and the production of the metabolic byproduct thiols (strong reducing agents) [229]. 3) Cisplatin has been reported to bind to different receptors, like Toll-like receptor 4 (TLR4) [85] and glucocorticoid receptor (GR) [86], inducing downstream reactions. In contrast, there is currently no evidence suggesting that gentamicin binds to these receptors. Although the lack of experiments to support whether the differences in toxicity mechanisms between cisplatin and gentamicin, as verified in other animal models, apply similarly in zebrafish larvae, using gentamicin as a substitute for cisplatin is currently the most rapid and effective method to validate the specificity of GPER regulation of cisplatin-induced nephrotoxicity. Our results indicated that the G36 inhibitor or GPER-targeted morpholinos did not affect edema severity and mortality induced by gentamicin in zebrafish larvae. This outcome further underscores the potential specific role of GPER in regulating cisplatin-induced nephrotoxicity.

The notable point is that ERK involvement in cisplatin-induced nephrotoxicity has been confirmed in various *in vitro* and *in vivo* models [57, 63]. However, there have been no reports indicating ERK involvement in gentamicin-induced nephrotoxicity. On the other hand, p38, another important member of the MAPK family, has been reported in different studies to be involved in the nephrotoxicity induced by both of these nephrotoxins [59, 230]. Our study verified in zebrafish larvae model that p-ERK is upregulated at the protein level after cisplatin stimulation, and functional inhibition of ERK can restore the abnormal phenotypes caused by cisplatin in zebrafish larvae. Future research could consider using zebrafish larva as a model to investigate the mechanisms of gentamicin-induced nephrotoxicity, particularly whether ERK participates in this process and whether it can replicate the conclusion of p38 MAPK observed in other models.

2 Selection of the kidney injury marker-*kim1* and summary of experimental methods with technical difficulties

Lastly, the preceding experiments were primarily based on zebrafish phenotypes, edema formation and mortality rate. Direct evidence demonstrating the restoration of cisplatin-induced renal abnormalities upon GPER inhibition was lacking. Initially, we utilized qPCR to assess kidney injury-related genes, including *kim1* [141, 142], *clu* [143], *ctgf* [144]. The mRNA levels of *kim1*, *clu*, and *ctgf* were found to be upregulated 24 hours after cisplatin injection, and these upregulations were mitigated upon functional inhibition of GPER. Secondly, the use of the ATP1A1 antibody to visualize the specific location of the pronephric tubule has been repeatedly confirmed in previous studies. Experimental results indicated that cisplatin leads to a reduction in the diameter of the proximal tubule, a finding consistent with observations from live zebrafish larvae through SYTO-59 dye staining. However, under the influence of the GPER inhibitor G36, the shortened diameter of the proximal tubule induced by cisplatin was restored. In Chapter 3,

Section 3.4, potential reasons for the change in proximal tubule diameter induced by cisplatin, such as tubule constriction or collapse, have been explained. The GPER inhibitor G36 might play a role as a vasodilator or apoptosis inhibitor in cisplatin-induced nephrotoxicity.

In summary, our study provides the first analysis of the potential of GPER as a modulator of cisplatin-induced nephrotoxicity. However, there are two crucial issues that require further elucidation in this context:

1. KIM1 is a transmembrane protein initially discovered to be expressed in renal tubular epithelial cells. In clinical settings, the measurement of KIM1 levels in urine or blood is used to determine the presence of kidney injury, particularly in the early diagnosis of acute kidney injury (AKI) [231, 232]. Rodent studies also confirmed *kim1* is expressed at very high levels in proximal tubule epithelial cells after ischemic or toxic injury [141, 233]. However, there has been an ongoing controversy regarding the expression of *kim1* in zebrafish, possibly due to the existence of two homologous genes, hepatitis A virus cellular receptor 1 (*havcr1*) [234] and 2 (*havcr2*) [235]. However, in previous studies, only Yin et al. utilized *havcr2* to represent *kim1*, and *havcr1* to represent *kim4* [235]. Yin et al. demonstrated an upregulation of *kim1* mRNA expression in renal tissues after injecting gentamicin into adult fish, while *kim4* showed no significant changes. In contrast, more zebrafish studies employ *havcr1* to represent *kim1* [99, 236, 237]. These studies use *havcr1* as a marker for zebrafish nephrotoxicity. For instance, Bauer et al. exposed 3 dpf zebrafish larvae to a 9 ng/ml gentamicin solution for 2 days, resulting in a two-fold upregulation of *havcr1* mRNA compared to the control group [99]. In our study, we adopted *havcr1* as a marker for zebrafish larval nephrotoxicity to measure changes in mRNA levels (personal communication by Benedikt Bauer and Angela Mally). In contrast, there is no controversy regarding the other kidney injury markers, including clusterin (*clu*) [238, 239] and connective tissue growth factor (*ctgf*) [240, 241].

2. Although the qPCR results provided supporting evidence at the mRNA level

that inhibiting GPER function mitigates cisplatin-induced nephrotoxicity, the IHC results were not as compelling. Still, we lack direct evidence to demonstrate the restoration of cisplatin-induced renal cell damage under GPER functional inhibition or knockdown. Over the past 3 years, we attempted various methods based on past research on nephrotoxicity, but ultimately get unconvincing results. The table below (Table 6.1 in Appendices) summarizes my analysis of these unsuccessful experiments.

These experimental methods with technical difficulties indicate that the proximal tubule and glomerulus in zebrafish larvae are located at a deeper position within the larvae's body. Conventional methods using acetone or proteinase K for whole-embryo tissue softening to enhance probe, dye, or antibody penetration into the proximal tubule are challenging to achieve. Future studies should focus more on precise identification of the proximal tubule and glomerulus positions through histological sections and combine histological dyes such as H&E staining [99], kidney injury antibodies like KIM1 [242], apoptosis antibodies like Caspase 3 [243], or electron microscopy to observe ultrastructural changes and cell death in renal structures [244]. It's worth mentioning that in our lab, epoxy resin [245] is used to embed zebrafish for subsequent sectioning. However, this type of plastic is too dense, causing many antibodies, dyes, and probes to fail to penetrate the plastic and reach the tissue. Even if pre-embedding labeling methods like whole mount IHC followed by embedding into epoxy resin are chosen, the fluorescence signal is quenched upon obtaining the sections. Therefore, future research should consider using alternative materials to replace epoxy resin for histological section studies, such as JB-4™ resin [98, 173]. This novel resin not only allows for a range of histological experiments on the obtained sections, including staining, antibodies, and probes, but also ensures that the fluorescence signal can be reliably detected in the pre-embedding labeling sections.

4.4.2 GPER-MAPK signaling in cisplatin-induced nephrotoxicity

Furthermore, by utilizing the MEK inhibitors U0126 and PD98059, along with the pan-caspase inhibitor Q-VD-OPh, a substantial decrease in abnormal phenotypes and mortality in zebrafish larvae was demonstrated. This corroborates the regulatory roles of MAPK and caspases in cisplatin-induced nephrotoxicity across various *in vivo* and *in vitro* models. These findings conclusively establish the participation of GPER, MAPK, and caspases in the regulation of cisplatin-induced nephrotoxicity, specifically implicating them in process of the zebrafish larvae malformation. However, while these results confirm the involvement of GPER, MAPK, and caspases, they do not definitively establish a sequential GPER-MAPK caspase regulatory pathway, in which GPER leads to MAPK activation which in turn triggers caspase activation leading to cell death.

To further study this regulatory pathway, we examined the activation of MAPK family members by monitoring phosphorylation at the protein level. Through specific antibodies, we confirmed that only p-ERK and p-p38 were detectable in zebrafish, while for phosphorylated JNK (pJNK) we could not identify a specific signal. Following cisplatin administration, a significant increase of p-ERK was observed, while p-p38 exhibited minimal change. Intriguingly, upon inhibiting GPER using inhibitors or morpholinos, the considerable increase in p-ERK induced by cisplatin was markedly attenuated, while p-p38 displayed negligible alterations.

It is noteworthy that we also examined the levels of p-H2AX, a DNA damage marker, at the whole mount protein level. Previous study confirmed the conservation of the phosphorylation site (Serine139) of H2AX in vertebrates [246]. The cisplatin treatment led to an upregulation of p-H2AX, but the inhibition of GPER function (G36 or GPER ATG-MO) did not impact this upregulation. Similar results were observed in the human non-small cell lung

cancer cell line A549 (unpublished data, personal communication by Iris Hansjosten). These findings indicate that GPER does not interfere with the initial DNA damage provoked by cisplatin, but acts downstream or in parallel to control cell fate. Still, whether cisplatin directly binds to GPER or indirectly, via e.g. the DNA damage response, triggers GPER signaling warrants further investigations.

These results definitively establish an upstream role of GPER in cisplatin-induced ERK activation (phosphorylation), underscoring the direct linkage of the GPER-ERK axis as a latent regulatory pathway in cisplatin-induced nephrotoxicity (Figure 4.15).

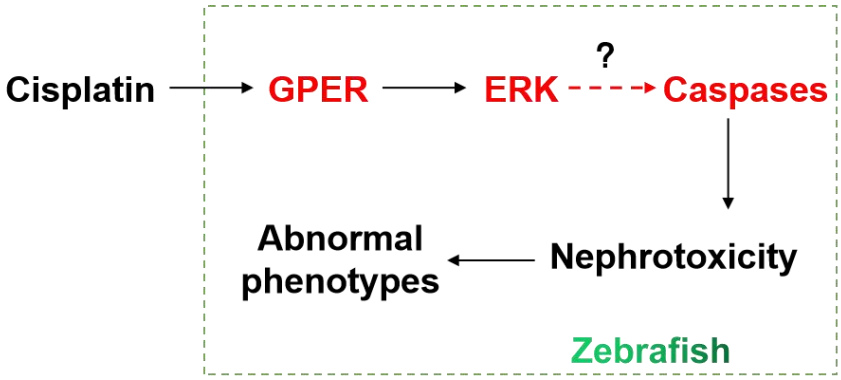

Figure 4.15 GPER-ERK signaling involves in cisplatin-induced nephrotoxicity in zebrafish larval model

Black solid arrows (—) represent signal transduction experimentally confirmed in this thesis. Red dotted arrows (— — —) with a question mark (**?**) represent potential signal transduction requiring additional experimental investigations.

There are four crucial issues that require further elucidation in this context:

1. All western blotting experiments were conducted with whole embryos, rather than focusing on embryonic kidney cells. Considering the early embryonic stage and the lack of a kidney reporter line, it was unfeasible to extract kidney-specific cells for analysis. Even if selective extraction of kidney cells would be possible, achieving the protein amounts essential for western blotting might be challenging.

2. Owing to the lack of a specific antibody to detect reliably ERK in zebrafish, the experiment could not assess the overall ERK protein levels. While other

models have confirmed that cisplatin does not induce a global increase in ERK proteins [247, 248], it remains uncertain whether this holds true for the zebrafish larval model. Similarly, the question arises whether inhibiting GPER function would lead to an overall downregulation of the zebrafish ERK protein.

3. Other studies in different models and species suggest an upregulation of p-p38 due to cisplatin, while overall p38 levels remain unaffected [248, 249]. It remains possible that the use of whole embryos masks a specific enhanced phosphorylation of p38 only in the kidney. Consequently, further experiments are essential to address the role of p-p38 in cisplatin-induced renal injury in zebrafish larvae.

4. The experiment also tried to assess the total levels of JNK and pJNK. Unfortunately, although the pJNK antibody detected some bands, they were inconsistent with the anticipated sizes of the zebrafish JNKs. Regrettably, also the JNK antibody entirely failed to yield detectable bands. Thus, no conclusions can be drawn concerning the role of JNK in the zebrafish larval model.

4.4.3 The role of the GPER-p53 signal in cisplatin-induced nephrotoxicity is unclear

In addition to the activation of MAPKs by cisplatin, we also assessed the effects on the levels of p53 and its phosphorylation (p-p53). The western blotting results revealed that cisplatin-induced an overall increase in p53 levels. Yet, inhibiting GPER did not influence the cisplatin-induced elevation of overall p53. However, cisplatin did lead to an increase in p-p53 levels, while GPER inhibition resulted in a reduction of cisplatin-induced p-p53.

Following functional experiments with a p53 knockout zebrafish line and p53 morpholino knockdown, a pro-apoptotic role resulting in enhanced lethality of zebrafish larvae upon cisplatin treatment could not be shown. On the contrary, the p53 knockout zebrafish line exhibited greater sensitivity to cisplatin than

normal zebrafish, with higher levels of edema and mortality. However, p53 knockdown by a specific morpholino had minimal impact on the extent of edema and mortality induced by cisplatin in zebrafish larvae. Previous *in vitro* and *in vivo* studies have confirmed that inhibiting p53 effectively counteracts cisplatin-induced nephrotoxicity.

There are four crucial issues that require further elucidation in this context:

1. All western blotting experiments of p53 and p-p53 were conducted with whole embryos, rather than focusing on embryonic renal cells, as discussed above for other antibodies used for detection of target proteins.

2. The p53 antibody has been validated in previous studies by Elabd [150] and others [250]. The upregulation of p53 expression in response to cisplatin stimulation is consistent with expectations [251, 252]. However, the fact that the functional inhibition of GPER does not alter cisplatin-induced upregulation of p53 suggests that GPER inhibition may affect the apoptotic process induced by cisplatin by potentially altering the levels of phosphorylated p53. Unlike the dependence of MAPK family function on phosphorylation, p53 also needs additional post-translational modifications to act as transcription factor, including phosphorylation [253], acetylation [254], methylation [255]. Previous studies confirmed over 20 phospho-acceptor sites on p53 in human [256], among which representative ones including serine 15 (S15), serine 20 (S20), and serine 392 (S392). The phosphorylation of S15 and S20 is typically associated with the activation and stability of p53, enhancing the accumulation and transcriptional activity of p53 under stress conditions. The phosphorylation of S392 is associated with the anti-apoptotic function of p53, affecting its interactions with other proteins, especially with anti-apoptotic proteins [253]. Our experiments utilized an antibody detecting the S15 phosphorylation site. While different studies have confirmed the conservation of zebrafish p53, limited research has focused on its phospho-acceptor sites, making it uncertain if the S15 phosphorylation site serves a similar function as in humans.

3. The p53 knockout zebrafish line might still maintain some residual p53 levels, which warrants further investigations.

4. While the p53 morpholinos used in this experiment has been extensively employed in previous studies by other laboratories [146, 257], encountering incomplete suppression of the target in morpholino knockdown experiments is not unprecedented. Compared to other gene targets, p53 knockdown is more prone to induce abnormal embryonic development. Consequently, selecting appropriate concentrations and injection doses becomes particularly crucial. It is currently unclear whether the insufficient p53 knockdown is due to inadequate dosage or other factors, such as off-target effects [257]. However, given that the total amount of p53 was clearly reduced by the morpholino at 9 hpf, it could also be possible that in this zebrafish model p53 does not have such a profound role in cisplatin mediating nephrotoxicity.

Thus, the existing data cannot confirm an involvement of the GPER-p53 signal in kidney injury provoked by cisplatin in zebrafish larval model.

Overall, Chapter 4 focused on functional inhibition of target proteins and biochemical assays to monitor expression levels and phosphorylation of target proteins in the zebrafish larval model. Combined with previous research outcomes, this study proposes for the first time a crucial involvement of the GPER-MAPK pathway in cisplatin-induced nephrotoxicity.

5 Conclusion and Outlook

The first part of our study employed previous research findings and combined them with relevant experiments to establish a method for investigating cisplatin-induced nephrotoxicity using zebrafish larvae as a model. This involved selecting appropriate days for larval injection, improving injection techniques, and implementing phenotypic classification methods. Despite the increasingly stringent ethical requirements for animal research imposed by various countries and organizations, the use of adult zebrafish or mouse models is subject to limitations. Therefore, developing a model centered around zebrafish larvae not only offers advantages in terms of efficiency, convenience, and affordability but also serves as a valuable complement to existing studies on cisplatin or platinum-based drug-induced nephrotoxicity.

The second part of our study utilized the zebrafish larvae model to uncover GPER-MAPK as a potential regulator of cisplatin-induced nephrotoxicity. This discovery is highly intriguing, not only because previous research had not reported the association between GPER and cisplatin-induced nephrotoxicity, but also because there were limited investigations into the pathophysiological function of GPER activation in inducing cell apoptosis. The inspiration to explore GPER as a potential regulator of cisplatin-induced nephrotoxicity stemmed from its role in cisplatin-induced cytotoxicity in cancer cells, and this finding further supports the notion that GPER-mediated regulation of cell death (in both normal and cancerous cells) induced by cisplatin is a universal phenomenon.

Based on the experimental findings of this study and previous research, the potential regulatory network is depicted (Figure 5.1). Cisplatin triggers the activation of GPER, MAPK, and caspases in a sequential manner, leading to the induction of apoptosis in renal cells. The present study provides the basis to further substantiate this potential regulatory mechanism.

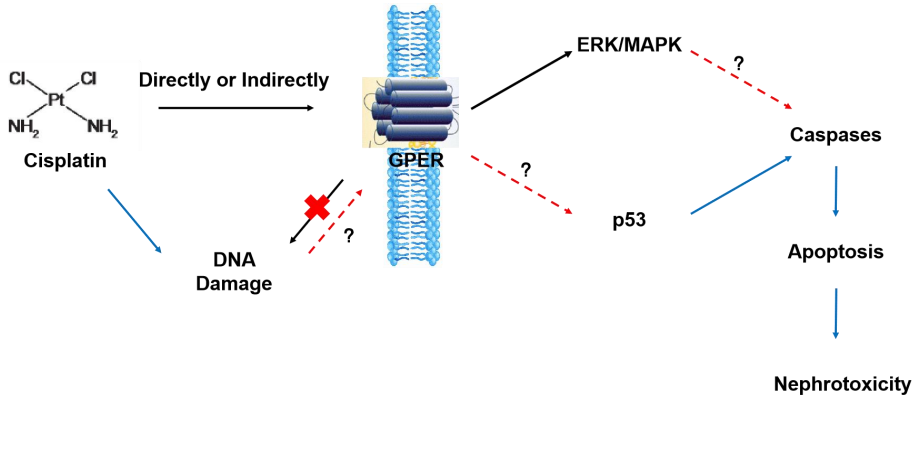

Figure 5.1 Putative regulatory network of cisplatin-induced nephrotoxicity established in the thesis

Blue solid arrows (—) represent known signal transduction. Black solid arrows (—) represent signal transduction experimentally confirmed in this thesis. Red dotted arrows (— — —) with a question mark (**?**) represent potential signal transduction requiring additional experimental investigations. Black solid arrows (—) with a red cross mark (**X**) represent signal transduction identified to be false in this thesis.

1. How does cisplatin activate GPER, directly or indirectly?

In Chapter 1, Section 1.3.4, it has been suggested that cisplatin may function as a 'metalloestrogen' by directly binding to GPER or activating alternative mechanisms, such as the DNA damage response (DDR), which subsequently triggers GPER activation. Our protein analysis targeting p-H2AX demonstrated that GPER does not interfere with the initial DNA damage provoked by cisplatin but acts downstream or in parallel to control cell fate. Although there is no research indicating the activation of GPER by the DNA Damage Response (DDR), future studies can consider comparing the differences in cell death induced by cisplatin when simultaneously inhibiting key DDR proteins like ATR alongside GPER versus inhibiting them individually. This comparison will help us better understand whether DDR has the ability to activate GPER.

Regarding whether GPER can directly bind to cisplatin, the highly developed surface plasmon resonance (SPR) technique provides a powerful and nondestructive tool for studying protein-small molecule interactions [258, 259].

2. How does cisplatin activate MAPK/ERK downstream of GPER?

To elucidate the mechanisms underlying MAPK/ERK activation following

GPER activation by cisplatin, and its role in inducing renal cell apoptosis, further investigation is required. Although Upadhayay et al. proposed in their review that GPER can directly activate ERK or the RAS/RAF/ERK pathway after being activated by SRC [260], it lacks experimental support. Currently, a more credible explanation comes from Filardo et al., who demonstrated that GPER can activate the epidermal growth factor receptor (EGFR) through transactivation in breast cancer cells [261], thereby activating the MAPK/ERK pathway. In fact, there have been multiple studies in the past reporting that cisplatin can activate EGFR signaling [262-264]. Combining these results suggests that the Cisplatin/GPER/EGFR/ERK signaling pathway may represent a potential sequential activation mechanism underlying cisplatin-induced apoptosis.

In conclusion, the specific mechanisms underlying GPER-mediated MAPK activation depend on the cellular context, physiological environment, and pathological conditions of different cells and the organism. Future investigations in this field should focus on renal cells to gain further insights into the intricacies of GPER activation and its impact on the MAPK pathway.

3. How can the activation of MAPK/ERK activate caspases?

Previous studies have confirmed that under specific conditions, the activation of MAPK/ERK can induce the activation of caspases, leading to cellular apoptosis [265, 266]. However, we did not verify the mechanism in our study. The lack of suitable western blotting antibodies for cleaved caspase 3/6/7 detection made it difficult to detect the respective proteins in zebrafish embryos. Therefore, additional validation in renal cells is required for further investigation.

4. Can the activation of GPER by cisplatin regulates p53?

p53 is also a key downstream target of our study. As an important regulator of the apoptosis pathway, previous studies have demonstrated that cisplatin can induce high expression of p53 [46, 267] and inhibiting p53 function can reduce cisplatin-induced renal cell death in *in vitro* [46] and *in vivo* [266] models.

However, our *in vivo* experiments conducted in zebrafish larvae yielded partially opposite results. In our study, the functional inhibition of p53 by a specific morpholino had no impact on cisplatin-induced edema and mortality. An even exacerbated cisplatin toxicity was observed in knock-out zebrafish where p53 function was completely absent. Furthermore, although the functional inhibition of GPER reduced the expression of p-p53 induced by cisplatin, it had no effect on the overall upregulation of p53 caused by cisplatin. These results reveal a potential crosstalk of GPER and p53. Future research needs to address the interaction of GPER and p53 and its role in the response to cisplatin.

As mentioned earlier, the specific mechanism of GPER as a modulator in cisplatin-induced nephrotoxicity requires further investigation in future experiments, but it serves as a valuable addition to the existing research. The significance and prospects of GPER as a potential modulator of cisplatin-induced nephrotoxicity can be summarized as follows:

A) Potential as a clinical therapeutic target: avoiding side effects, especially nephrotoxicity, presents the greatest objective to fully exploiting the anticancer effects of cisplatin. Previous studies lacked an understanding of the upstream regulators involved in cisplatin-induced nephrotoxicity. GPER, as a membrane receptor protein, holds immense potential as a therapeutic target. By modulating GPER, it may be possible to explore methods to alleviate or reverse cisplatin-induced nephrotoxicity, thereby enhancing treatment efficacy and reducing adverse reactions.

B) Expanding the functionality and role of GPER in cisplatin-induced other adverse effects: Our research findings demonstrate the regulatory role of GPER in cisplatin-induced kidney injury. However, as GPER is widely expressed in different tissues and organs, further investigation into its pathophysiological function in cisplatin-induced neuro- or ototoxicity holds significant importance.

C) Advancing our understanding of kidney injury mechanisms: the research

highlights the scarcity of studies on GPER in relation to the kidney. Considering our study's identification of GPER as a potential modulator for cisplatin-induced nephrotoxicity, exploring whether the GPER-MAPK regulatory network is applicable to other renal injury models or toxicity mechanisms induced by different toxins would be an intriguing research direction.

D) Providing a novel perspective on GPER-mediated regulation of apoptosis: Most of the physiological studies on GPER have primarily focused on its involvement in cell proliferation, migration, and differentiation. However, there has been relatively less exploration of its specific role and mechanisms in apoptosis regulation. Our research results reveal that GPER also plays a role in regulating normal/cancer cell apoptosis. This provides a rationale for further investigating its involvement in apoptotic signaling pathways, cell survival and death balance, and related diseases.

Acknowledgement

Time flies, and my four years of overseas doctoral life are coming to an end. I still remember the day I arrived in Germany for the first time - the excitement and anticipation, as well as the pressure. Looking back at the past years, I'd like to express my gratitude to everyone who has supported me, making my doctoral journey enriching and colorful.

First and foremost, I would like to extend my heartfelt gratitude to my supervisor, PD Dr. Carsten Weiss. Thank you for giving me the opportunity to join your team. Your continuous encouragement, patience, and guidance have been invaluable. You've consistently emphasized the essence of scientific research and the cultivation of scientific thinking as the core aspects of doctoral education, rather than merely chasing experimental results. This perspective has deeply influenced me. From designing research topics to their practical implementation, I've experienced your thoughtful intentions every step of the way. You've helped me overcome some bad research habits, aiming to shape me into someone who is more rigorous and passionate about scientific work.

I also want to sincerely thank my co-supervisor, Dr. Thomas Dickmeis, for your guidance. Considering that our laboratory had relatively little experience with using zebrafish as a model organism, the technological platforms you've established saved us a lot of exploratory time and unnecessary complications. Moreover, during critical phases of my research, your extensive knowledge always came to my aid in resolving problems and shortcomings in the projects. Here, I'd like to express my gratitude once again to Dr. Masanari Takamiya. Many experiments over these four years were accomplished with your assistance, and we've collectively tackled numerous experimental challenges. You've taught me various experimental methods and techniques, which have been immensely beneficial for my subsequent research topics. Every discussion with you has introduced me to novel ways of thinking. Our

collaboration has always been remarkably smooth.

My appreciation extends to all my colleagues: Silvia, Susanne, Dorit, Christina, Marian, Gaelle, Gao. During one of the most challenging phases of my life, I'm thankful for your understanding and support.

I'm grateful for our excellent fish facilities and all members of EZRC who took care of my zebrafish over these four years.

I want to acknowledge the financial support of the China Scholarship Council (CSC) for my doctoral studies in Germany. Four years of study made me even prouder of our nation. I'm thankful for the country's substantial medical assistance during the pandemic.

Lastly, I want to thank my family for their love and encouragement. You've always been my role models, and while I still have many areas to improve compared to you, I firmly believe that with steady progress, I will one day make you proud.

References

1. Rosenberg, B., L. Vancamp, and T. Krigas, *Inhibition of Cell Division in Escherichia Coli by Electrolysis Products from a Platinum Electrode.* Nature, 1965. **205**: p. 698-9.
2. Rosenberg, B. and L. VanCamp, *The successful regression of large solid sarcoma 180 tumors by platinum compounds.* Cancer Res, 1970. **30**(6): p. 1799-802.
3. Kelland, L., *The resurgence of platinum-based cancer chemotherapy.* Nat Rev Cancer, 2007. **7**(8): p. 573-84.
4. Pabla, N. and Z. Dong, *Cisplatin nephrotoxicity: mechanisms and renoprotective strategies.* Kidney Int, 2008. **73**(9): p. 994-1007.
5. Kanat, O., H. Ertas, and B. Caner, *Platinum-induced neurotoxicity: A review of possible mechanisms.* World J Clin Oncol, 2017. **8**(4): p. 329-335.
6. Rybak, L.P., et al., *Cisplatin ototoxicity and protection: clinical and experimental studies.* Tohoku J Exp Med, 2009. **219**(3): p. 177-86.
7. Wagstaff, A.J., et al., *Carboplatin. A preliminary review of its pharmacodynamic and pharmacokinetic properties and therapeutic efficacy in the treatment of cancer.* Drugs, 1989. **37**(2): p. 162-90.
8. Yarbro, C.H., *Carboplatin: a clinical review.* Semin Oncol Nurs, 1989. **5**(2 Suppl 1): p. 63-9.
9. Alcindor, T. and N. Beauger, *Oxaliplatin: a review in the era of molecularly targeted therapy.* Curr Oncol, 2011. **18**(1): p. 18-25.
10. Kelland, L.R., et al., *Mini-review: discovery and development of platinum complexes designed to circumvent cisplatin resistance.* J Inorg Biochem, 1999. **77**(1-2): p. 111-5.
11. Ivanov, A.I., et al., *Cisplatin binding sites on human albumin.* J Biol Chem, 1998. **273**(24): p. 14721-30.
12. Ishida, S., et al., *Uptake of the anticancer drug cisplatin mediated by the copper transporter Ctr1 in yeast and mammals.* Proc Natl Acad Sci U S A, 2002. **99**(22): p. 14298-302.
13. Davies, M.S., S.J. Berners-Price, and T.W. Hambley, *Slowing of cisplatin aquation in the presence of DNA but not in the presence of phosphate: improved understanding of sequence selectivity and the roles of monoaquated and diaquated species in the binding of cisplatin to DNA.* Inorg Chem, 2000. **39**(25): p. 5603-13.
14. Moggs, J.G., et al., *Differential human nucleotide excision repair of paired and mispaired cisplatin-DNA adducts.* Nucleic Acids Res, 1997. **25**(3): p. 480-91.
15. Damia, G., et al., *Cisplatinum and taxol induce different patterns of p53 phosphorylation.* Neoplasia, 2001. **3**(1): p. 10-6.
16. Appella, E. and C.W. Anderson, *Post-translational modifications and activation of p53 by genotoxic stresses.* Eur J Biochem, 2001. **268**(10): p. 2764-72.
17. Dasari, S. and P.B. Tchounwou, *Cisplatin in cancer therapy: molecular mechanisms of action.* Eur J Pharmacol, 2014. **740**: p. 364-78.

18. Lin, X., et al., *The copper transporter CTR1 regulates cisplatin uptake in Saccharomyces cerevisiae.* Mol Pharmacol, 2002. **62**(5): p. 1154-9.
19. Brozovic, A., A. Ambriovic-Ristov, and M. Osmak, *The relationship between cisplatin-induced reactive oxygen species, glutathione, and BCL-2 and resistance to cisplatin.* Crit Rev Toxicol, 2010. **40**(4): p. 347-59.
20. Zhang, J., et al., *Status of bi- and multi-nuclear platinum anticancer drug development.* Anticancer Agents Med Chem, 2010. **10**(4): p. 272-82.
21. Gunes, D.A., et al., *Co-application of arsenic trioxide (As2O3) and cisplatin (CDDP) on human SY-5Y neuroblastoma cells has differential effects on the intracellular calcium concentration ([Ca2+]i) and cytotoxicity.* Neurotoxicology, 2009. **30**(2): p. 194-202.
22. Byun, J.M., et al., *Tetraarsenic oxide and cisplatin induce apoptotic synergism in cervical cancer.* Oncol Rep, 2013. **29**(4): p. 1540-6.
23. Shahid, F., Z. Farooqui, and F. Khan, *Cisplatin-induced gastrointestinal toxicity: An update on possible mechanisms and on available gastroprotective strategies.* Eur J Pharmacol, 2018. **827**: p. 49-57.
24. Akbarali, H.I., et al., *Chemotherapy induced gastrointestinal toxicities.* Adv Cancer Res, 2022. **155**: p. 131-166.
25. Alberts, D.S. and J.K. Noel, *Cisplatin-associated neurotoxicity: can it be prevented?* Anticancer Drugs, 1995. **6**(3): p. 369-83.
26. Quasthoff, S. and H.P. Hartung, *Chemotherapy-induced peripheral neuropathy.* J Neurol, 2002. **249**(1): p. 9-17.
27. Laurell, G. and U. Jungnelius, *High-dose cisplatin treatment: hearing loss and plasma concentrations.* Laryngoscope, 1990. **100**(7): p. 724-34.
28. Kitcher, S.R., et al., *ORC-13661 protects sensory hair cells from aminoglycoside and cisplatin ototoxicity.* JCI Insight, 2019. **4**(15).
29. Miettinen, S., et al., *Radiotherapy enhanced ototoxicity of cisplatin in children.* Acta Otolaryngol Suppl, 1997. **529**: p. 90-4.
30. Fausti, S.A., et al., *High-frequency monitoring for early detection of cisplatin ototoxicity.* Arch Otolaryngol Head Neck Surg, 1993. **119**(6): p. 661-6.
31. Ress, B.D., et al., *Effects of cis-platinum chemotherapy on otoacoustic emissions: the development of an objective screening protocol. Third place--Resident Clinical Science Award 1998.* Otolaryngol Head Neck Surg, 1999. **121**(6): p. 693-701.
32. Lebwohl, D. and R. Canetta, *Clinical development of platinum complexes in cancer therapy: an historical perspective and an update.* Eur J Cancer, 1998. **34**(10): p. 1522-34.
33. Shiraishi, F., et al., *Heme oxygenase-1 gene ablation or expression modulates cisplatin-induced renal tubular apoptosis.* Am J Physiol Renal Physiol, 2000. **278**(5): p. F726-36.
34. Miller, R.P., et al., *Mechanisms of Cisplatin nephrotoxicity.* Toxins (Basel), 2010. **2**(11): p. 2490-518.
35. Volarevic, V., et al., *Molecular mechanisms of cisplatin-induced nephrotoxicity: a balance on the knife edge between renoprotection and tumor toxicity.* J Biomed Sci, 2019. **26**(1): p. 25.

36. Santoso, J.T., et al., *Saline, mannitol, and furosemide hydration in acute cisplatin nephrotoxicity: a randomized trial.* Cancer Chemother Pharmacol, 2003. **52**(1): p. 13-8.
37. de Jongh, F.E., et al., *Weekly high-dose cisplatin is a feasible treatment option: analysis on prognostic factors for toxicity in 400 patients.* Br J Cancer, 2003. **88**(8): p. 1199-206.
38. Pabla, N., et al., *The copper transporter Ctr1 contributes to cisplatin uptake by renal tubular cells during cisplatin nephrotoxicity.* Am J Physiol Renal Physiol, 2009. **296**(3): p. F505-11.
39. Ciarimboli, G., et al., *Organic cation transporter 2 mediates cisplatin-induced oto- and nephrotoxicity and is a target for protective interventions.* Am J Pathol, 2010. **176**(3): p. 1169-80.
40. Hanigan, M.H. and P. Devarajan, *Cisplatin nephrotoxicity: molecular mechanisms.* Cancer Ther, 2003. **1**: p. 47-61.
41. Yamashita, N., et al., *Cumulative DNA damage by repeated low-dose cisplatin injection promotes the transition of acute to chronic kidney injury in mice.* Sci Rep, 2021. **11**(1): p. 20920.
42. Kasherman, Y., S. Sturup, and D. Gibson, *Is glutathione the major cellular target of cisplatin? A study of the interactions of cisplatin with cancer cell extracts.* J Med Chem, 2009. **52**(14): p. 4319-28.
43. Domingo, I.K., A. Latif, and A.P. Bhavsar, *Pro-Inflammatory Signalling PRRopels Cisplatin-Induced Toxicity.* Int J Mol Sci, 2022. **23**(13).
44. Ozkok, A., et al., *NF-kappaB transcriptional inhibition ameliorates cisplatin-induced acute kidney injury (AKI).* Toxicol Lett, 2016. **240**(1): p. 105-13.
45. Sancho-Martinez, S.M., et al., *Necrotic concentrations of cisplatin activate the apoptotic machinery but inhibit effector caspases and interfere with the execution of apoptosis.* Toxicol Sci, 2011. **122**(1): p. 73-85.
46. Wei, Q., et al., *Activation and involvement of p53 in cisplatin-induced nephrotoxicity.* Am J Physiol Renal Physiol, 2007. **293**(4): p. F1282-91.
47. Cummings, B.S. and R.G. Schnellmann, *Cisplatin-induced renal cell apoptosis: caspase 3-dependent and -independent pathways.* J Pharmacol Exp Ther, 2002. **302**(1): p. 8-17.
48. Molitoris, B.A., et al., *siRNA targeted to p53 attenuates ischemic and cisplatin-induced acute kidney injury.* J Am Soc Nephrol, 2009. **20**(8): p. 1754-64.
49. Jiang, M., et al., *Regulation of PUMA-alpha by p53 in cisplatin-induced renal cell apoptosis.* Oncogene, 2006. **25**(29): p. 4056-66.
50. Seth, R., et al., *p53-dependent caspase-2 activation in mitochondrial release of apoptosis-inducing factor and its role in renal tubular epithelial cell injury.* J Biol Chem, 2005. **280**(35): p. 31230-9.
51. Jiang, M., et al., *Cisplatin-induced apoptosis in p53-deficient renal cells via the intrinsic mitochondrial pathway.* Am J Physiol Renal Physiol, 2009. **296**(5): p. F983-93.
52. Yuan, Y., et al., *p53 Contributes to Cisplatin Induced Renal Oxidative Damage via Regulating P66shc and MnSOD.* Cell Physiol Biochem, 2015. **37**(4): p. 1240-56.

53. Liu, X., et al., *Functional Role of p53 in the Regulation of Chemical-Induced Oxidative Stress.* Oxid Med Cell Longev, 2020. **2020**: p. 6039769.
54. Rivlin, N., et al., *Mutations in the p53 Tumor Suppressor Gene: Important Milestones at the Various Steps of Tumorigenesis.* Genes Cancer, 2011. **2**(4): p. 466-74.
55. Zhang, C., et al., *Gain-of-function mutant p53 in cancer progression and therapy.* J Mol Cell Biol, 2020. **12**(9): p. 674-687.
56. Chen, Z., et al., *MAP kinases.* Chem Rev, 2001. **101**(8): p. 2449-76.
57. Jo, S.K., et al., *MEK inhibitor, U0126, attenuates cisplatin-induced renal injury by decreasing inflammation and apoptosis.* Kidney Int, 2005. **67**(2): p. 458-66.
58. Francescato, H.D., et al., *Effect of JNK inhibition on cisplatin-induced renal damage.* Nephrol Dial Transplant, 2007. **22**(8): p. 2138-48.
59. Ramesh, G. and W.B. Reeves, *p38 MAP kinase inhibition ameliorates cisplatin nephrotoxicity in mice.* Am J Physiol Renal Physiol, 2005. **289**(1): p. F166-74.
60. Kim, Y.K., et al., *Role of ERK activation in cisplatin-induced apoptosis in OK renal epithelial cells.* J Appl Toxicol, 2005. **25**(5): p. 374-82.
61. Clark, J.S., et al., *Cisplatin induces apoptosis through the ERK-p66shc pathway in renal proximal tubule cells.* Cancer Lett, 2010. **297**(2): p. 165-70.
62. Nowak, G., *Protein kinase C-alpha and ERK1/2 mediate mitochondrial dysfunction, decreases in active Na+ transport, and cisplatin-induced apoptosis in renal cells.* J Biol Chem, 2002. **277**(45): p. 43377-88.
63. Arany, I., et al., *Cisplatin-induced cell death is EGFR/src/ERK signaling dependent in mouse proximal tubule cells.* Am J Physiol Renal Physiol, 2004. **287**(3): p. F543-9.
64. Mishima, K., et al., *Protective effect of cyclic AMP against cisplatin-induced nephrotoxicity.* Free Radic Biol Med, 2006. **40**(9): p. 1564-77.
65. Hansjosten, I., *Modulation der Cisplatin-induzierten Apoptose durch bioaktive kleine Moleküle*. 2017: Karlsruher Institut für Technologie (KIT).
66. Carmeci, C., et al., *Identification of a gene (GPR30) with homology to the G-protein-coupled receptor superfamily associated with estrogen receptor expression in breast cancer.* Genomics, 1997. **45**(3): p. 607-17.
67. Yan, M., et al., *Nuclear and cytoplasmic expressions of ERbeta1 and ERbeta2 are predictive of response to therapy and alters prognosis in familial breast cancers.* Breast Cancer Res Treat, 2011. **126**(2): p. 395-405.
68. Revankar, C.M., et al., *A transmembrane intracellular estrogen receptor mediates rapid cell signaling.* Science, 2005. **307**(5715): p. 1625-30.
69. Prossnitz, E.R. and H.J. Hathaway, *What have we learned about GPER function in physiology and disease from knockout mice?* J Steroid Biochem Mol Biol, 2015. **153**: p. 114-26.
70. Thomas, P., et al., *Identity of an estrogen membrane receptor coupled to a G protein in human breast cancer cells.* Endocrinology, 2005. **146**(2): p. 624-32.
71. Ding, X., et al., *Activation of the G Protein-Coupled Estrogen Receptor Elicits Store Calcium Release and Phosphorylation of the Mu-Opioid Receptors in the Human Neuroblastoma SH-SY5Y Cells.* Front Neurosci, 2019. **13**: p. 1351.

72. Petrie, W.K., et al., *G protein-coupled estrogen receptor-selective ligands modulate endometrial tumor growth.* Obstet Gynecol Int, 2013. **2013**: p. 472720.
73. Prossnitz, E.R., et al., *Estrogen signaling through the transmembrane G protein-coupled receptor GPR30.* Annu Rev Physiol, 2008. **70**: p. 165-90.
74. Prossnitz, E.R. and M. Barton, *The G-protein-coupled estrogen receptor GPER in health and disease.* Nat Rev Endocrinol, 2011. **7**(12): p. 715-26.
75. Yuan, J., et al., *Acquisition of epithelial-mesenchymal transition phenotype in the tamoxifen-resistant breast cancer cell: a new role for G protein-coupled estrogen receptor in mediating tamoxifen resistance through cancer-associated fibroblast-derived fibronectin and beta1-integrin signaling pathway in tumor cells.* Breast Cancer Res, 2015. **17**(1): p. 69.
76. Torres-Lopez, L., et al., *The G-Protein-Coupled Estrogen Receptor Agonist G-1 Inhibits Proliferation and Causes Apoptosis in Leukemia Cell Lines of T Lineage.* Front Cell Dev Biol, 2022. **10**: p. 811479.
77. Han, Z.W., et al., *GPER agonist G1 suppresses neuronal apoptosis mediated by endoplasmic reticulum stress after cerebral ischemia/reperfusion injury.* Neural Regen Res, 2019. **14**(7): p. 1221-1229.
78. Cheng, S.B., et al., *Anatomical location and redistribution of G protein-coupled estrogen receptor-1 during the estrus cycle in mouse kidney and specific binding to estrogens but not aldosterone.* Mol Cell Endocrinol, 2014. **382**(2): p. 950-9.
79. Lindsey, S.H., et al., *Estrogen receptor GPR30 reduces oxidative stress and proteinuria in the salt-sensitive female mRen2.Lewis rat.* Hypertension, 2011. **58**(4): p. 665-71.
80. Qiao, C., et al., *Icariin modulates mitochondrial function and apoptosis in high glucose-induced glomerular podocytes through G protein-coupled estrogen receptors.* Mol Cell Endocrinol, 2018. **473**: p. 146-155.
81. Kurt, A.H., et al., *The protective role of G protein-coupled estrogen receptor 1 (GPER-1) on methotrexate-induced nephrotoxicity in human renal epithelium cells.* Ren Fail, 2016. **38**(5): p. 686-92.
82. Gohar, E.Y., et al., *Does G Protein-Coupled Estrogen Receptor 1 Contribute to Cisplatin-Induced Acute Kidney Injury in Male Mice?* Int J Mol Sci, 2022. **23**(15).
83. Meyer, M.R., et al., *Obligatory role for GPER in cardiovascular aging and disease.* Sci Signal, 2016. **9**(452): p. ra105.
84. Hutchens, M.P., et al., *Estrogen-mediated renoprotection following cardiac arrest and cardiopulmonary resuscitation is robust to GPR30 gene deletion.* PLoS One, 2014. **9**(6): p. e99910.
85. Babolmorad, G., et al., *Toll-like receptor 4 is activated by platinum and contributes to cisplatin-induced ototoxicity.* EMBO Rep, 2021. **22**(5): p. e51280.
86. Pan, C., et al., *Cisplatin-mediated activation of glucocorticoid receptor induces platinum resistance via MAST1.* Nat Commun, 2021. **12**(1): p. 4960.
87. Tran, Q.K. and M. Vermeer, *Biosensor-based approach identifies four distinct calmodulin-binding domains in the G protein-coupled estrogen receptor 1.* PLoS One, 2014. **9**(2): p. e89669.

88. Schmidt-Wolf, R. and G. Zissel, *Interaction Between CCL18 and GPR30 Differs from the Interaction Between Estradiol and GPR30.* Anticancer Res, 2020. **40**(6): p. 3097-3108.
89. Roque, C. and G. Baltazar, *G protein-coupled estrogen receptor 1 (GPER) activation triggers different signaling pathways on neurons and astrocytes.* Neural Regen Res, 2019. **14**(12): p. 2069-2070.
90. Qiu, Y.A., et al., *GPER-Induced ERK Signaling Decreases Cell Viability of Hepatocellular Carcinoma.* Front Oncol, 2021. **11**: p. 638171.
91. Kabir, M.E., et al., *G Protein-Coupled Estrogen Receptor 1 Mediates Acute Estrogen-Induced Cardioprotection via MEK/ERK/GSK-3beta Pathway after Ischemia/Reperfusion.* PLoS One, 2015. **10**(9): p. e0135988.
92. Yu, X., et al., *The activation of G protein-coupled estrogen receptor induces relaxation via cAMP as well as potentiates contraction via EGFR transactivation in porcine coronary arteries.* PLoS One, 2018. **13**(1): p. e0191418.
93. Filardo, E.J., et al., *Estrogen-induced activation of Erk-1 and Erk-2 requires the G protein-coupled receptor homolog, GPR30, and occurs via trans-activation of the epidermal growth factor receptor through release of HB-EGF.* Mol Endocrinol, 2000. **14**(10): p. 1649-60.
94. Scaling, A.L., E.R. Prossnitz, and H.J. Hathaway, *GPER mediates estrogen-induced signaling and proliferation in human breast epithelial cells and normal and malignant breast.* Horm Cancer, 2014. **5**(3): p. 146-160.
95. Ding, Q., et al., *Estradiol-mediated ERK phosphorylation and apoptosis in vascular smooth muscle cells requires GPR 30.* Am J Physiol Cell Physiol, 2009. **297**(5): p. C1178-87.
96. Teame, T., et al., *The use of zebrafish (Danio rerio) as biomedical models.* Anim Front, 2019. **9**(3): p. 68-77.
97. Balon, E.K., *Terminology of intervals in fish development.* Journal of the Fisheries Board of Canada, 1975. **32**(9): p. 1663-1670.
98. Cianciolo Cosentino, C., et al., *Intravenous microinjections of zebrafish larvae to study acute kidney injury.* J Vis Exp, 2010(42).
99. Bauer, B., et al., *Exploration of zebrafish larvae as an alternative whole-animal model for nephrotoxicity testing.* Toxicol Lett, 2021. **344**: p. 69-81.
100. Choi, T.Y., et al., *Zebrafish as an animal model for biomedical research.* Exp Mol Med, 2021. **53**(3): p. 310-317.
101. Astell, K.R. and D. Sieger, *Zebrafish In Vivo Models of Cancer and Metastasis.* Cold Spring Harb Perspect Med, 2020. **10**(8).
102. D'Costa, A. and I.T. Shepherd, *Zebrafish development and genetics: introducing undergraduates to developmental biology and genetics in a large introductory laboratory class.* Zebrafish, 2009. **6**(2): p. 169-77.
103. Marques, I.J., E. Lupi, and N. Mercader, *Model systems for regeneration: zebrafish.* Development, 2019. **146**(18).
104. Major, R.J. and K.D. Poss, *Zebrafish Heart Regeneration as a Model for Cardiac Tissue Repair.* Drug Discov Today Dis Models, 2007. **4**(4): p. 219-225.

105. Noorimotlagh, Z., et al., *Mechanisms of spinal cord injury regeneration in zebrafish: a systematic review.* Iran J Basic Med Sci, 2017. **20**(12): p. 1287-1296.
106. Uemoto, T., G. Abe, and K. Tamura, *Regrowth of zebrafish caudal fin regeneration is determined by the amputated length.* Sci Rep, 2020. **10**(1): p. 649.
107. Patton, E.E. and L.I. Zon, *The art and design of genetic screens: zebrafish.* Nat Rev Genet, 2001. **2**(12): p. 956-66.
108. Wiley, D.S., S.E. Redfield, and L.I. Zon, *Chemical screening in zebrafish for novel biological and therapeutic discovery.* Methods Cell Biol, 2017. **138**: p. 651-679.
109. Vaz, R.L., T.F. Outeiro, and J.J. Ferreira, *Zebrafish as an Animal Model for Drug Discovery in Parkinson's Disease and Other Movement Disorders: A Systematic Review.* Front Neurol, 2018. **9**: p. 347.
110. Avdesh, A., et al., *Regular care and maintenance of a zebrafish (Danio rerio) laboratory: an introduction.* J Vis Exp, 2012(69): p. e4196.
111. Drummond, I.A. and A.J. Davidson, *Zebrafish kidney development.* Methods Cell Biol, 2010. **100**: p. 233-60.
112. Drummond, I., *Making a zebrafish kidney: a tale of two tubes.* Trends Cell Biol, 2003. **13**(7): p. 357-65.
113. Gerlach, G.F. and R.A. Wingert, *Kidney organogenesis in the zebrafish: insights into vertebrate nephrogenesis and regeneration.* Wiley Interdiscip Rev Dev Biol, 2013. **2**(5): p. 559-85.
114. Elmonem, M.A., et al., *Genetic Renal Diseases: The Emerging Role of Zebrafish Models.* Cells, 2018. **7**(9).
115. Fatma, S., U. Nayak, and R.K. Swain, *Methods to generate and evaluate zebrafish models of human kidney diseases.* Int J Dev Biol, 2021. **65**(7-8-9): p. 475-485.
116. Desgrange, A. and S. Cereghini, *Nephron Patterning: Lessons from Xenopus, Zebrafish, and Mouse Studies.* Cells, 2015. **4**(3): p. 483-99.
117. *EU. Directive 2010/63/EU of the European parliament and of the council of 22 September 2010 on the protection of animals used for scientific purposes.* Off J EU, 2010. **L 276**: p. 33-79.
118. McCampbell, K.K. and R.A. Wingert, *New tides: using zebrafish to study renal regeneration.* Transl Res, 2014. **163**(2): p. 109-22.
119. Perse, M. and Z. Veceric-Haler, *Cisplatin-Induced Rodent Model of Kidney Injury: Characteristics and Challenges.* Biomed Res Int, 2018. **2018**: p. 1462802.
120. Wang, Y., et al., *Progressive adriamycin nephropathy in mice: sequence of histologic and immunohistochemical events.* Kidney Int, 2000. **58**(4): p. 1797-804.
121. Suzuki, S., et al., *Comparison of gentamicin nephrotoxicity between rats and mice.* Comp Biochem Physiol C Pharmacol Toxicol Endocrinol, 1995. **112**(1): p. 15-28.
122. Nguyen, L., et al., *The Nephrotoxin Puromycin Aminonucleoside Induces Injury in Kidney Organoids Differentiated from Induced Pluripotent Stem Cells.* Cells, 2022. **11**(4).
123. Westhoff, J.H., et al., *In vivo High-Content Screening in Zebrafish for Developmental Nephrotoxicity of Approved Drugs.* Front Cell Dev Biol, 2020. **8**: p. 583.

124. Cirio, M.C., M.P. de Caestecker, and N.A. Hukriede, *Zebrafish Models of Kidney Damage and Repair.* Curr Pathobiol Rep, 2015. **3**(2): p. 163-170.
125. Hentschel, D.M., et al., *Acute renal failure in zebrafish: a novel system to study a complex disease.* Am J Physiol Renal Physiol, 2005. **288**(5): p. F923-9.
126. Zennaro, C., et al., *Podocyte developmental defects caused by adriamycin in zebrafish embryos and larvae: a novel model of glomerular damage.* PLoS One, 2014. **9**(5): p. e98131.
127. Rider, S.A., et al., *The Efficacy of Puromycin and Adriamycin for Induction of Glomerular Failure in Larval Zebrafish Validated by an Assay of Glomerular Permeability Dynamics.* Zebrafish, 2018. **15**(3): p. 234-242.
128. Scheidecker, S., et al., *Exome sequencing of Bardet-Biedl syndrome patient identifies a null mutation in the BBSome subunit BBIP1 (BBS18).* J Med Genet, 2014. **51**(2): p. 132-6.
129. Hanke, N., et al., *"Zebrafishing" for novel genes relevant to the glomerular filtration barrier.* Biomed Res Int, 2013. **2013**: p. 658270.
130. Poureetezadi, S.J. and R.A. Wingert, *Little fish, big catch: zebrafish as a model for kidney disease.* Kidney Int, 2016. **89**(6): p. 1204-10.
131. Zhou, W. and F. Hildebrandt, *Inducible podocyte injury and proteinuria in transgenic zebrafish.* J Am Soc Nephrol, 2012. **23**(6): p. 1039-47.
132. Naylor, R.W., et al., *A novel nanoluciferase transgenic reporter measures proteinuria in zebrafish.* Kidney Int, 2022. **102**(4): p. 815-827.
133. Wen, X., et al., *A zebrafish model of infection-associated acute kidney injury.* Am J Physiol Renal Physiol, 2018. **315**(2): p. F291-F299.
134. Zhou, W., et al., *Characterization of mesonephric development and regeneration using transgenic zebrafish.* Am J Physiol Renal Physiol, 2010. **299**(5): p. F1040-7.
135. Wang, X., et al., *Evaluation of nephrotoxic effects of aristolochic acid on zebrafish (Danio rerio) larvae.* Hum Exp Toxicol, 2016. **35**(9): p. 974-82.
136. Hentschel, D.M., et al., *Rapid screening of glomerular slit diaphragm integrity in larval zebrafish.* Am J Physiol Renal Physiol, 2007. **293**(5): p. F1746-50.
137. Bollig, F., et al., *Identification and comparative expression analysis of a second wt1 gene in zebrafish.* Dev Dyn, 2006. **235**(2): p. 554-61.
138. Coffey, C.M., et al., *Novel oxytocin gene expression in the hindbrain is induced by alcohol exposure: transgenic zebrafish enable visualization of sensitive neurons.* PLoS One, 2013. **8**(1): p. e53991.
139. Jin, M., et al., *Claudin-7b and Claudin-h are required for controlling cilia morphogenesis in the zebrafish kidney.* Mech Dev, 2020. **161**: p. 103595.
140. Wang, Y., et al., *Grouper tshbeta promoter-driven transgenic zebrafish marks proximal kidney tubule development.* PLoS One, 2014. **9**(6): p. e97806.
141. Han, W.K., et al., *Kidney Injury Molecule-1 (KIM-1): a novel biomarker for human renal proximal tubule injury.* Kidney Int, 2002. **62**(1): p. 237-44.
142. Bonventre, J.V., *Kidney Injury Molecule-1 (KIM-1): a specific and sensitive biomarker of kidney injury.* Scand J Clin Lab Invest Suppl, 2008. **241**: p. 78-83.

143. Guo, J., et al., *Relationship of clusterin with renal inflammation and fibrosis after the recovery phase of ischemia-reperfusion injury.* BMC Nephrol, 2016. **17**(1): p. 133.
144. Toda, N., et al., *CTGF in kidney fibrosis and glomerulonephritis.* Inflamm Regen, 2018. **38**: p. 14.
145. Chaturantabut, S., et al., *Estrogen Activation of G-Protein-Coupled Estrogen Receptor 1 Regulates Phosphoinositide 3-Kinase and mTOR Signaling to Promote Liver Growth in Zebrafish and Proliferation of Human Hepatocytes.* Gastroenterology, 2019. **156**(6): p. 1788-1804 e13.
146. Weger, M., et al., *MondoA regulates gene expression in cholesterol biosynthesis-associated pathways required for zebrafish epiboly.* Elife, 2020. **9**.
147. Finckbeiner, S., et al., *Transient knockdown and overexpression reveal a developmental role for the zebrafish enosf1b gene.* Cell Biosci, 2011. **1**: p. 32.
148. Hansjosten, I., et al., *Surface functionalisation-dependent adverse effects of metal nanoparticles and nanoplastics in zebrafish embryos.* Environmental science / Nano, 2022. **91**(1): p. 375-392.
149. Hayashi, Y., et al., *Differential Nanoparticle Sequestration by Macrophages and Scavenger Endothelial Cells Visualized in Vivo in Real-Time and at Ultrastructural Resolution.* ACS Nano, 2020. **14**(2): p. 1665-1681.
150. Elabd, S., et al., *Delay in development and behavioural abnormalities in the absence of p53 in zebrafish.* PLoS One, 2019. **14**(7): p. e0220069.
151. Westerfield, M. and T. Book, *A guide for the laboratory use of zebrafish Danio (Brachydanio) rerio*. 1994, University of Oregon Press, Eugene.
152. Alestrom, P., et al., *Zebrafish: Housing and husbandry recommendations.* Lab Anim, 2020. **54**(3): p. 213-224.
153. Kobayashi, M., A. Jamieson-Lucy, and M.C. Mullins, *Microinjection Method for Analyzing Zebrafish Early Stage Oocytes.* Front Cell Dev Biol, 2021. **9**: p. 753642.
154. Zakaria, Z.Z., et al., *Design and Microinjection of Morpholino Antisense Oligonucleotides and mRNA into Zebrafish Embryos to Elucidate Specific Gene Function in Heart Development.* J Vis Exp, 2022(186).
155. Stainier, D.Y.R., et al., *Guidelines for morpholino use in zebrafish.* PLoS Genet, 2017. **13**(10): p. e1007000.
156. Eisen, J.S. and J.C. Smith, *Controlling morpholino experiments: don't stop making antisense.* Development, 2008. **135**(10): p. 1735-43.
157. Lubke, L., et al., *mdka Expression Is Associated with Quiescent Neural Stem Cells during Constitutive and Reactive Neurogenesis in the Adult Zebrafish Telencephalon.* Brain Sci, 2022. **12**(2).
158. Livak, K.J. and T.D. Schmittgen, *Analysis of relative gene expression data using real-time quantitative PCR and the 2(-Delta Delta C(T)) Method.* Methods, 2001. **25**(4): p. 402-8.
159. Vo, A.H., et al., *Loss of fibrinogen in zebrafish results in symptoms consistent with human hypofibrinogenemia.* PLoS One, 2013. **8**(9): p. e74682.

160. O'Brien, L.L., et al., *Wt1a, Foxc1a, and the Notch mediator Rbpj physically interact and regulate the formation of podocytes in zebrafish.* Dev Biol, 2011. **358**(2): p. 318-30.
161. He, B., et al., *Podocin-green fluorescence protein allows visualization and functional analysis of podocytes.* J Am Soc Nephrol, 2011. **22**(6): p. 1019-23.
162. Huang, J., et al., *A zebrafish model of conditional targeted podocyte ablation and regeneration.* Kidney Int, 2013. **83**(6): p. 1193-200.
163. Rieke, J.M., et al., *SLC20A1 Is Involved in Urinary Tract and Urorectal Development.* Front Cell Dev Biol, 2020. **8**: p. 567.
164. Liu, Y., et al., *Notch signaling controls the differentiation of transporting epithelia and multiciliated cells in the zebrafish pronephros.* Development, 2007. **134**(6): p. 1111-22.
165. Cha, Y.R. and B.M. Weinstein, *Use of PCR template-derived probes prevents off-target whole mount in situ hybridization in transgenic zebrafish.* Zebrafish, 2012. **9**(2): p. 85-9.
166. Westerfield, S.O.S.a.M., *The Zebrafish Book. Guide for the Laboratory Use of Zebrafish (Danio rerio)*. 1995.
167. Mahmood, T. and P.C. Yang, *Western blot: technique, theory, and trouble shooting.* N Am J Med Sci, 2012. **4**(9): p. 429-34.
168. Gallo-Oller, G., R. Ordonez, and J. Dotor, *A new background subtraction method for Western blot densitometry band quantification through image analysis software.* J Immunol Methods, 2018. **457**: p. 1-5.
169. Abraham-Juárez, M.J., *Western Blot in Maize.* Bio-Protocol, 2019. **9**(11).
170. Takamiya, M., et al., *Molecular description of eye defects in the zebrafish Pax6b mutant, sunrise, reveals a Pax6b-dependent genetic network in the developing anterior chamber.* PLoS One, 2015. **10**(2): p. e0117645.
171. Ghnenis, A.B., et al., *Toluidine Blue Staining of Resin-Embedded Sections for Evaluation of Peripheral Nerve Morphology.* J Vis Exp, 2018(137).
172. Sridharan, G. and A.A. Shankar, *Toluidine blue: A review of its chemistry and clinical utility.* J Oral Maxillofac Pathol, 2012. **16**(2): p. 251-5.
173. Sullivan-Brown, J., M.E. Bisher, and R.D. Burdine, *Embedding, serial sectioning and staining of zebrafish embryos using JB-4 resin.* Nat Protoc, 2011. **6**(1): p. 46-55.
174. Christou-Savina, S., P.L. Beales, and D.P. Osborn, *Evaluation of zebrafish kidney function using a fluorescent clearance assay.* J Vis Exp, 2015(96): p. e52540.
175. Buckley, C., et al., *Precise spatio-temporal control of rapid optogenetic cell ablation with mem-KillerRed in Zebrafish.* Sci Rep, 2017. **7**(1): p. 5096.
176. Yin, C. and L. Solnica-Krezel, *Convergence and extension movements affect dynamic notochord-somite interactions essential for zebrafish slow muscle morphogenesis.* Dev Dyn, 2007. **236**(10): p. 2742-56.
177. Morales Fenero, C., et al., *Acute Kidney Injury Model Induced by Cisplatin in Adult Zebrafish.* J Vis Exp, 2021(171).

178. Kim, M.J., et al., *Cisplatin nephrotoxicity is induced via poly(ADP-ribose) polymerase activation in adult zebrafish and mice.* Am J Physiol Regul Integr Comp Physiol, 2020. **318**(5): p. R843-R854.
179. Perse, M., *Cisplatin Mouse Models: Treatment, Toxicity and Translatability.* Biomedicines, 2021. **9**(10).
180. Gersten, B.K., et al., *Ototoxicity and Platinum Uptake Following Cyclic Administration of Platinum-Based Chemotherapeutic Agents.* J Assoc Res Otolaryngol, 2020. **21**(4): p. 303-321.
181. Marmiroli, P., et al., *Susceptibility of different mouse strains to oxaliplatin peripheral neurotoxicity: Phenotypic and genotypic insights.* PLoS One, 2017. **12**(10): p. e0186250.
182. Shi, M., et al., *Cisplatin nephrotoxicity as a model of chronic kidney disease.* Lab Invest, 2018. **98**(8): p. 1105-1121.
183. Attia, A., et al., *Cisplatin-induced neurotoxicity in cerebellar cortex of male mice involves oxidative stress and histopathology.* The Journal of Basic and Applied Zoology, 2021. **82**(1): p. 1-10.
184. Fernandez, K., et al., *An optimized, clinically relevant mouse model of cisplatin-induced ototoxicity.* Hear Res, 2019. **375**: p. 66-74.
185. Dalian, D., et al., *Ototoxic Effects of Carboplatin in Organotypic Cultures in Chinchillas and Rats.* J Otol, 2012. **7**(2): p. 92-101.
186. Lee, D.S., et al., *Evaluation of Cisplatin-Induced Pathology in the Larval Zebrafish Lateral Line.* Int J Mol Sci, 2022. **23**(22).
187. Di Paola, D., et al., *Environmental Risk Assessment of Oxaliplatin Exposure on Early Life Stages of Zebrafish (Danio rerio).* Toxics, 2022. **10**(2).
188. Wertman, J.N., et al., *The identification of dual protective agents against cisplatin-induced oto- and nephrotoxicity using the zebrafish model.* Elife, 2020. **9**.
189. Ma, L., et al., *A Cancer Cell-Selective and Low-Toxic Bifunctional Heterodinuclear Pt(IV)-Ru(II) Anticancer Prodrug.* Inorg Chem, 2018. **57**(5): p. 2917-2924.
190. Bolten, J.S., et al., *Zebrafish (Danio rerio) larvae as a predictive model to study gentamicin-induced structural alterations of the kidney.* PLoS One, 2023. **18**(4): p. e0284562.
191. Khan, A.H., et al., *Effect of calcium channel blockade on adrenergically induced renal vasoconstriction in rat models of renal impairment.* Clin Exp Pharmacol Physiol, 2009. **36**(5-6): p. 501-8.
192. Tusgaard, B., et al., *Cisplatin decreases renal cyclooxygenase-2 expression and activity in rats.* Acta Physiol (Oxf), 2011. **202**(1): p. 79-90.
193. Ozkok, A. and C.L. Edelstein, *Pathophysiology of cisplatin-induced acute kidney injury.* Biomed Res Int, 2014. **2014**: p. 967826.
194. Lieberthal, W., V. Triaca, and J. Levine, *Mechanisms of death induced by cisplatin in proximal tubular epithelial cells: apoptosis vs. necrosis.* Am J Physiol, 1996. **270**(4 Pt 2): p. F700-8.
195. Zsengeller, Z.K., et al., *Cisplatin nephrotoxicity involves mitochondrial injury with impaired tubular mitochondrial enzyme activity.* J Histochem Cytochem, 2012. **60**(7): p. 521-9.

196. Li, J., et al., *Blocking Macrophage Migration Inhibitory Factor Protects Against Cisplatin-Induced Acute Kidney Injury in Mice.* Mol Ther, 2018. **26**(10): p. 2523-2532.
197. Inoue, T., *M1 macrophage triggered by Mincle leads to a deterioration of acute kidney injury.* Kidney Int, 2017. **91**(3): p. 526-529.
198. Drummond, I.A., et al., *Early development of the zebrafish pronephros and analysis of mutations affecting pronephric function.* Development, 1998. **125**(23): p. 4655-67.
199. McKeage, M.J., *Comparative adverse effect profiles of platinum drugs.* Drug Saf, 1995. **13**(4): p. 228-44.
200. Duan, J., et al., *Low-dose exposure of silica nanoparticles induces cardiac dysfunction via neutrophil-mediated inflammation and cardiac contraction in zebrafish embryos.* Nanotoxicology, 2016. **10**(5): p. 575-85.
201. Vasamsetti, B.M.K., et al., *Developmental Toxic Effects of Thiram on Developing Zebrafish (Danio rerio) Embryos.* Toxics, 2022. **10**(7).
202. Quan, H., et al., *Fimasartan, an angiotensin II receptor antagonist, ameliorates an in vivo zebrafish model of heart failure.* Korean J Intern Med, 2020. **35**(6): p. 1400-1410.
203. Kumar, D., et al., *Microvillar and ciliary defects in zebrafish lacking an actin-binding bioactive peptide amidating enzyme.* Sci Rep, 2018. **8**(1): p. 4547.
204. Kasher, P.R., et al., *Characterization of samhd1 morphant zebrafish recapitulates features of the human type I interferonopathy Aicardi-Goutieres syndrome.* J Immunol, 2015. **194**(6): p. 2819-25.
205. Ren, Z., et al., *Assessment of eco-toxic effects of commonly used water disinfectant on zebrafish (Danio rerio) swimming behaviour and recovery responses: an early-warning biomarker approach.* Environ Sci Pollut Res Int, 2022. **29**(27): p. 41849-41862.
206. Young-Sun, M., et al., *Acute toxicity and gene responses induced by endosulfan in zebrafish (Danio rerio) embryos.* Environmental Pollutants & Bioavailability, 2016. **28**(1-4).
207. Wan-Mohtar, W., et al., *Use of Zebrafish Embryo Assay to Evaluate Toxicity and Safety of Bioreactor-Grown Exopolysaccharides and Endopolysaccharides from European Ganoderma applanatum Mycelium for Future Aquaculture Applications.* Int J Mol Sci, 2021. **22**(4).
208. Capek, D., et al., *EmbryoNet: using deep learning to link embryonic phenotypes to signaling pathways.* Nat Methods, 2023. **20**(6): p. 815-823.
209. Chen, Z., et al., *Transgenic zebrafish modeling low-molecular-weight proteinuria and lysosomal storage diseases.* Kidney Int, 2020. **97**(6): p. 1150-1163.
210. Morozov, D., et al., *Mapping kidney tubule diameter ex vivo by diffusion MRI.* Am J Physiol Renal Physiol, 2021. **320**(5): p. F934-F946.
211. Du, Z., et al., *Mechanosensory function of microvilli of the kidney proximal tubule.* Proc Natl Acad Sci U S A, 2004. **101**(35): p. 13068-73.
212. Tadagavadi, R.K. and W.B. Reeves, *Renal dendritic cells ameliorate nephrotoxic acute kidney injury.* J Am Soc Nephrol, 2010. **21**(1): p. 53-63.

213. Gonzales-Vitale, J.C., et al., *The renal pathology in clinical trials of cis-platinum (II) diamminedichloride.* Cancer, 1977. **39**(4): p. 1362-71.
214. van Angelen, A.A., et al., *Cisplatin-induced injury of the renal distal convoluted tubule is associated with hypomagnesaemia in mice.* Nephrol Dial Transplant, 2013. **28**(4): p. 879-89.
215. Allen, G.G. and L.J. Barratt, *Effect of cisplatin on the transepithelial potential difference of rat distal tubule.* Kidney Int, 1985. **27**(6): p. 842-7.
216. Ambrosini, G., et al., *The GPER Agonist LNS8801 Induces Mitotic Arrest and Apoptosis in Uveal Melanoma Cells.* Cancer Res Commun, 2023. **3**(4): p. 540-547.
217. Dennis, M.K., et al., *Identification of a GPER/GPR30 antagonist with improved estrogen receptor counterselectivity.* J Steroid Biochem Mol Biol, 2011. **127**(3-5): p. 358-66.
218. McCurley, A.T. and G.V. Callard, *Characterization of housekeeping genes in zebrafish: male-female differences and effects of tissue type, developmental stage and chemical treatment.* BMC Mol Biol, 2008. **9**: p. 102.
219. Bolar, N.A., et al., *Heterozygous Loss-of-Function SEC61A1 Mutations Cause Autosomal-Dominant Tubulo-Interstitial and Glomerulocystic Kidney Disease with Anemia.* Am J Hum Genet, 2016. **99**(1): p. 174-87.
220. Hultman, K.A., A.W. Scott, and S.L. Johnson, *Small molecule modifier screen for kit-dependent functions in zebrafish embryonic melanocytes.* Zebrafish, 2008. **5**(4): p. 279-87.
221. Hawkins, T.A., et al., *The small molecule Mek1/2 inhibitor U0126 disrupts the chordamesoderm to notochord transition in zebrafish.* BMC Dev Biol, 2008. **8**: p. 42.
222. Palchaudhuri, R., et al., *A Small Molecule that Induces Intrinsic Pathway Apoptosis with Unparalleled Speed.* Cell Rep, 2015. **13**(9): p. 2027-36.
223. Colombo, E.A., et al., *A zebrafish model of Poikiloderma with Neutropenia recapitulates the human syndrome hallmarks and traces back neutropenia to the myeloid progenitor.* Sci Rep, 2015. **5**: p. 15814.
224. Parra, M.K., et al., *Deep intron elements mediate nested splicing events at consecutive AG dinucleotides to regulate alternative 3' splice site choice in vertebrate 4.1 genes.* Mol Cell Biol, 2012. **32**(11): p. 2044-53.
225. Olive, P.L. and J.P. Banath, *Kinetics of H2AX phosphorylation after exposure to cisplatin.* Cytometry B Clin Cytom, 2009. **76**(2): p. 79-90.
226. Guan, B.Z., et al., *Activation of G protein coupled estrogen receptor (GPER) promotes the migration of renal cell carcinoma via the PI3K/AKT/MMP-9 signals.* Cell Adh Migr, 2018. **12**(2): p. 109-117.
227. Natale, C.A., et al., *Activation of G protein-coupled estrogen receptor signaling inhibits melanoma and improves response to immune checkpoint blockade.* Elife, 2018. **7**.
228. Randjelovic, P., et al., *Gentamicin nephrotoxicity in animals: Current knowledge and future perspectives.* EXCLI J, 2017. **16**: p. 388-399.

229. Zhang, J., et al., *Cisplatin chemotherapy and renal function.* Adv Cancer Res, 2021. **152**: p. 305-327.
230. Ozbek, E., et al., *Atorvastatin prevents gentamicin-induced renal damage in rats through the inhibition of p38-MAPK and NF-kappaB pathways.* Ren Fail, 2009. **31**(5): p. 382-92.
231. Dieterle, F., et al., *Renal biomarker qualification submission: a dialog between the FDA-EMEA and Predictive Safety Testing Consortium.* Nat Biotechnol, 2010. **28**(5): p. 455-62.
232. Faught, L.N., et al., *Drug-induced acute kidney injury in children.* Br J Clin Pharmacol, 2015. **80**(4): p. 901-9.
233. Ichimura, T., et al., *Kidney injury molecule-1 (KIM-1), a putative epithelial cell adhesion molecule containing a novel immunoglobulin domain, is up-regulated in renal cells after injury.* J Biol Chem, 1998. **273**(7): p. 4135-42.
234. Rider, S.A., et al., *Zebrafish mesonephric renin cells are functionally conserved and comprise two distinct morphological populations.* Am J Physiol Renal Physiol, 2017. **312**(4): p. F778-F790.
235. Yin, W., et al., *Mammalian Target of Rapamycin Mediates Kidney Injury Molecule 1-Dependent Tubule Injury in a Surrogate Model.* J Am Soc Nephrol, 2016. **27**(7): p. 1943-57.
236. Liao, Z., et al., *Innate Immune Response to Fasting and Refeeding in the Zebrafish Kidney.* Biomolecules, 2021. **11**(6).
237. Babich, R., et al., *Kidney developmental effects of metal-herbicide mixtures: Implications for chronic kidney disease of unknown etiology.* Environ Int, 2020. **144**: p. 106019.
238. Jeong, Y.M., et al., *Induction of clusterin expression by neuronal cell death in Zebrafish.* J Genet Genomics, 2014. **41**(11): p. 583-9.
239. Dieterle, F., et al., *Urinary clusterin, cystatin C, beta2-microglobulin and total protein as markers to detect drug-induced kidney injury.* Nat Biotechnol, 2010. **28**(5): p. 463-9.
240. Yang, L., X. Li, and H. Wang, *Possible mechanisms explaining the tendency towards interstitial fibrosis in aristolochic acid-induced acute tubular necrosis.* Nephrol Dial Transplant, 2007. **22**(2): p. 445-56.
241. Stemmer, K., et al., *Molecular characterization of preneoplastic lesions provides insight on the development of renal tumors.* Am J Pathol, 2009. **175**(4): p. 1686-98.
242. Brilli Skvarca, L., et al., *Enhancing regeneration after acute kidney injury by promoting cellular dedifferentiation in zebrafish.* Dis Model Mech, 2019. **12**(4).
243. Chambers, J.M., et al., *ppargc1a controls nephron segmentation during zebrafish embryonic kidney ontogeny.* Elife, 2018. **7**.
244. Schenk, H., et al., *Disease modeling in genetic kidney diseases: zebrafish.* Cell Tissue Res, 2017. **369**(1): p. 127-141.
245. Takamiya, M., et al., *Melanosomes in pigmented epithelia maintain eye lens transparency during zebrafish embryonic development.* Sci Rep, 2016. **6**: p. 25046.

246. Ota, S., et al., *NLK positively regulates Wnt/beta-catenin signalling by phosphorylating LEF1 in neural progenitor cells.* EMBO J, 2012. **31**(8): p. 1904-15.
247. Bar, J., et al., *Induction of Activating Transcription Factor 3 Is Associated with Cisplatin Responsiveness in Non-Small Cell Lung Carcinoma Cells.* Neoplasia, 2016. **18**(9): p. 525-35.
248. Leng, Y., et al., *Ghrelin enhances cisplatin sensitivity in HO-8910 PM human ovarian cancer cells.* J Ovarian Res, 2021. **14**(1): p. 162.
249. Kim, D.U., et al., *Ojeoksan Ameliorates Cisplatin-Induced Acute Kidney Injury in Mice by Downregulating MAPK and NF-kappaB Pathways.* Int J Mol Sci, 2022. **23**(20).
250. Babu, S., Y. Takeuchi, and I. Masai, *Banp regulates DNA damage response and chromosome segregation during the cell cycle in zebrafish retina.* Elife, 2022. **11**.
251. Kutuk, O., et al., *Cisplatin overcomes Bcl-2-mediated resistance to apoptosis via preferential engagement of Bak: critical role of Noxa-mediated lipid peroxidation.* Carcinogenesis, 2009. **30**(9): p. 1517-27.
252. Jiang, M., et al., *Nutlin-3 protects kidney cells during cisplatin therapy by suppressing Bax/Bak activation.* J Biol Chem, 2007. **282**(4): p. 2636-45.
253. Maclaine, N.J. and T.R. Hupp, *The regulation of p53 by phosphorylation: a model for how distinct signals integrate into the p53 pathway.* Aging (Albany NY), 2009. **1**(5): p. 490-502.
254. Reed, S.M. and D.E. Quelle, *p53 Acetylation: Regulation and Consequences.* Cancers (Basel), 2014. **7**(1): p. 30-69.
255. West, L.E. and O. Gozani, *Regulation of p53 function by lysine methylation.* Epigenomics, 2011. **3**(3): p. 361-9.
256. MacLaine, N.J. and T.R. Hupp, *How phosphorylation controls p53.* Cell Cycle, 2011. **10**(6): p. 916-21.
257. Robu, M.E., et al., *p53 activation by knockdown technologies.* PLoS Genet, 2007. **3**(5): p. e78.
258. Kuo, W.T., et al., *Quantitative analysis of ligand-EGFR interactions: a platform for screening targeting molecules.* PLoS One, 2015. **10**(2): p. e0116610.
259. Patching, S.G., *Surface plasmon resonance spectroscopy for characterisation of membrane protein-ligand interactions and its potential for drug discovery.* Biochim Biophys Acta, 2014. **1838**(1 Pt A): p. 43-55.
260. Upadhayay, S., et al., *Involvement of the G-Protein-Coupled Estrogen Receptor-1 (GPER) Signaling Pathway in Neurodegenerative Disorders: A Review.* Cell Mol Neurobiol, 2023. **43**(5): p. 1833-1847.
261. Filardo, E.J., *Epidermal growth factor receptor (EGFR) transactivation by estrogen via the G-protein-coupled receptor, GPR30: a novel signaling pathway with potential significance for breast cancer.* J Steroid Biochem Mol Biol, 2002. **80**(2): p. 231-8.
262. Benhar, M., D. Engelberg, and A. Levitzki, *Cisplatin-induced activation of the EGF receptor.* Oncogene, 2002. **21**(57): p. 8723-31.

263. Liccardi, G., J.A. Hartley, and D. Hochhauser, *EGFR nuclear translocation modulates DNA repair following cisplatin and ionizing radiation treatment.* Cancer Res, 2011. **71**(3): p. 1103-14.
264. Winograd-Katz, S.E. and A. Levitzki, *Cisplatin induces PKB/Akt activation and p38(MAPK) phosphorylation of the EGF receptor.* Oncogene, 2006. **25**(56): p. 7381-90.
265. Yue, J. and J.M. Lopez, *Understanding MAPK Signaling Pathways in Apoptosis.* Int J Mol Sci, 2020. **21**(7).
266. Kishi, T., et al., *Angiotensin II type 1 receptor-activated caspase-3 through ras/mitogen-activated protein kinase/extracellular signal-regulated kinase in the rostral ventrolateral medulla is involved in sympathoexcitation in stroke-prone spontaneously hypertensive rats.* Hypertension, 2010. **55**(2): p. 291-7.
267. Jiang, M. and Z. Dong, *Regulation and pathological role of p53 in cisplatin nephrotoxicity.* J Pharmacol Exp Ther, 2008. **327**(2): p. 300-7.

Appendices

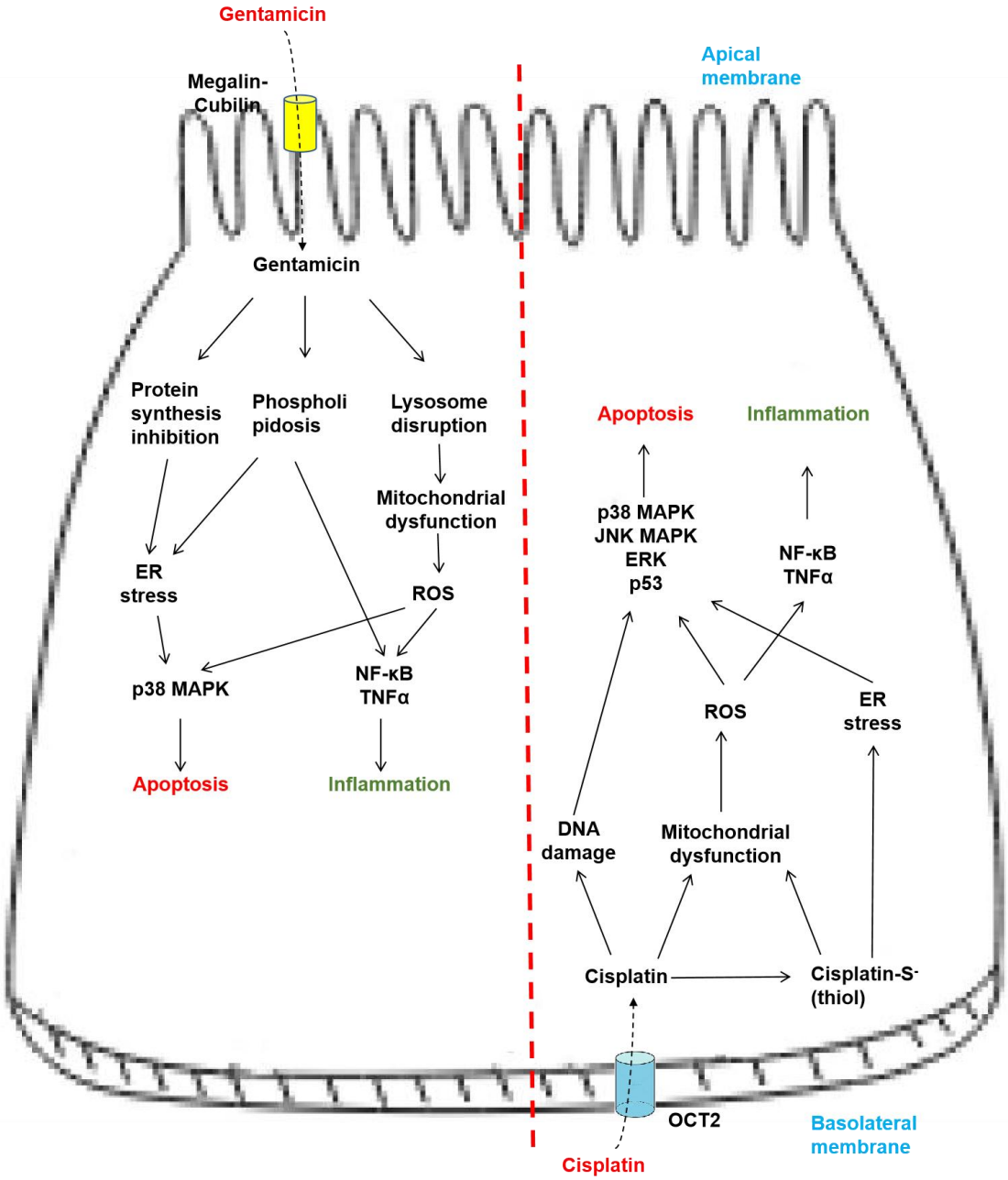

Figure S.1 Gentamicin and cisplatin-induced nephrotoxicity mechanisms comparison
The red dotted arrow separates gentamicin on the left and cisplatin on the right.

Methods of observation	ISH (Stained with ***podocin*** probe)	ISH (Stained with ***cdh17*** probe)	ISH (Stained with ***nephrin*** probe)	ISH (Stained with ***slc20a1a*** probe)	ISH (Stained with ***trpm7*** probe)	Tunel staining with whole mount IHC (Stained with **ATP1A1**antibody)	Acridine orange	DAPI staining with whole mount IHC (Stained with **ATP1A1**antibody)
Endpoint	Glomerulus	pronephric tubules	Glomerulus	Proximal tubule	Distal tubule	Apoptotic cells in pronephric tubules	apoptotic cells	Apoptotic cells in pronephric tubules
Life stage of zebrafish	4 dpf	4 dpf	4 dpf	4 dpf	4 dpf	3 or 4 dpf	3 to 5 dpf	4 dpf
References	Zhang et at. [267]	Bauer et at. [99]	Zhang et at. [267]	Wingert et al.[268]	Wingert et al.[268]	Drummondet al.[197]	Parng et al.[269]	Wingert et al.[268]
Results	Signal was successfully detected in the target area	Signal was successfully detected in the distal tube, not proximal tubule	No signal was detected in the target area			All apoptotic Signal was detected in the surface of zebrafish	Embryos fixation would caused Fluorescence quenching	No signal was detected in the pronephric tubules
The reasons why follow-up experiments cannot be carried out	We observed disarray in the cell structure of glomeruli induced by cisplatin. However, there is a lack of criteria for determining the restorative effect of GPER inhibition on cisplatin-induced nephrotoxicity.	Compared to the position of the proximal tubule, which is located deeper in the zebrafish body, the distal tubule is closer to the surface of the zebrafish. This allows ISH probes to easily enter the distal tubule but not the proximal tubule.	The majority of the literature utilizes early-stage zebrafish embryos (1-2 dpf). Considering that zebrafish embryos at 3-5 dpf have a more compact structure, conventional tissue softening methods such as proteinase K or acetone treatment may not adequately facilitate probe penetration.			Similar to the ISH results, the probes from the TUNEL kit were unable to penetrate the tissue and enter the pronephron region.	Acridine orange detection needs to be performed in live zebrafish larvae. In the absence of a zebrafish reporter line, it is difficult to accurately detect apoptotic signals. Any tissue fixation method leads to fluorescence quenching, making it challenging to combine IHC (stained with α6F monoclonal antibody) to show apoptotic cells in pronephric tubules.	1. IHC samples were fixed using Dent's fixative (80% methanol + 20% DMSO) instead of the conventional 4% PFA. It is uncertain whether this fixation method would lead to DNA degradation within the internal cells. 2. Similar to the ISH results, the DAPI dye was unable to penetrate the tissue and enter the kidney region.

Table S.1 Summary of experimental methods with technical difficulties and analysis of potential reasons for detecting cisplatin-induced zebrafish larval renal structural damage